RSC Advances

REVIEW

View Article Online
View Journal | View Issue

Cite this: *RSC Adv.*, 2025, **15**, 32833

Golden eyes on pollutants: colorimetric detection of emerging contaminants with AuNPs

Evana Sultana[a] and Muhammad Shamim Al Mamun *[ab]

Emerging contaminants (ECs), including pharmaceuticals, endocrine disruptors, heavy metals, and per- and polyfluoroalkyl substances (PFAS), are becoming increasingly crucial to identify because of their toxicity, persistence, and resistance to traditional water treatment techniques. Even if they are accurate, traditional analytical methods are frequently costly, time-consuming, and instrumentally complex. With its ease of use, quick visual reaction, high sensitivity, and affordability, colorimetric sensing based on gold nanoparticles (AuNPs) has become a viable substitute in this regard for on-site EC monitoring. The synthesis, functionalization, and use of AuNPs for the colorimetric detection of new pollutants have advanced recently, as this review illustrates. Because of their special localized surface plasmon resonance (LSPR) characteristics, AuNPs can interact with target analytes to produce noticeable color changes. We talk about different synthesis techniques, such as the reduction of citrate and borohydride, and how they affect the optical characteristics and particle shape. Additionally, we investigate functionalization techniques that provide selectivity toward ECs using thiol ligands, DNA aptamers, polymers, and chelating agents. A thorough analysis is conducted of colorimetric detection techniques, encompassing both aggregation-based and non-aggregation-based systems. Detecting ions (cation, anion), pesticides, metals (heavy metals, alkali and alkaline earth metals, coinage metals, rare-earth metals), food (formalin, melamine, rhodamine dye, *etc.*), pathogens, mycotoxins, oligonucleotides (DNA, nucleic acids, protein, *etc.*), glucose, and drugs (antibiotics, allergens, *etc.*) has been examined in this review. Lastly, we discuss present issues such as probe stability and matrix interference and suggest future paths for the development of portable and field-deployable sensors.

Received 1st August 2025
Accepted 26th August 2025

DOI: 10.1039/d5ra05615b

rsc.li/rsc-advances

1. Introduction

A wide range of synthetic and naturally occurring chemicals are included in emerging contaminants (ECs), also known as contaminants of emerging concern (CECs). These include heavy metals, industrial additives, pesticides, pharmaceuticals and personal care products (PPCPs), endocrine-disrupting chemicals (EDCs), and per- and polyfluoroalkyl substances (PFAS).[1,2] Despite the fact that these contaminants are frequently found in aquatic ecosystems at trace levels (ng L^{-1} to μg L^{-1}), many of them are bioactive, persistent, and difficult for traditional wastewater treatment methods to eliminate, endangering the health of people and the environment.[3–5] Therefore, for environmental monitoring and cleanup efforts, it is essential to create sensitive, selective, and field-deployable detection systems.

For identifying ECs, conventional analytical methods including inductively coupled plasma mass spectrometry (ICP-MS), gas chromatography-mass spectrometry (GC-MS), and high-performance liquid chromatography (HPLC) provide exceptional sensitivity and precision.[6] Nevertheless, these techniques are frequently costly, time-consuming, and necessitate specialized equipment and skilled workers. However, because of its ease of use, quick reaction time, affordability, and potential for on-site detection without the need for complex laboratory equipment, colorimetric sensing based on gold nanoparticles (AuNPs) has become a viable substitute.[7,8] In the visible spectrum, AuNPs' distinctive localized surface plasmon resonance (LSPR) characteristics cause strong optical absorption and scattering. The dielectric environment, particle size, shape, and interparticle distance all have a significant impact on this characteristic.[9,10] The presence of analytes causes AuNPs to aggregate or change their surface environment, which shifts the LSPR band and frequently results in a visible color change from red (the dispersed state) to blue or purple (the aggregated state). This can be seen visually or using UV-vis spectrophotometry.[11] Controlled synthesis and surface functionalization are essential for the effective use of AuNPs in colorimetric detection. The citrate reduction approach, which was initially created by Turkevich *et al.*[12] and subsequently improved by Frens,[13] is the most widely used technique for creating spherical

[a]*Chemistry Discipline, Khulna University, Khulna-9208, Bangladesh. E-mail: s.mamun@chem.ku.ac.bd*
[b]*Chemical and Materials Engineering, University of Nevada, Reno, 1664 N. Virginia, Reno, NV, 89557, USA*

AuNPs. It permits control over particle size by varying the citrate-to-gold ratio. Green synthesis employing plant extracts,[14] seed-mediated growth, and sodium borohydride reduction are further techniques. These methods produce AuNPs with a range of sizes and shapes (spheres, rods, stars), each of which makes a unique contribution to the plasmonic behavior and sensing capabilities.

AuNPs are functionalized with ligands, polymers, biomolecules, or chelating agents to provide selectivity for particular ECs. Thiols, amines, and carboxylates are examples of surface ligands that bind firmly to the AuNP surface and act as target analyte recognition elements. For instance, through coordination chemistry or aptamer–target interactions, thiol- or DNA-functionalized AuNPs can bind selectively to small molecules or heavy metal ions (such as Hg^{2+}, Cd^{2+}), causing aggregation and a detectable colorimetric response.[15–17] Functionalization with aptamers or antibodies enhances specificity even more and makes it possible to detect complex chemical ECs like pesticides, hormones, and antibiotics.[18,19]

In general, there are two types of colorimetric sensing methods: aggregation-based and non-aggregation-based. In aggregation-based systems, the target analyte's binding causes interparticle crosslinking, which modifies the LSPR and causes a color shift. In non-aggregation-based techniques, the interaction causes morphological changes or modifies the local refractive index surrounding AuNPs without causing aggregation.[20] The efficiency of AuNP-based colorimetric tests for identifying different ECs has been documented in numerous research. For instance, selective detection of mercury ions with detection limits in the nanomolar range has been achieved using citrate-stabilized AuNPs functionalized with glutathione or cysteine. Similarly, by target-induced aggregation or dispersion,[21,22] AuNPs modified with DNA aptamers have shown promise in detecting antibiotics including tetracycline, streptomycin, and kanamycin. To enable portable and real-time EC detection in the field, AuNP sensors that are embedded into smartphones and paper have also been developed.[23] Despite its benefits, there are still certain obstacles to overcome before these technologies may be put to real-world use. These include the scalability of production, the limited stability or shelf life of functionalized AuNPs, and interference from matrix components in environmental samples. However, AuNP-based colorimetric sensors are a very appealing platform for quick EC screening due to their visual readout, adjustable surface chemistry, and simplicity of manufacturing.

The EC has been the subject of numerous review publications. For instance, a thorough analysis detailed the chemical properties, origins, and types of ECs. Here, they highlighted areas that need further research to fully understand the impact of these chemicals and made recommendations for future studies.[24] The health effects and exposure risk profiles of seven legacy and new drinking water contaminants or contaminant groups-uranium, lead, nitrate, disinfection byproducts, fracking-related compounds, arsenic, and per- and polyfluorinated alkyl substances (PFAS)-were compiled by Ronnie Levin *et al.*[25] The types of ECs and their effects on soil and water quality have been summarized in a mini-review work by Haimanote K. Bayabil *et al.*[26] While assessing existing treatment technologies and regulatory frameworks, a different study team released a review that sought to offer a thorough understanding of the occurrence, detection, and environmental implications of ECs. The most recent developments in analytical methods that improve EC detection in water were examined in this research.[27] There are some remarkable details in this review that set it apart from others. Our research study has covered every potential method for creating AuNPs, including physical and biosynthetic processes, whereas the other review paper only covered the chemical and green synthesis pathway. Here, the rationale, steps, and drawbacks of modification have all been clearly and concisely illustrated. In order to explore the morphological character of AuNPs, we have attempted to discuss their distinctive properties, including Raman spectra analysis, Density Functional Theory (DFT)-simulation data, XRD analysis, and some information regarding SEM-EDX data. Everyone is aware that AuNPs have attracted a lot of interest in the field of sensors these days simply due to their surface plasmon resonance property, which is thoroughly covered here. Every potential mechanism has been covered with an appropriate example based on SPR. Following that, we have included a comparison table that highlights the fundamental distinctions between a few different sensing systems. We have attempted to cover all contaminants-detection methods in our evaluation under four general headings: environment-based detection, food-based detection, biological detection, and drug detection. Each phrase includes a brief explanation of the mechanism and an example. Following the conversation, we attempted to briefly discuss a few difficulties with the detection procedure.

With an emphasis on their use in the detection of newly developing contaminants, this study attempts to present a thorough summary of current developments in AuNP synthesis, surface functionalization techniques, and colorimetric detection mechanisms. Along with the prospects for practical application in the future, important factors such selectivity, sensitivity, detection limits, and integration into portable devices will also be covered.

2. Synthesis of gold nanoparticles (AuNPs)

2.1. Chemical synthesis of AuNPs

In the chemical synthesis process two concepts must be fulfilled. One is selecting the reducing agent which will reduce the Au^{+} or Au^{3+} to corresponding Au^{0} which is the electrical state of nanoparticles. Other one is choosing the suitable stabilizing agents which will stabilize the nanoparticles against aggregation by providing a repulsive force that then controls the growth rate, final size, or geometric shape of the nanoparticles.[28] Chemical reduction can be performed using various chemical reductants such as sodium citrate ($Na_3C_6H_5O_7$), hydrazine (N_2H_4), ascorbic acid ($HC_6H_7O_6$), and sodium borohydride ($NaBH_4$).[29] The stabilizing agent was absorbed onto the AuNPs surface to prevent agglomeration. The most common are

phosphorus ligands, trisodium citrate dihydrate ($C_6H_9Na_3O_9$), cetyltrimethylammonium bromide (CTAB), chitosan, surfactants, and other polymers.[30–32] Sometimes reducing agents also can act as a stabilizing agent.[33]

2.1.1. Turkevich method. Turkevich method provides a relatively simple and reliable way to produce well-defined gold nanoparticles for various applications. The principle of this method involves reduction of gold ions (Au^{3+}) to gold atoms (Au^0) in the presence of reducing agents like citrate[12,34,35] amino acids, ascorbic acid or UV light.[36,37] In this method sodium citrate used as both reducing and stabilizing agent.[38] The color changed from pale yellow ($HAuCl_4 \cdot 3H_2O$) to a transparent colorless suspension almost immediately after citrate addition. The suspension remained colorless for 10 s and rapidly turned bluish gray. The next minute, the suspension continued to darken to a dark blue/purple color that was almost black. At this point, the suspension started to turn deep wine red, which is a characteristic of AuNPs.[39] Two mechanisms are generally used to explain the Turkevich method. The mechanism of Turkevich method consists of three steps. Step one is the oxidation of citric acid by various reagents, acetone dicarboxylic acid has been described as the first intermediate step.[40] First, trivalent gold (Au^{3+}) is reduced to monovalent gold (Au^+) by citrate. Simultaneously, citrate (Cit^{3+}) is oxidized to acetone dicarboxylate ($ACDC^{2-}$). The second step involves a disproportionation reaction in which metallic gold (Au^0) and trivalent gold (Au^{3+}) are produced. The overall reaction is given below.[41–43] Acetone dicarboxylate ($ACDC^{2-}$) is rapidly degraded to acetone at a synthesis temperature of approximately 100 °C, as shown in Fig. 1 The degradation products reduce trivalent gold (Au^{3+}) and lead to a complete conversion to Au^0. Therefore, $ACDC^{2-}$ acts as an auxiliary reducing agent.[41,42] In 1973, Frens experienced that by varying the ratio of reducing to stabilizing agents, the size of AuNPs range from 16 nm to 147 nm can be achieved.[13,44,45]

2.1.2. Brust method. The Brust method was first described in 1994.[47] In this method there is two phase process to produce AuNPs which size range varies from 1.5–5.2 nm. AuNPs was synthetized by using organic solvents and by varying the ratio of thiol to gold. The Brust method was inspired from Faraday's two-phase system. First, chloroauric acid (Au^{3+}) is phase transferred into toluene from an aqueous phase using a phase transfer catalyst called tetraethylammonium bromide (TOAB).[48] Another aqueous solution containing sodium borohydride, the main reducing agent, is contacted with the organic phase next in presence of alkanethiol which stabilize the AuNPs.[49] The extraordinary stability of the synthesized particles is attributed to alkanethiols which form a strong bond with the particle surface and also cause passivation of the surface of AuNPs.[50–53] The particle formation was indicated by changing the color from orange to blue.[48,50] A great variety of functionalized nanoparticles of noble metals have been synthesized over the years using this method (Fig. 2).[54,55]

2.1.3. Seeded growth method. We have already discussed that Turkevich and brust method can only produce the spherical AuNPs. But AuNPs can exhibits its nanoparticle characteristics in many other nanostructures such as rod,[57,58] cube[59] and tubes[60] *etc.* Unlike the Frens method, seed-mediated growth synthesis introduces students to a more advanced nanofabrication technique.[61] While the seed-mediated growth is the most common method for the synthesis of rod-shaped AuNPs, spherical AuNPs are also reported, with a size range of 1.5–86 nm.[30] Mainly the size of AuNPs is increased by the growth of seed of AuNPs. The basic principle of this synthesis process involves two parts. The first part is the synthesis of AuNPs following the Frens method. After that the synthesized AuNPs solution will be used as seed for further growth. The seed particles are then added to a solution of metal salt in the presence of a weak reducing agent (ascorbic acid) and structure directing agent to prevent further nucleation. Addition of excess amount of reagent to a seed-mediated synthesis, the nanoparticles become the larger in size. In this process, one can observe the color change of the nanoparticles according to the increase order of size. Since this method uses step-by-step increase of the size, it allows for the controllable synthesis of AuNPs with desired shape and size.[62] Behind this controllable synthesis process some influential factors are involved like

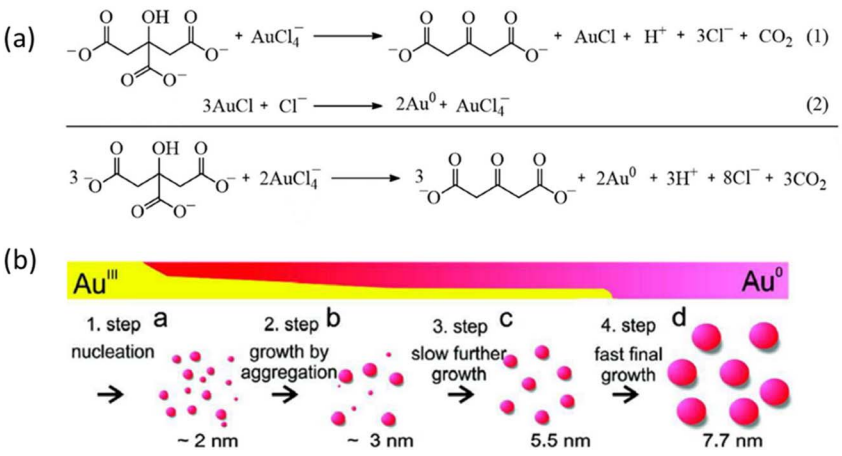

Fig. 1 (a) Accepted reduction mechanism of $AuCl_4^-$ using citrate in two step redox reaction. (b) Synthesis of spherical AuNPs in the size range of 10–20 nm by Turkevich method.[46] This figure has been adapted from ref. 46 with permission from American Chemical Society, copyright 2010.

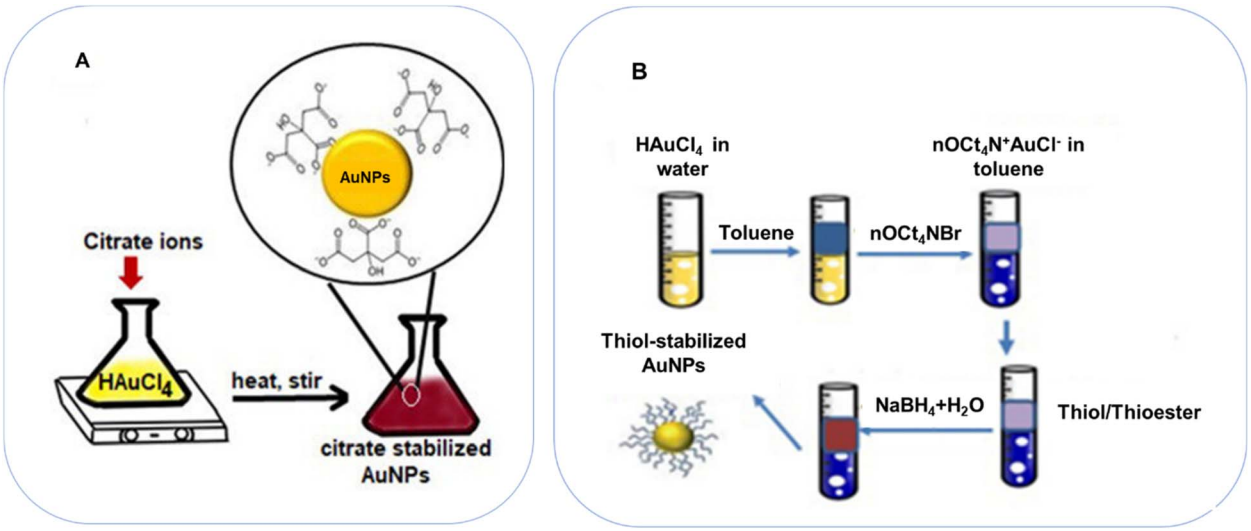

Fig. 2 (A) The synthesis of AuNPs using Turkevich method. (B) Burst method for the synthesis of AuNPs. This figure has been adapted from ref. 56 with permission from Tailor & Francis Group, copyright 2020.[56]

temperature, reducing agent and precursor concentrations, seed concentration, and the rate of the addition of the reducing agent.[63] The increase of size more than seed AuNPs can also be observed by UV-vis spectroscopy (Fig. 3).

2.1.4. The sulfhydryl ligand method. In this method the gold salt ($HAuCl_4$) is mixed with sulfhydryl ligands into a single or double phase solvent. In the single-phase method, a water-soluble sulfhydryl ligand such as thioglycolic acid, cysteine, or glutathione, is used as a ligand to prepare AuNPs that have good dispersity in water.[64] Mainly these two-phase solvents are classified according to the polarity of solvents. The double-phase method, alkyl sulfhydryl is often used as a ligand, and the synthesized AuNPs possess good oil solubility and are stable in organic solvent.[65] Then the sodium borohydride as a strong reducing agents use to reduce Au^{3+} ion to AuNPs.[66] The sulfhydryl ligands bind on the Surface of AuNPs through the Au–S bond.[67] In this method, the size distribution of AuNPs normally ranged between 0.8–8 nm.

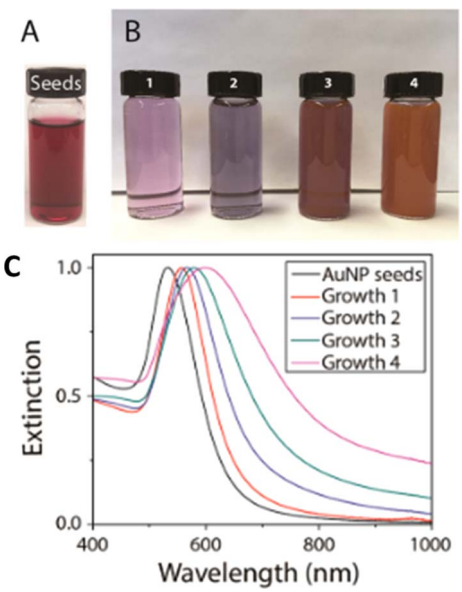

Fig. 3 Seed-mediated growth of varying sizes of spherical gold nanoparticles. (A) ~40 nm Au nanoparticles act as seeds in the seed-mediated synthesis. (B) Images of nanoparticle growth after seed-mediated synthesis of group 1, group 2, group 3, and group 4. (C) The extinction spectra of groupwise synthesized AuNP seeds. This figure has been adapted from ref. 61 with permission from American Chemical Society, copyright 2024.

2.2. Green synthesis of AuNPs

In order to produce biocompatible and ecofriendly AuNPs, green synthesis is increasingly favored alignment with sustainable practices. Mainly this synthetic process can be divided into two broad categories of physical and biological approach.

2.2.1. Physical synthesis of gold nanoparticles. Physical methods allow for synthesis of AuNPs with controllable size and structure with reduced time and the possibility of simultaneous synthesis and sterilization of the products.[62] This method involves some physical techniques those utilize the energy of electromagnetic and particle-like radiation to induce chemical reactions in the solution, leading to the reduction of Au ions without the need for chemical reducing agents.[63] These techniques include gamma and X-ray radiations techniques[68–70] microwave-assisted methods[71,72] ultra-violet (UV),[73] laser ablation,[74] ultrasonic[75,76] and electron beam irradiation[77] and enclose methodologies such as photochemical, thermolytic procedures. Gamma irradiation allows controllable synthesis for AuNPs which are specially in spherical, and rod shaped in the range of 2–22 nm. A photochemical reaction uses light from sun or UV light produces free radicals that acts as a reducing agents in the AuNPs synthesis.[73,78] Microwave assisted methods produce heat in the system that leads to reduction, and the procedure is rapid.[72,79,80]

2.2.2. Biosynthesis of gold nanoparticles

2.2.2.1. Using plant constituents. Biosynthesis of gold nanoparticles has recently gain much interest because of its non-toxic effects on environments and cost effective green method that applies plant based constituents like leaf, root and seeds, flowers, fruits, bark and flower.[81–83] Some benefits of using this method for the synthesis of AuNPs is using its biocompatible parts like flavonoids, phytosterols, saponins, steroids, tannins, quinones and other natural compounds *etc.* which possess some important functional group that catalyze the reduction of gold salt and stabilize AuNPs.[84] The gold salt solution is reduced into AuNPs and the reaction completes in minutes to a few hours. The reaction mixture is further incubated to reduce the gold salt completely and is visually monitored by color change. Finally, the synthesized AuNPs are purified by centrifugation and washed thoroughly in water for further us.[85] In this process, there is no need for extra purification steps and all the plants constituents are easily available. AuNPs synthesized *via* green synthesis method are also reported to exhibit antibacterial, antifungal, anticancer, and anti-inflammatory properties, and antioxidant and catalytic activity due to the presence of phytochemicals from the bio extract.[86,87] Regarding the biosynthesis of AuNPs, plant extracts have little diversity in functional groups resulting in a restricted choice of surface functionalities around AuNPs. Moreover, the procedure is often time-consuming due to issues related to the extraction of raw materials, often low yielded and produces less uniform particle size due to complexity of natural reducing agents (Table 1).[88]

2.2.2.2. Using microorganisms. Synthesis of AuNPs from microorganisms generally are of two kinds like intracellular and extracellular. But the later one is more suitable for taking less purification steps and hence take less time and effort.[62] Size dependent biosynthesis of AuNPs is possible by using virus, bacteria[99] and algae[100] fungi[101] which reveals non-toxic, non-genotoxic, and non-oxidative properties on human cells.[102] Fungi are advantageous over bacteria and algae, due to their high metal tolerance and bioaccumulation ability.[103] Upon treatment on microbial cells, gold salts synthesize nanostructures then size and shape of AuNPs can be controlled by altering different growth factors. From the literature review we have come to know that extracellular biosynthesis of AuNPs used different types of microbes which are illustrated in a Table 2.

Table 1 A list of some of the different plants which have been used for synthesis of AuNPs

Plant	Parts of plants	Size of AuNPs (nm)	References
Rosa hybrid	Petal	10 nm	89
Garcinia mangostana	Peel extract	32.96 ± 5.25 nm	90
Magnolia kobus	Leaf	5–300 nm	91
Cassia auriculata	Leaf	15–25 nm	92
Prunus domestica	Fruit	14–26 nm	93
Zingiber officinale	Root	5–15 nm	94
Salvia officinalis	Leaf	6–27 nm	95
Cicer arietinum L.	Bean extract	25 nm	96
Nyctanthesarbortristis	Flower extract	19.8 nm	97
Gnidia glauca	Flower extract	50–150 nm	98

Table 2 Different microorganisms have been used for synthesis of AuNPs of different sizes and shapes

Microorganism	Genius	Size of AuNPs (nm)	References
Shewanella algae	Bacteria	10–20 nm	104
Pseudomonas fluorescens	Bacteria	50–70 nm	105
Marinobacter Pelagius	Bacteria	10 nm	106
Stenotrophomonas maltophilia	Bacteria	40 nm	107
Rhodopseudomonas capsulate	Bacteria	10–20 nm	108
Acanthella elongate	Sponge	7–20 nm	109
Sargassum wightii Greville	Algae	8–12 nm	110
Candida albicans	Fungi	20–80 nm	111

2.2.2.3. Using biomolecules. A biomolecule molecule is loosely defined as a molecule produced by a living organism. Nowadays AuNPs can be synthesized by using different biomolecules including proteins (*e.g.* sulfite reductase),[112] amino acids (*e.g.* histidine)[113] and carbohydrates (*e.g.* dextrose).[114] Recently inorganic nanoparticles protected by organic ligands have attracted much interest due to their diverse technological applications.[115,116] Amine-capped AuNPs were reported using primary amines.[117] Oleyl amine (OLA)[118] aromatic amines[119] amino acids[120,121] diamines[122] have been used as reducing/capping agents in synthesis of AuNPs. These molecules contain hydroxyl and carbonyl functional groups which can reduce the Au^{3+} to Au^{0}.

3. Modification/fabrication of AuNPs

Modification of AuNPs means the addition of new functional groups on the surface of AuNPs which may be come from any biological constituents like DNA, oligonucleotides *etc.* Functionalization in the case of AuNPs is usually referred to anchoring molecules to the AuNPs with specific properties and functions in addition to simple stabilization.[123] The first functionalization of AuNPs was carried out in 1996 by using thiolated oligonucleotides to detect DNA as a sensor of AuNPs.[124,125] For the sensors and biosensors activity of AuNPs, these specific functions will facilitate a specific response to target analytes in case of providing high selectivity and sensitivity. For the functionalization of AuNPs, there are three strategies are available to functionalize their surface: (a) covalent interactions[126] (b) electrostatic interactions[127] and (c) attachment of small molecules for specific recognition of the analyte.[128] For the covalent bonding thiol containing biological or organic compounds are used to conjugate on the surface of AuNPs *via* Au–S bond. One end of the thiol group is anchored on the surface of AuNPs and by using the other thiol group connected with chemical bonds (–COOH and $-NH_2$) to functionalize modification of DNA, RNA, amino acids.[129] Notably, the thiolated DNA forms a high-density DNA monolayer on AuNPs, causing high stability, even in highly ionic media, such as seawater.[130] Functionalizing agents can be added on the surface of AuNPs *via* physical adsorption based on electrostatic forces between oppositely charges molecules.[131] Electrostatic modification involves the functionalization of AuNPs with ligands *via* electrostatic interaction. This type of

Table 3 Summary of different functionalizing units for the modification of AuNPs[140]

SL no.	Type of AuNPs	Modifying agents	Mechanism of modification	Ref.
1	Gold chromophore	Thiourea	Desulfurization reaction with AuNPs	141
2	MA-GNPs	Maleic acid (–COOH)	Acts as reducing and stabilizing agents	142
3	TA-AuNPs	Disulfides, –COOH	Covalent S–Au linkage	143
4	AA stabilized AuNP	Glycine	Photochemical synthesis	144
5	DTET-AuNPs	Dithioerythritol	Ligand exchange interaction	145
6	BSA-AuNPs	Cysteine, polyethylene glycol (PEG)	Ligand exchange reaction	146
7	Green synthesis	Chitosan	Core or shell formation	147
8	DNA-AuNP	Probe A: 5′HS-C10-A10-T-A103′ Probe B: 5′HS-C10-T10-T-T10 3′	Through the thiol group present in DNA	148
9	Amino acid modified	L-Cysteine	Through the S- atom present in L-Cys	149
10	Acid modified	3-MPA and AMP	Electrostatic interaction	150
11	Naphthol modified	1,8-Naphtholimide	Aqueous phase synthesis	151
12	DNA functionalized	Poly thymine (T33) oligo in Mn^{2+}	Mn^{2+} groups on AuNP bind to backbone of DNA	152
13	Acid stabilized AuNP	3-Mercaptopropionic acid	Coordination chemistry	153
14	Optically modified	MPA-H-Cys-PDCA	Incubating AuNP with MPA-H-Cys-PDCA	154
15	Nanogold aptamer	Single stranded DNA (ssDNA)	Self-assembly of the aptamer by catalytic reaction	155
16	GSH-AuNPs	Glutathione ($–NH_2$, –SH, –COOH)	Self-assembly of the GSH	156
17	Peptide-AuNPs	Cys-$(Arg)_8$-Asp-Ser (CRRRRRRRRGDS)	Cross-linking of cysteine's thiol with AuNPs	157
18	T-SH-AuNP	*N*-1-(2-Mercaptoethyl) thymine	Ligand exchange interaction	158
19	Amine-AuNPs	Polyethylene glycol (PEG)	siRNA delivery	159
20	PVP-AuNPs	Polyvinylpyrrolidone	Rapid oxidation of the PVP under UV radiation	160
21	Papain-AuNPs	Cysteine, thiol (–SH)	Covalent bond Au–S/Au–SH	161
22	RNA-AuNPs	Polyvalent RNA-gold nanoconjugates	RNA delivery	162
23	NTA-AuNP	3-Nitro-1-*H*-1,2,4-triazole	Triazole ring of NTA interacts with AuNP surface	163
24	AuNPs	6-Aza-2-thiothymine (ATT)	Aggregation	164

interaction involves very weak bonds with AuNPs and ligands in respect to covalent bond which exhibit very low stability under various environmental conditions (PH, ionic strength).[132] Ligands, such as DNA, on AuNPs are easily removed under high salinity or strong acid/base conditions, resulting in AuNP aggregation which is really undesirable and may be occurred in absence of any analytes.[133] For example, unfolded single stranded DNA (ssDNA)[16,134] and streptavidin[135] were bound to the citrate-capped AuNPs *via* electrostatic forces. Furthermore, modifying AuNPs with small molecules, especially antibodies, induces specific recognition of target antigens in the matrix. For example, streptavidin AuNPs can specifically interact with biotinylated antibodies *via* a streptavidin–biotin reaction.[136] AuNPs without surface modification may lead to aggregation of particles. So, capping agents/protective agents must be added on the surface of AuNPs which will prevent aggregation keeping them apart from each other. Most effective/common type of stabilizing agents are thiols, citrate, surfactants, polymers, and different types of chelating ligands. The protecting agent generally forms a monolayer, a ligand shell, and serves a critical role in imparting the particles a large number of properties such as stability against aggregation, improved solubility, controlled shape and orderly assembly of nanoparticles, improved electron-transfer efficiency and provides a platform for the sensing of specific molecules or ions.[137] The most common mechanism for the stabilization of nanoparticles involves charge stabilization and steric stabilization. Charge stabilization faces difficulties in the presence of salts. Adsorbing charged ligands like citrate on the surface, the induced charge on surface of NPs repels each other inhibiting aggregation. Steric stabilization is achieved by coating the nanoparticles' surface with large molecules like polymers, which prevent them from touching each other by steric effects. A wide variety of different thiolated molecules can be placed in the ligand shell which can produce thiol–gold bond either directly during synthesis[138] or place exchange reaction (Table 3).[54,139]

4. Characterization of AuNPs

Once the AuNPs is synthetized then it is obvious to justify whether the synthesis is conducted correctly or whether the procedures need to be modified and optimized according to the desired properties. For the confirmation of the AuNPs synthesis, only characterization of AuNPs based on different aspects is appropriate. The common characteristics of AuNPs are the size distribution, shape, surface charge, crystallinity and surface chemistry. There are many tools and techniques available for the characterization of AuNPs. The most common method to understand the size, shape and morphology of AuNPs is transmission electron microscopy (TEM).[165] Scanning electron microscopy (SEM) is another technique which help us to know the shape and size distribution of each AuNPs.[166] The SEM image of NPs help the diameter distribution of AuNPs using ImageJ Software, in which the diameter was calculated 25.67 ± 0.30011 nm.[167] Another size distribution technique is dynamic light scattering (DLS).[168] The ultraviolet visible (UV-vis) spectroscopy, another conventional method which is used to confirm the formation and aggregation of AuNPs with another elements. Based on literature review, the distinct absorption peak from the surface plasmon absorption of the gold

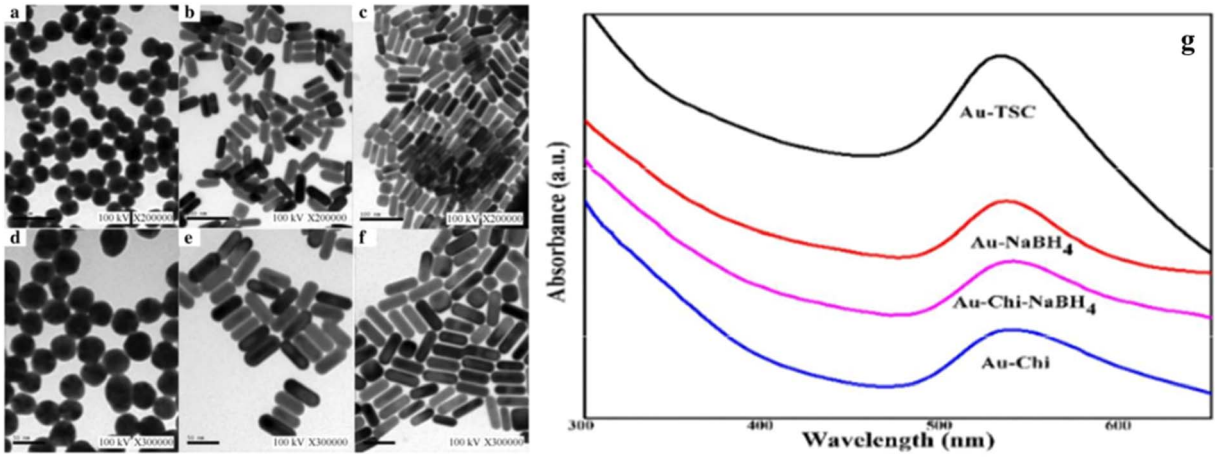

Fig. 4 TEM images of gold nanoparticles with different shapes. (a and d) Spherical nanoparticles, (b and e) short nanorods (c and f) long nanorods[187] (g) the UV-vis spectroscopy of synthetized AuNPs (size range <20 nm) by using different reducing agents. This figure has been adapted from ref. 140 with permission from Royal Society of Chemistry, copyright 2016.

nanoparticles is located between 510 and 530 nm.[140] The characteristic peak at 524 nm at UV-vis spectroscopy confirms the successful formation of Na_2EDTA capped AuNPs.[169] Near-infrared (NIR) spectroscopy is also reported to investigate AuNP aggregates and different shapes of AuNPs.[170] To understand the surface chemistry of AuNPs, Attenuated Total Reflectance (ATR) and Fourier-transform infrared (FT-IR) spectroscopy are effective technique which gives us information about the functional group present on AuNPs.[167,171] In the Na_2-EDTA capped AuNPs, the O–H bond stretching at 3400 cm^{-1}, CH_2 (wag vibration) at 1388 cm^{-1} and the C–O bond stretching at 1630 cm^{-1} was depicted *via* ATR spectroscopy.[172] When a laser beam (532 nm N_2) was focused on the AuNPs, the electrostatic fields surrounding the particles increased, matching previously reported result which shows that AuNPs gives Raman band at around 479 cm^{-1} indicates the presence of metal, by the ν(metal–O) band.[173] This finding has a striking resemblance to previously reported study of chitosan-capped AuNPs, which revealed a Raman band peak at 493 cm^{-1}.[174] Atomic force microscopy (AFM) provides the unique opportunity to

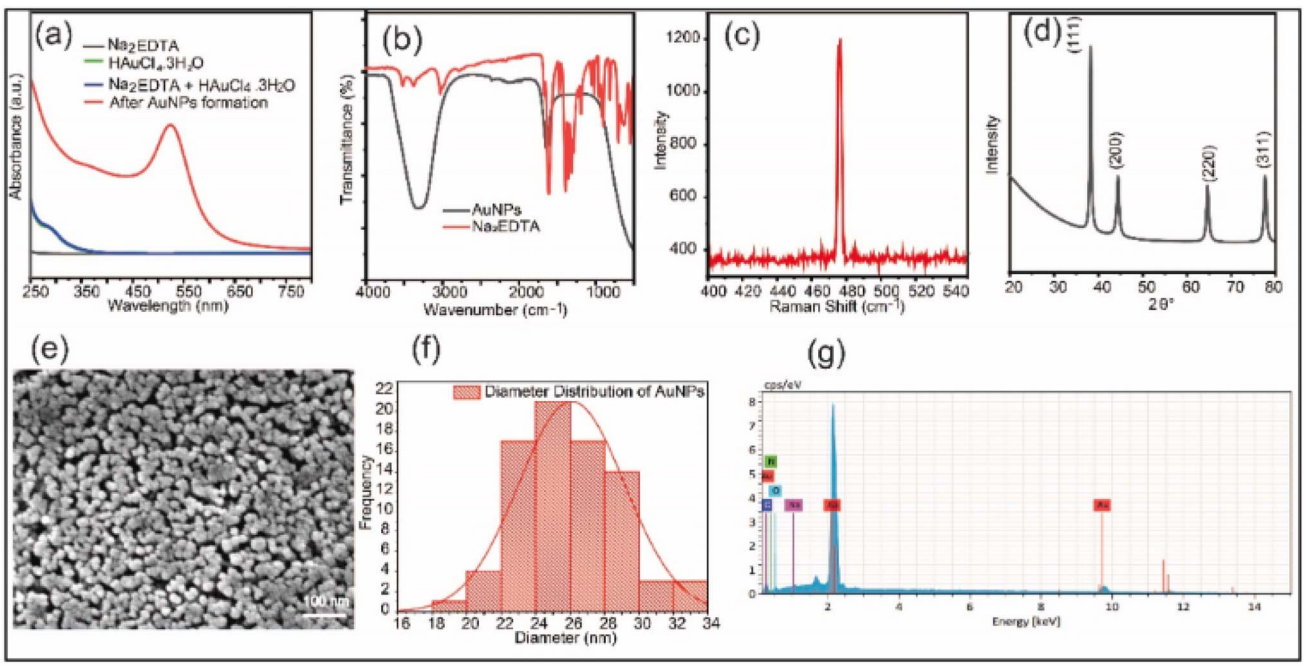

Fig. 5 (a) UV-visible spectrum of the formation of AuNPs. (b) IR spectrum of Na_2EDTA and synthesized AuNPs solution. (c) Raman spectrum of AuNPs. (d) XRD spectrum of synthesized AuNPs solution. (e) Morphological analysis of the synthesized AuNPs using SEM. (f) Diameter distribution of AuNPs using ImageJ software. (g) EDX spectra analysis of the AuNPs. This figure has been adapted from ref. 167 with permission from Elsevier, copyright 2025.

characterize a single nm-sized spot by a combination of methods.[175] The instrument characterizes the morphology of the samples with quantitative information about properties such as roughness or height distributions. Samples are measured in AFM without special surface preparation at ambient pressure or in liquids.[176,177] To verify the elemental composition of the synthesized AuNPs, EDX can be a good technical approach. Approximately 91% of the particles identified by this approach were gold, according to EDX analysis, indicating an effective production of AuNPs.[178] Gel electrophoresis is a technique that is mainly used to confirm the successful attachment of the oligonucleotides/polymers onto the surface of AuNPs through separating nano-conjugates based on their size and charge.[179,180] An electrophoresis approach with online thermal lens can also be used for monitoring the surface energy of AuNPs.[181] To estimate the surface charge and stability of AuNPs, Zeta potential technique can be a very smart choice. Zeta potential is a measure of the effective electric charge on the nanoparticle's surface and quantifies the charge stability of the colloidal particles.[182] Under an electric field, the optical measurement of the particle's motion can be used to determine the Zeta potential[183,184] The higher magnitude of Zeta potential represents increased stability due to increased electrostatic repulsion (Highly stable particles are in the range 40+ mV).[182] The crystallinity of AuNPs can be measured by X-ray diffraction (XRD).[185] The crystalline and stable nature of the AuNPs is confirmed by the existence of strong peaks. These peaks (at 38°, 44°, 65°, and 77°) presence suggested that AuNPs had a face-centered cubic (fcc) structure which was verified by peak matching with JCPDS data file no. 04-0784.[186,187] The average crystallite size of Na_2EDTA capped AuNPs was estimated to be 19.71 ± 3.2288 nm by using the Debye–Scherrer equation (Fig. 4 and 5).[167]

5. Properties of AuNPs

AuNPs exhibits different physical and chemical properties varying different sizes and shapes. The spherical shape of AuNPs is synthesized using Isotropic growth of gold nuclei.[56] According to the anisotropic properties, based on dimensions, the shape of AuNPs can be classified into three categories such as (a) one-dimensional shape: nanorods, nanowires, nanotubes *etc.*(b) two-dimensional shape: nanoplates such as stars, pentagons, squares/rectangles, dimpled nanoplates, hexagon *etc.*(c) three-dimensional shape: gold nanotadpoles, gold nanodumbbells (AuNDs), nanopods.[188] Depending on the size, the color of AuNPs varies include brown, purple, blue, orange and red. The shape of nanoparticles also influences their optical[189,190] and catalytic properties. AuNPs has been a great field of interest due to its two separate SPR bands called longitudinal plasmon band (LSPR) and transverse (TSPR).[191] The transverse band appears in the visible region, while the longitudinal band is observed in the near-infrared (NIR) region.[192] The SPR bands of AuNPs ranges from 500–550 nm depending on size of nanoparticles[193,194] As the aspect ratio (length-to-width ratio) of gold nanorods increases, the longitudinal plasmon resonance becomes more intense and shifts to longer wavelengths. Therefore, by adjusting the aspect ratio, the plasmon resonance can be precisely tuned across the visible spectrum. On the other hand, the transverse surface plasmon resonance does not depend on the aspect ratio and provide the same wavelength of plasmon resonance of spheres.[194]

5.1. Surface plasmon resonance of AuNPs/electronic and optoelectronic properties of AuNPs

In the era of nanotechnology, AuNPs is called the nano plasmon due to the free electron density around the particles which possess limited motion due to its small size (~50 nm mean free path) than the adequate motion in case of bulk materials. Due to this amazing strategy optical properties are significant in nano materials. Because of small size, AuNPs exhibits various physicochemical properties *e.g.* good optical characteristics, high electron densities, and good biocompatibility and catalytic performance.[195] Among all of these wonderful properties, the most applied optical properties are their surface plasmon resonance[196] and fluorescence quenching.[197] SPR is defined as the collective oscillation of electrons (diameter $d \ll \lambda$, where λ is the wavelength of the light), which is dependent on both the nature and size of the material.[198,199] In 1908, Mie first elucidated the origin of this phenomenon by solving Maxwell's electromagnetic equation for small homogeneous spherical particles interacting with an electromagnetic field.[200] Surface plasmon resonance occurs when the vibrational frequency of free electrons interacts with the frequency of incident light to generate resonance.[201] As the light wave passes over the particle, it causes the electron density to become polarized toward one surface, leading the electrons to oscillate in sync with the light's frequency, resulting in a standing wave-like oscillation. The resonance condition can be determined from absorption and scattering spectroscopy depending on shape and size and dielectric constants of both metal and surrounding materials. The change in shape or size of AuNPs causes the change in electric field resulting in the change in oscillation frequency of electron. This generates different cross-sections for the optical properties including absorption and scattering. Strong optical absorption occurred in the visible range by the collective excitation of free electron clouds when Au nanoparticles are exposed to light irradiation. Changing the solvent eventually changes the dielectric constants which will influence the oscillation frequency due to the varying ability of the surface to accommodate electron charge density from the AuNPs. Thus, the chemically bonded molecules can be detected by observing the change they induce the electron density on the surface of AuNPs resulting in the shifts in surface plasmon absorption maximum. This phenomenon is the basic of sensing strategy.[194] This generated resonance is responsible for the characteristic absorption of AuNPs in the UV-vis region. Due to the absorption λ_{max} changes varying the size, shape and interparticle distance of AuNPs.[202] The molecules or ligands used to coat the AuNPs surface imparts positive or negative charge. Positively charged surface of AuNPs is most stable in nature. Another reason is the coulombic attraction between the electron and nuclei.[62] It has been proposed that only electron–electron interactions are

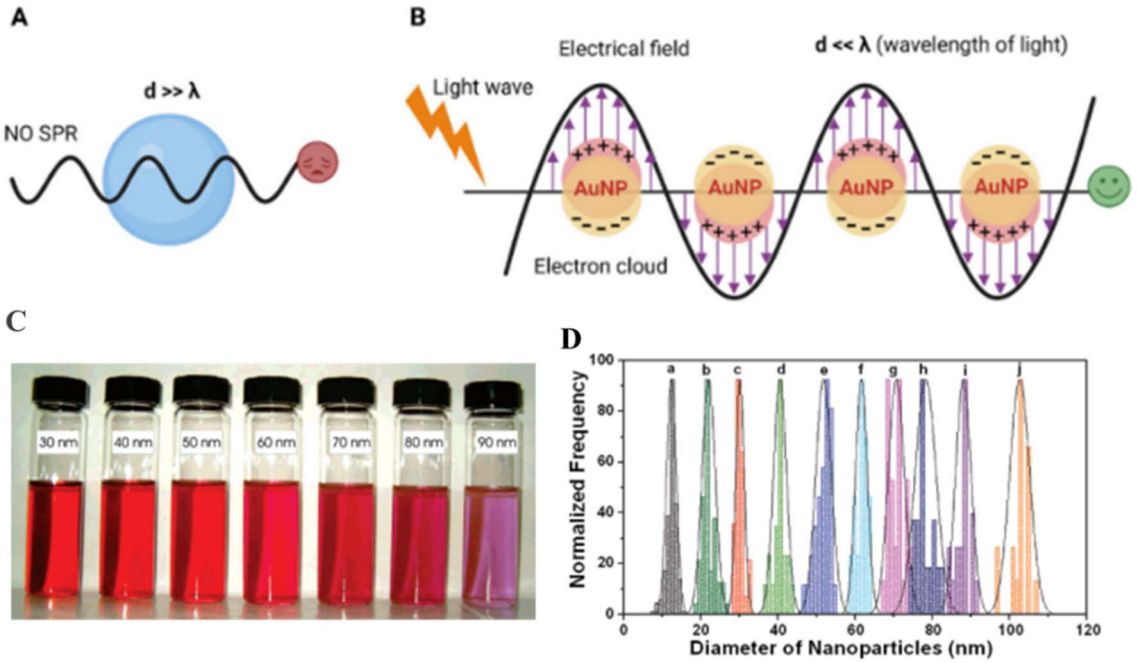

Fig. 6 Principle of surface plasmon resonance-based colorimetric sensor due to surface plasmon resonance (SPR) phenomena (A) no SPR happens when particle size is greater than the wavelength of light (B) SPR phenomena take place successfully when the wavelength of light is greater than AuNPs size to get a colorimetric response.[208] (C) Photo showing the colors of gold nanoparticles with different particle sizes. (D) Size distributions of AuNPs of different sizes. (a) 12.3 (1.3 nm; b) 20.6 (1.5 nm; c) 30.0 (1.1 nm; d) 40.3 (1.7 nm; e) 51.6 (2.0 nm; f) 61.3 (1.5 nm; g) 70.6 (2.0 nm; h) 78.3 (2.7 nm; i) 88.1 (2.0 nm; and j) 102.2 (2.6 nm) (the *y*-axis represents normalized frequency). This figure has been adapted from ref. 208 with permission from American Chemical Society, copyright 2017.

involved in the SPR process rather than electron–phonon coupling.[203] For example a typical spherical shaped AuNPs of 13 nm size absorb maximum wavelength of 520–523 nm which is responsible for wine red color of solution.[66] In fact absorption of AuNPs is mainly dependent on various factors like size, shape, functionalization, synthesis process, solvents and inter-particle distance of AuNPs.[123,199] Murray and co-workers have observed spectral shift induced by solvent refractive index changes that are consistent with Mie theory.[204] Therefore, the aggregation of nanoparticles results in significant red-shifting (from ~520 to ~650 nm) and broadening in the SPB, changing the solution color from red to blue due to the inter-particle plasmon coupling.[205,206] The more increased diameter of spherical shaped AuNPs gives more longer wavelength of absorption (red shift) (Fig. 6).[207]

6. Mechanisms of SPR-based colorimetric sensors using AuNPs/ principle of gold nanoparticles-based colorimetric sensor

Gold nanoparticle (AuNP)-based colorimetric sensors have become a great field of interest because of having some unique features like amazing optical properties (surface plasmon resonance), controllable size, catalytic properties and surface chemistry.[208] Mostly, the surface chemistry of AuNPs provides a significant capability of being linked towards a range of molecular units with thiol group for conjugation and detection of biological targets.[209–212] These intriguing properties and advantages of GNPs are explicitly responsible for its escalating applicability in detection. Mainly, sensor is a systematic unit of group of devices that intend to generate physical or chemical change in its surroundings.[213] Colorimetric sensors possess two critical elements that determine their selectivity, sensitivity, response time and signal-to-noise ratio.[201,214] One of these is the recognition unit which gives selective response with target molecules (small organic molecules and biomacromolecules *etc.*).[215] The other element is he conduction unit that transforms the detection response into a color change in the visible light region (390–750 nm) and determines the detection sensitivity.[216] Colorimetric analysis of gold nanoparticles is based on change of surface plasmon resonance caused by the aggregation of AuNPs and changing the surface morphologies or interparticle distance.[217,218] In the past decades, the colorimetric detection method regarding NPs which sensing mechanism was based on interparticle distance dependent properties.[219] Nowadays, the sensing mechanism depends on nanoparticles aggregation and dispersion grade variation induced by analyte that changes the interparticle plasmon coupling detected by LSPR spectral lines.[220] Nanotechnology launched a lot of advancements from the first detected colorimetric method[125] to several LSPR-based colorimetric sensors for detection different types of analytes *e.g.* nucleic acids,[221–223] proteins[224,225] and small molecules.[226,227] The changes in the Au nanoparticles' size, shape and composition induced by analyte are followed by shift in the SPR and color

changes.[228] The mechanisms based on AuNPs can be classified in the following categories:

6.1. The growth-based colorimetric sensing mechanisms of AuNPs

The growth of small -sized AuNPs to longer-sized AuNPs or different shaped AuNPs by means of reduction of $AuCl_4^-$ to AuNPs, causes color change of the system. The enzymatic reaction or the chemical transformation may cause the morphology change of AuNPs which has become a new trend in designing a biological and chemical colorimetric sensing strategy.

6.1.1. Non-enzymatic growth of AuNPs. For the growth reaction, a reducing agent plays a vital role to convert $AuCl_4^-$ to AuNPs. H_2O_2 is a well-known reducing agent for the AuNPs growth[229] and it also act as a catalyst for the metalation of AuNPs.[230] Based on the reducing property of H_2O_2, a colorimetric sensing system was designed to detect metal ions like Hg^{2+}.[231] H_2O_2 was decomposed by the catalytic activity of AuNCs following the less reduction of $AuCl_4^-$ to AuNPs occur, resulting the less growth of AuNPs which led to the formation of ill-modified morphology of aggregated AuNPs. Mainly the decomposition happened due to the absence of target Hg^{2+}. Thus, the partially aggregated AuNPs gives purple color. On the other hand, in the presence of target analyte Hg^{2+}, the H_2O_2 perfectly reduce the $AuCl_4^-$ to AuNPs with fast rate resulting the perfect growth of AuNPs. This phenomenon produces the non-aggregated AuNPs.[232] In the mentioned system H_2O_2 was incorporate in the system which was prepared separately but *in situ* production of reducing agents are also designed. A new system has been established by Liu *et al.*[233] showed that H_2O_2 can be generated by the oxidation of glucose through the glucose oxidase catalytic reaction. By using this *in situ* produced reducing agent, the glucose oxidized catalyst growth AuNPs can be used for the detection of the cancer biomarker prostate-specific antigen. Hydroxylamine (NH_2OH) is another most commonly used reducing agents which has been used in colorimetric sensing strategy based on target mediated growth of AuNPs.[234] Hydroxylamine also acts as a reducing agent for the detection of Hg^{2+} which is adsorbed on the surface of AuNPs and formed an amalgam like (Hg^{2+}–Au) structure. Thus, Zhao *et al.*[235] merged these two sensing strategies for the development of Hg^{2+} detection. The growth of AuNPs can be controlled by controlling the amount of adsorption of Hg^{2+} on AuNPs surface, thus giving rise to different structures of AuNPs resulting different colors of solutions (Fig. 7).

Researchers have found a new mechanism where the target itself acts as a reducing agents like tetracyclic antibiotics based on *in situ* growth of AuNPs. Tetracyclic antibiotics reduce Au^{3+} to Au^0, which could spontaneously form AuNPs with the oxidation of phenol group associated with benzene ring. With the increase of tetracycline, the SPR effect of AuNPs is intensified, resulting in the appearance of slightly blue color. In this method Shen *et al.*[236] developed a colorimetric method to detect tetracycline broad-spectrum antibiotics. Though this method gives fast result but cannot differentiate between different types of tetracycline.

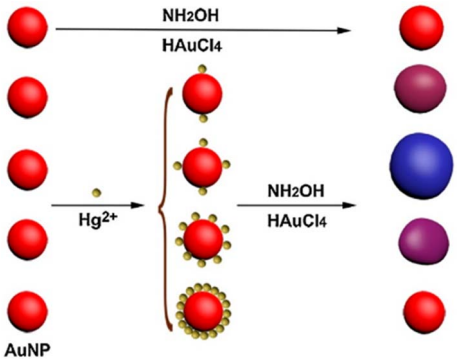

Fig. 7 The schematic illustration of the amount of Hg^{2+} on the surface which controls the growth of AuNPs. Reproduced with permission from reference. This figure has been adapted from ref. 236 with permission from Elsevier, copyright 2017.

Nowadays, DNA molecule plays a vital role on the diffusion of Au^{3+} to the seed which help changing in morphology of AuNPs.[237,238] Researchers have found out a way to use DNA-aptamer to the colorimetric diagnosis method by DNA-mediated AuNPs growth. Ochratoxin A (OTA) can be detected by using a method of aptamer controlled AuNPs growth which has been described.[234] Here, DNA aptamer acts as a capping agent which adsorbed on the surface of pre-prepared AuNPs by the physical adsorption process. In this process, aptamer strands were controlled by managing the aptamer–target interaction depending on the concentration of the target. The higher the OTA concentration, the lower the Aptamer capped on AuNPs. Highly covered aptamer exhibits a branched morphology and gives blue color solution while the lower aptamer coverage gives spherical morphology resulting in a red color solution.

6.1.2. Enzyme-mediated AuNPs growth. In this method the size of AuNPs can be larger by reduction of Au^{3+} to Au^0 with the help of enzymatic reaction. For example, GOx mediated nanocrystal growth for the attomolar detection of prosthetic specific antigen (PSA) was reported in Liu *et al.*[233] Here, secondary antibody (Ab2)-GOx conjugate functionalized magnetic beads were used as a capture probe, and primary antibodies (Ab1) were used as a detection probe. After the formation of immunocomplex (Ab1-PSA-Ab2-Gox), Gox trigger the oxidation of glucose, leading to the formation of H_2O_2. This H_2O_2 mainly enlarges the 5 nm AuNPs to larger size which is responsible for the color change of the solution. The formation of immunocomplex (Ab1-PSA-Ab2-Gox) was mandatory because the small sized (5 nm) AuNPs exhibits colorless solution whereas larger size (>10 nm) AuNPs gives red color solution. The calculated LOD of this method is 93 aM which is more than 4 orders of magnitude higher than the conventional ELISA method. An enzymatic silver deposition on AuNPs assay was developed by Gao *et al.*[239] for the developed a high-resolution colorimetric sensor to monitor alkaline phosphate (ALP) activity.

6.2. Aggregation-based colorimetric sensor

6.2.1. Labeled detection method. In the labeled based colorimetric sensing mechanism, the controlled aggregation of

AuNPs can be achieved by cross-linking, non-cross linking or destabilization process.[240] The labeled method directly attaches ligands like DNA, aptamers, peptides and antibodies on the AuNPs surface through chemical interaction prior to detection of target molecules. Ligand modified AuNPs are very stable at higher ionic strength, because there are two types of repulsions available (steric and hydration based interparticle). In the cross-linking aggregation, aggregation induced by the controlled assembly of ligands functionalized-AuNPs in the formation of intermolecular bonds (H-bonding, hydrophobic bond, chelation, base pairing *etc.*).[241] In cross-linking methods, the target compound and ligand on the gold nanoparticle surface form a complex, which decreases the interparticle distance and causes aggregation.[242] For the modification of AuNPs with specific ligands, one terminal of the ligands should have a sulfhydryl group that will bind on the surface of AuNPs with the bond Au–S and other part of ligand will interact with the target[243] that will reduce the interparticle distances resulting aggregation.[244] Peptide-functionalized AuNPs have been developed in colorimetric diagnosis of biological constituents by using cross-linking aggregation.[245–247] Chandrawati *et al.* utilized peptide-conjugated AuNPs for monitoring the concentration of blood coagulation factor XIII, (LOD 0.01 U mL^{-1}) which require thrombin and Ca^{2+} for activation.[248] AuNPs was modified with melamine and aggregation occurred due to the Au–N bond formation.[249] AuNPs was modified with Triton X-100 which formed multiple cross-link with melamine leading to aggregation and color changed.[250] For understanding the rapidity of color change for both cross-linking and non-cross linking aggregation method, the ssDNA-AuNPs based cross-linking and non-cross linking method has been developed by Wang *et al.*[251] The study demonstrated that the rapidity of cross and non-cross-linking aggregation of ssDNA-AuNPs are reversed on the increase of complementary/crosslinker DNA. When a small number/low concentrated of the crosslinker/complementary DNAs are provided, the crosslinking mode proceeds faster than the non-crosslinking mode because the intraparticle (non-cross linking) hybridization precedes over the interparticle (cross-linking) hybridization. The cross-linked aggregation is most stable and gives a color change from red to purple but non-cross-linked aggregation is less stable showing color change from purple to red. The change of length/structure of ligands on the surface of AuNPs can influence the aggregation process in case of destabilization-induced aggregation. AuNPs aggregation is induced by controlled loss of electrostatic stabilization when a part of ligands is cleaved.[240] For example, McVey *et al.* reported a method to detect pathogenic bacterial DNA by using RNase H-controlled aggregation of AuNPs. RNA-functionalized AuNPs (RNA-AuNPs) were cleaved by RNase H when the formation of DNA–RNA hybridization and the cleavage made target DNA free which could hybridize with the other RNA probe on AuNPs.[252] Another colorimetric detection method has been established for real time monitoring of dipeptidyl peptidase-IV activity based on the hydrolysis of peptide-AuNPs.[253,254]

6.2.2. Labeled-free detection method. The label-free colorimetric methods are mostly regulated by electrostatic stabilization where a repulsive electric layer can be generated by the surface charges of AuNPs to stabilize colloids. Thus, neutralization of surface charge results the formation of unstable AuNPs leading to the formation of aggregation. Due to this unstable aggregation the color changes from red to purple. The principle of the anti-aggregation of AuNPs can be classified into two categories. One is the target shows stronger attraction towards the aggregation agents which results the detachments of aggregation agents from the aggregated AuNPs.[255,256] The other principle is that the target shows larger interaction toward AuNPs which keep aggregation agent far from AuNPs.[257] The analyte-triggered aggregation for sensing purpose is performed based on the affinity of analyte to interact (electrostatic or H-bond) with unmodified AuNPs. From a reported dada, heparin was detected by using colorimetric sensing method. Ma *et al.* showed that the poly (diallyl dimethylammonium chloride) (PDDA) with positive charges can easily adsorb onto the citrate-capped AuNP surfaces (negatively charged) by electrostatic attraction in the absence of heparin. This behavior leads to the aggregation of AuNPs leading to color change to red-to-purple. On the other hand, heparin bears negative charge which interact with PDDA in an electrostatic manner forming a stable complex. This complex inhibits the PDDA-AuNPs aggregation, leading to back red color solution (Fig. 8).[258]

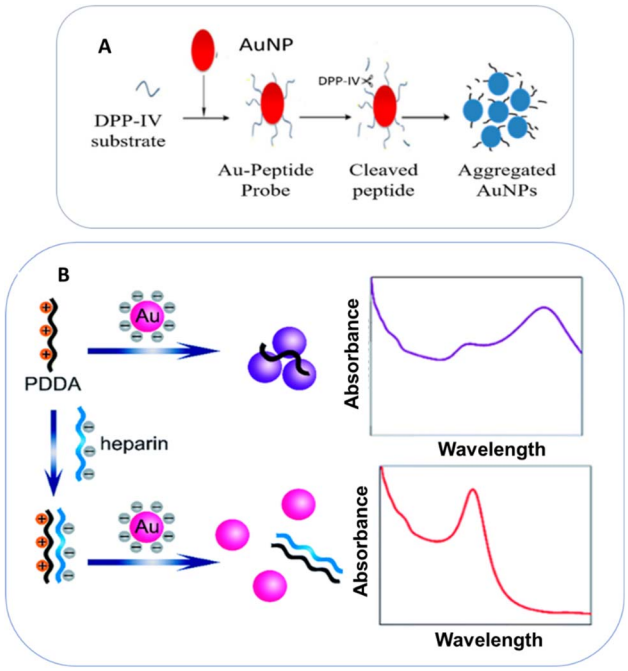

Fig. 8 (A) The schematic representation of the measurement of dipeptidyl peptidase-IV(DPP-IV) activity. (B) The schematic illustration of heparin detection using a label-free colorimetric method. This figure has been adapted from ref. 259 with permission from Royal Society of Chemistry, copyright 2019.

6.3. Etching of AuNPs

Mainly, various shape of AuNPs like gold nanospheres (AuNSs), gold nanorods (AuNRs)[260,261] gold nanotriangles and gold

nanourchins have been used as etching-based colorimetric sensors. Etching-based sensing mechanism is totally reversed of growth-based sensing mechanism. In the etching-based sensing mechanism, the oxidizing agent oxidizes Au^0 to Au^{3+} which is necessary for etching of AuNPs. Etching process is also different from an anti-aggregation process where the growth of AuNPs is suppressed whereas the etching process is to dissolve the AuNPs to some degree which causes the size and shape changes of AuNPs. These size changes result in the shifting of LSPR extinction peak and thus color changes. Based on these shape-induced anisotropic optical properties, AuNRs are more ideal gold nanostructures over all the shaped AuNPs discussed above for etching-based sensing strategies. Depending on the aspects ration of AuNRs longitudinal SPR[262] gives color shift. As the lower the aspect ratio, the color shifts from red to blue. Moreover, the AuNRs tip has high surface energy that eases the etching reaction to occur. Depending on the addition of etchants, the etching process can be modified in two segments.

6.3.1. H_2O_2-mediated etching method. Among various types of etchants H_2O_2 (ref. 248) can potentially etches the terminal ends of AuNRs which leads to lower aspect ratio or spherical AuNP resulting the color change of solution. Although the etching capacity of H_2O_2 has been reported, it has many disadvantages such as high conc. Of H_2O_2, high temperature and acidic environments which are responsible for limiting the applicability of this system for sensing strategy. Zhang *et al.* developed a method to detect Co^{2+} based on the Fenton-like reaction mediated reactions in which Co^{2+} induced the decomposition of H_2O_2 producing hydroxyl (OH^-) radicals. This hydroxyl radical etched the AuNRs in the presence of SCN^- and the AuNRs turn into spherical AuNPs which undergo color change from green to red.[263] Different metal cations such as Cu^{2+},[259] Co^{2+}, Mn^{2+} (ref. 264) and Pb^{2+} (ref. 265) are used to accelerate the etching rate of AuNPs or catalyze the production of oxidizing effect that etches AuNPs. Mainly Cu^{2+} and Co^{2+} accelerate the etching rate by using H_2O_2 as an oxidizing agent. Weng *et al.* recently studied that cetyltrimethylammonium bromide (CTAB) accelerate the rate of H_2O_2 etching effect in presence of Cu^{2+}.[266] Not only metal ion but also enzymes are used remarkably to enhance the etching reaction rate. For example, Saa *et al.* reported that the H_2O_2-triggered etching of AuNRs occurred in presence of horseradish peroxidase (HRP) which show a considerable color change from pink, blue to yellow as a function of glucose concentration.[267] The enzyme horseradish peroxidase (HRP) that is able to induce a gradual oxidation of AuNRs in the presence of trace concentrations of H_2O_2 (Fig. 9).

6.3.2. Ion-mediated etching method. Some metal cations such as Cr(VI)[268] and Au(III)[269] can be directly used as oxidizing agents to etch AuNPs. For example, Cr(VI) ion shows strong etching capacity towards AuNRs, which gives color change and thus the Cr(VI) can be detected with a limit of detection of 88 nM.[270] It has already been reported that most of the halide ion effectively increase the etching of AuNRs due to promoting the solubility property of gold monoxide.[271,272] Mainly iodide-mediated etching shows considerable effects on etching of AuNRs.[273] Substantial colorimetric sensing strategies based on iodine-mediated etching of AuNPs have been developed in which I_2 was produced by the oxidation of I^- with metal cations or H_2O_2 or by the reduction of IO_3^-.[274,275] For example, due to having low surface passivation at the end terminal of CTAB, iodine (as a oxidant) etches AuNRs in the presence to CTA^- and thus the shape and color change occurs.[276,277] Ultrasonic visual detection of molybdate has been designed using iodine-mediated etching assay. Although I_2 could be produced by the oxidation of I^- with H_2O_2 to etch AuNRs but the reaction kinetic is very low due to corrosion occur of CTAB stabilized AuNRs in the presence of a weak acid solution. The addition of molybdate which is peroxide-like molecule, accelerates of the reaction between H_2O_2 and I^- resulted in the production of I_2 and etching of AuNRs. By this process the molybdate was detected with the limit of detection 1 nM.[278] Another colorimetric method that relies on the I_2-mediated method assays has been experienced of the on-site detection of dissolved oxygen. In this method, Mn^{2+} was oxidized in the presence of dissolved oxygen to first Mn^{3+} to Mn^{4+} and after acidification I^- was oxidized to I_2 by Mn^{3+} and Mn^{4+}. Thus the color change from blue to red was observed (Fig. 10).[264]

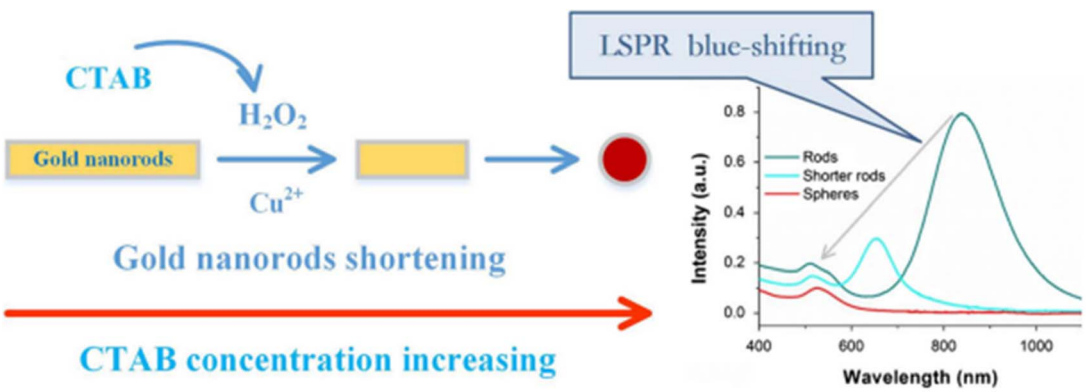

Fig. 9 Shape changes leading to LSPR blue shift of gold nanorods etched by Cu^{2+}-mediated H_2O_2 oxidation in the presence of CTAB. This figure has been adapted from ref. 267 with permission from Springer, copyright 2014.

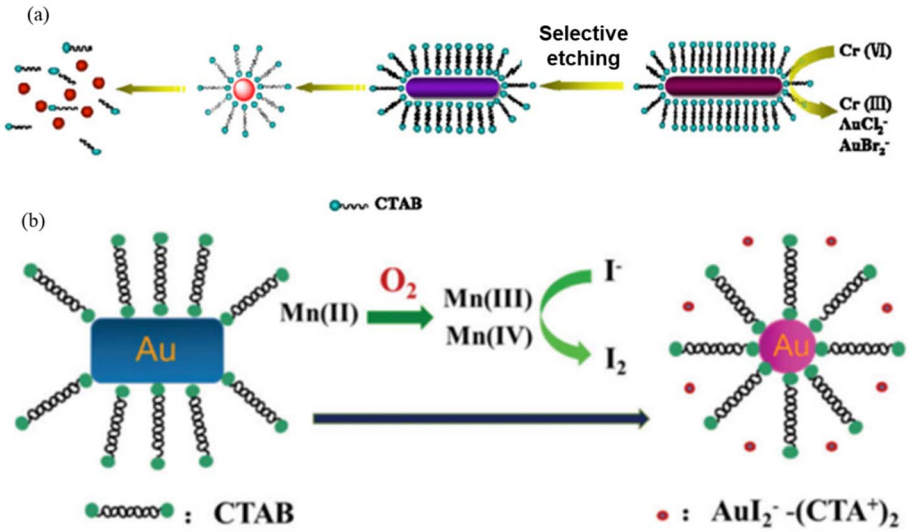

Fig. 10 (a) Schematic illustration on the etching mechanism of the AuNRs induced by Cr(VI). Reproduced with the permission.[279] (b) The schematic illustration for the detection of dissolved oxygen based on the iodine-mediated etching of AuNRs. This figure has been adapted from ref. 265 with permission from Royal Society of Chemistry, copyright 2016.

6.4. Nano-enzyme based colorimetric sensor mechanism

A nano enzyme-based colorimetric sensing strategy is a powerful and innovative approach used in chemical and biological sensing. Nanozymes (nanomaterial-based artificial enzymes) which mimics the activity of enzymes, responsible for the color change that can be visually detected. Compared to natural enzymes, this nano enzyme has some unique advantages *e.g.* high stability against denaturing and inactivation, easy synthesis, cost-effectiveness, high sensitivity and facile storage.

6.4.1. AuNPs exhibits peroxidase-like activity. In the nanozyme mechanism, positive/negative charged AuNPs mimic the function of biological enzymes such as peroxidase, reductase, catalase, glucose oxidase, or superoxidase due to their enzyme-mimetic properties.[280,281] AuNPs not only exhibits SPR properties but also show peroxidase-like catalytic activity which has been explored to fabricate colorimetric sensing mechanism. The SPR-based or peroxidase activity-based catalytic sensing behavior of AuNPs mainly depends on surface modifications of nanoparticles which is suitably selected according to the nature of analyte to be detected. In the nanozyme sensors, AuNPs themselves do not contribute in visual read-out, so chromogenic substances such as 3,3,5,5-tetramethylbenzi-dine (TMB), 2,2-azino-bis (3-ethylbenzothiazoline-6-sulphonic acid) (ABTS), and *o*-phenylenediamine (OPD) are required to generate color in the presence of analytes.[282] For this purpose, choice of chromogenic substances depends on some parameters like pH, temperature, and chemical moieties of the target analyte and functionalized-AuNPs.[62] Peroxidase behavior on AuNPs surface to detect analyte mainly based on two principles; one is the enhancement of peroxidase-like activity or the inhibition of peroxidase-like activity in presence of analyte. In case of peroxidase-like enhancement, OH ion adsorbed on the surface of AuNPs that trigger the decomposition of H_2O_2 into H_2O and O_2 in the basic conditions. Thus, the charge transform of Au^0 to Au^{1+} occurred and produce a signal to detect analyte.[283] On the other hand, sulphides (S^{2-}) and halides (X^-) inhibits the active sites forming Au_2S and Au-X species on the surface of AuNPs that ease the aggregation of AuNPs in presence of analyte, thus color change occurred.[284] But this inhibition activity is less prevalent than enhancement process. Positively-charged ((cysteamine-capped AuNPs) and negatively-charged (citrate-capped AuNP) AuNPs have been reported to possess intrinsic peroxidase activity and have been used in biochemical analyses.[285,286] Jv *et al.* reported that, AuNPs catalyze the oxidation of peroxidase-like substance 3,3,5,5-tetramethylbenzidine (TMB) by H_2O_2 to develop blue color in aqueous solution providing simple method to detect H_2O_2. In this detection process H_2O_2 can be adsorbed on the surface of AuNPs, and the O–O bond of H_2O_2 might be broken up into double HO radical.[287] The generated OH radical might be stabilized by AuNPs *via* partial electron exchange interaction.[288,289] Shah *et al.* reported that the adenosine triphosphate (ATP) improved the peroxidase activity of negatively charged AuNPs[290] and developed a colorimetric assay to detect ATP. Peroxidase activity of AuNPs has been used for various detection purposes including the environmental assays and also for food safety.

The reason behind the higher peroxidase-like activity of the AuNPs can be the negatively charged capping agent, citrate having several carboxylic groups (COOH–) on the surface of AuNPs which can facilitate the electrostatic attraction between the amino group of TMB and citrate. Thus, the TMB on the surface of AuNPs facilitates the oxidation of hydroxyl radicals due to the reaction between AuNPs and H_2O_2.

6.4.2. Other enzyme-like activity of AuNPs. Besides peroxidase-like activity, AuNPs exhibits other enzyme-mimicking like activities for the colorimetric sensing mechanism like glucose oxidase, superoxidase dismutase, and catalase-like activity. Zhao *et al.* has reported that synthesized supramolecular factionalized AuNPs, cyclodextrin-modified AuNPs (CD@AuNPs) possess dual enzymatic-mimic activity

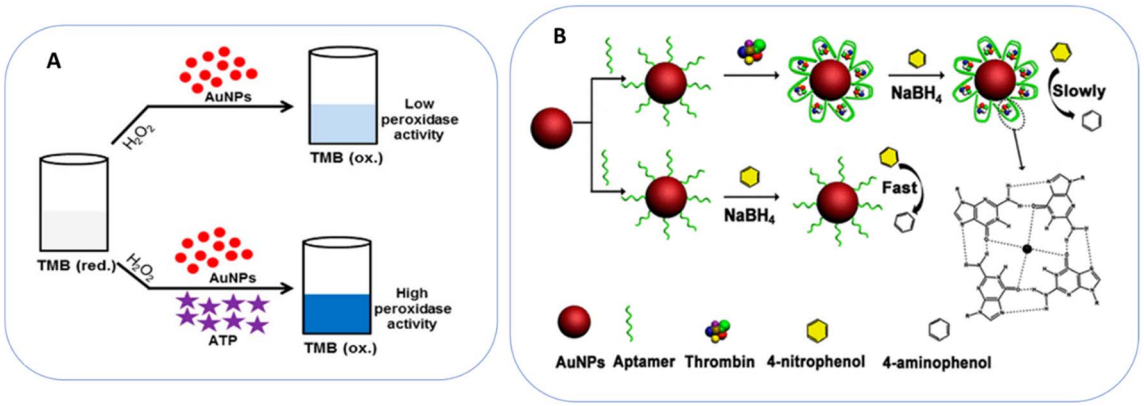

Fig. 11 (A) The schematic illustration of the colorimetric sensing mechanism for adenosine triphosphate (ATP) based on the ATP-promoted nanozyme activity of AuNPs. This figure has been adapted from ref. 290 with permission from Elsevier, copyright 2015. (B) Thrombin interacts with the aptamer leading to mask the surface of AuNPs, reduced by $NaBH_4$ but the yellow color remains same. But in absence of thrombin, the surface was free to interact with 4-nitrophenol which was reduced at a fast rate showing a color change. This figure has been adapted from ref. 293 with permission from American Chemical Society, copyright 2016.

where cyclodextrin acts as both reducing agents and stabilizers. The CD@AuNPs possess unpredictable catalytic activity and exhibit mimicking properties of both glucose oxidase and horseradish peroxidase simultaneously. In the cascade reaction in which glucose is first oxidized to gluconic acid and H_2O_2 in presence of glucose oxidase mimicking activity of CD@AuNPs. Then, H_2O_2 and preadded TMB (3,3′,5,5′-tetramethylbenzidine) are further catalyzed into H_2O and oxTMB, respectively mimicking the horseradish peroxidase enzyme.[291] Chen *et al.* developed a simple colorimetric strategy for protein detection by using aptamer-AuNPs. Thrombin can be quantified in the presence of catalytic AuNP surface by using color-change time of 4-nitrophenol. In the presence of thrombin, the aptamer interacts with the thrombin which masks the surface of AuNPs, inhibiting the attachment of upcoming 4-nitrophenol resulting in the yellow solution that remains unchanged during reaction. On the other hand, in absence of thrombin, 4-nitrophenol easily adsorbs on the surface of aptamer-AuNPs, resulting in the color change from yellow to colorless. In this sensing process the limit of detection (LOD) of 0.1 nM was achieved with naked eyes.[292] Colorimetric assays are extremely attractive compare to various traditional detection technique due to its convenience, simplicity and easy to use features.[281] Moreover, it is very easy to monitor its colorimetric response with naked eye. Besides it does not require any sophisticated instrumentation for detection method, thus has become the most suitable choice for on-site-detection/on-spot detection (Fig. 11).

7. Comparison of different sensing mechanisms

The development of simple and convenient sensors is of significant importance for the detection of chemical and biological detection processes. Compared with other sensing methods, AuNP-based colorimetric assays are promising because the whole sensing method proceeds with a simple solution of target and the probe without sophisticated instruments and the most attractive feature of this technique is to detect the color change with naked eye. The colorimetric sensor is now engineered by the functionalized AuNPs using smartphones that make the detection process available to all the general mass. Though these approaches simplify the operation procedure, shorten the detection time, reduce the assay cost, there are still some limitations that should be overcome in future research work (Table 4).

8. Applications of GNPs based colorimetric probes/sensors

8.1. Environment-based detection

Nowadays, AuNPs has been emerged as the most attractive and powerful sensor in the field of environmental science due to its amazing optical properties such as surface plasmon resonance (SPR) activity which causes distinct color changes upon

Table 4 Comparison of basic features among different sensing mechanisms of AuNPs

Sensing mechanism	Basic requirements	Limitations
Aggregation of AuNPs	Depending on dispersion states are readily affected by solvent, pH, temperature and salinity	Suffer from sensitivity issues
Growth of AuNPs	Always require a reducing agent	Sometimes tough to handle (affected by side reaction)
Etching of AuNRs	Commonly limited to AuNRs	Restrict the application of other AuNPs
Nano-enzyme based AuNPs	Supramolecular functionalized AuNPs needed to detect and quantify target	The production of enzyme-like NPs is sensitive and costly

aggregation or interaction with specific analytes for sensing a wide range of environmental pollutants like heavy metals, disposable gas, toxic chemicals produced from inorganic, organic, and biomolecules dispersed in water, soil and air.[293] These types of toxic materials release in the environments through various natural and anthropogenic sources like industrial wastes, agricultural fertilizers, and medical diagnostics.[294] These chemical pollutants offer great threat to humans, animals, plants, and ecosystems through many ways like direct ingestion, food chains, absorption by plants *etc.* Exposure over the threshold limit of these contaminants may act as poisonous and mainly responsible for cardiac diseases, brain stroke, kidney failure and infertility and miscarriages.[294] Hence, some effective methods to detect these substances is a crying need for this crucial moment. AuNPs have been rapidly used for this detection purpose using colorimetric sensing strategy. AuNPs-based sensors are not only effective portable devices but also real-time on spot monitoring probe offering a promising approach for environmental monitoring and pollution control.

8.1.1. Metal ion detection

8.1.1.1. Alkali (K, Cs) and alkaline earth metal ions (calcium/barium/strontium). Alkali and alkaline earth metal mainly occupy the 1st and 2nd group of periodic tables *e.g.* Li, Na, K, Rb, Ca, Mg, Be *etc.* These alkali and alkaline earth metals are named after the physical properties of each group of periodic tables. Among all the other alkali and alkaline earth metal ion Na^+, K^+, and Ca^{2+} are the most important ions to be detected in water or food samples. Moreover, these ions can be considered as biomarkers in biological fluids like urine, blood, serum, saliva and sweat samples. The first alkaline metal detection method was introduced by Zhang *et al.* In this detection method Zhang and his co-workers used MSA-AuNPs (Au–S bond affinity) to recognize Ca^{2+}, Sr^{2+} and Ba^{2+} ions over other cations. In the presence of Ca^{2+}, Sr^{2+} and Ba^{2+} ion, aggregates were formed which was mirrored by the appearance of color change from red to blue. The aggregation occurred due to the interaction of metal ion with the carboxylic acid group of mercaptosuccinic acid (MSA). The LOD were detected 20, 8 and 2.5 mM for Ca^{2+}, Sr^{2+} and Ba^{2+}, respectively.[295] K^+ ion was also detected naked eye by using potassium binding aptamer (PBA)-AuNPs. Firstly, AuNPs functionalized with PBA and capped with citrate ion. In the presence of K^+, due to the high affinity between aptamer and K^+, a g-quadruplex structure[296] was formed resulting the dissociation of aptamer from the surface of AuNPs. Then, AuNPs being uncapped, aggregated forming blue color solution. Upon addition of a cationic dye (Y5GL) the solution turns to green.[297] A new strategy for colorimetric detection of Cs^+ using Au NPs and Prussian blue (PB) based on nonmorphological transition mechanism. When the PB-P was added on the AuNPs surface, the Fe^{3+} reduced to Fe^{2+} in the presence of citrate present as a capping agent for AuNPs. So, the adsorption of PB on AuNPs cause color change but in presence of Cs^+, the PB reacts with Cs^+ due to the great affinity and thus the AuNPs remain free, resolving its red color back.[298] A sheet-based colorimetric detection device has been developed using gold nanoparticles (AuNPs) modified by 4-amino-6-hydroxy-2-mercaptopyrimidine monohydrate (AHMP) to detect Ca^{2+}. AHMP was chemisorbed on the surface of AuNPs by the thiol group but the other two groups ($-NH_2$ and –OH) remained free to provide lone pair electron to Ca^{2+} ion so that it could undergo electrostatic attraction. This indicates that Ca^{2+} could quickly bind to their functional groups ($-NH_2$ and –OH) onto modified AuNPs.[299] These contribute to the aggregation mechanism of the AuNPs resulting the color change from red to blue. By this method, Ca^{2+} was detected with LOD of 3.05 ppm at pH 6. Another visual detection method in which Ba^{2+} can be detected, has been established by Bai *et al.* In this detection method, the citrate-stabilized GNPs was modified using tiopronin. Tio could bind to the GNP surfaces through the sulfur atom, and the cross-linking of Tio-functionalized GNPs could be rapidly achieved by chelation in the presence of Ba^{2+} occurring color change from red to blue (Fig. 12).[300]

8.1.1.2. Heavy metal ions. Heavy metals refer to elements characterized by metallic behavior, high atomic mass, and densities typically exceeding 5 g cm^{-3}. These metals (Pb, Cd, Hg, As, Cr) are widely used in the industrial activities and also recognized for their potential toxicity to humans and the environment, even at low concentrations.[301] They can accumulate in biological systems and persist in ecosystems due to their non-biodegradable nature, posing long-term risks to public health and ecological stability.[302] Designing efficient and sensitive colorimetric sensors based on AuNP-related surface plasmon resonance (SPR) and peroxidase-like activity for detecting heavy metals such as Ni^{2+}, Hg^{2+}, Cd^{2+}, As^{3+}, Cr^{3+}, Cr^{6+}, and Pb^{2+} necessitates specific chemical or biological surface modifications of nanoparticles to develop functional colorimetric probes.[303,304] A viable colorimetric strategy for identifying Pb^{2+} ions was put forward Chai *et al.* using GSH-AuNPs. In this technique, addition of Pb^{2+} induced the aggregation of AuNPs following the color change from red to blue.[305] Ratnarathorn *et al.* developed another method to detect Pb^{2+} by using maleic acid- AuNPs in which Pb^{2+} was interact with –COOH inducing the aggregation of AuNPs that results in interparticle plasmon coupling and color shift from red to blue.[142] Cd is another toxic heavy metal generally used in fertilizers, metal alloys and battery.[306] Another SPR-based colorimetric sensor has been developed based on analyte aptamer affinity approach for the quantitative detection of Cd^{2+} using AuNPs. Here aptamer provides strength to AuNPs for not being involved in aggregation due to repulsive forces. Addition of Cd^{2+} influences the aggregation binding with aptamer which made free aptamer. This aggregation led to color change from red to blue.[307] A unique Hg^{2+} detection process was investigated by Hamaguchi *et al.* using glycine capped gold nanoparticles. In this method, Hg^{2+} induced aggregation results the detection of Hg^{2+} with LOD of 5 M.[144] Qi *et al.* reported a colorimetric method associated with nano enzyme sensor using oxidase mimetic activity of unmodified AuNPs in which the negative surface of AuNPs offer oxidation of TMB in presence of Cr^{6+} resulting the color change from red to blue. in this method the detection limit was estimated 0.52 μg L^{-1}.[308]

In short, heavy metal ions are the most extensively studied analytes among various metals because they readily form complexes with gold nanoparticles (AuNPs) and are commonly

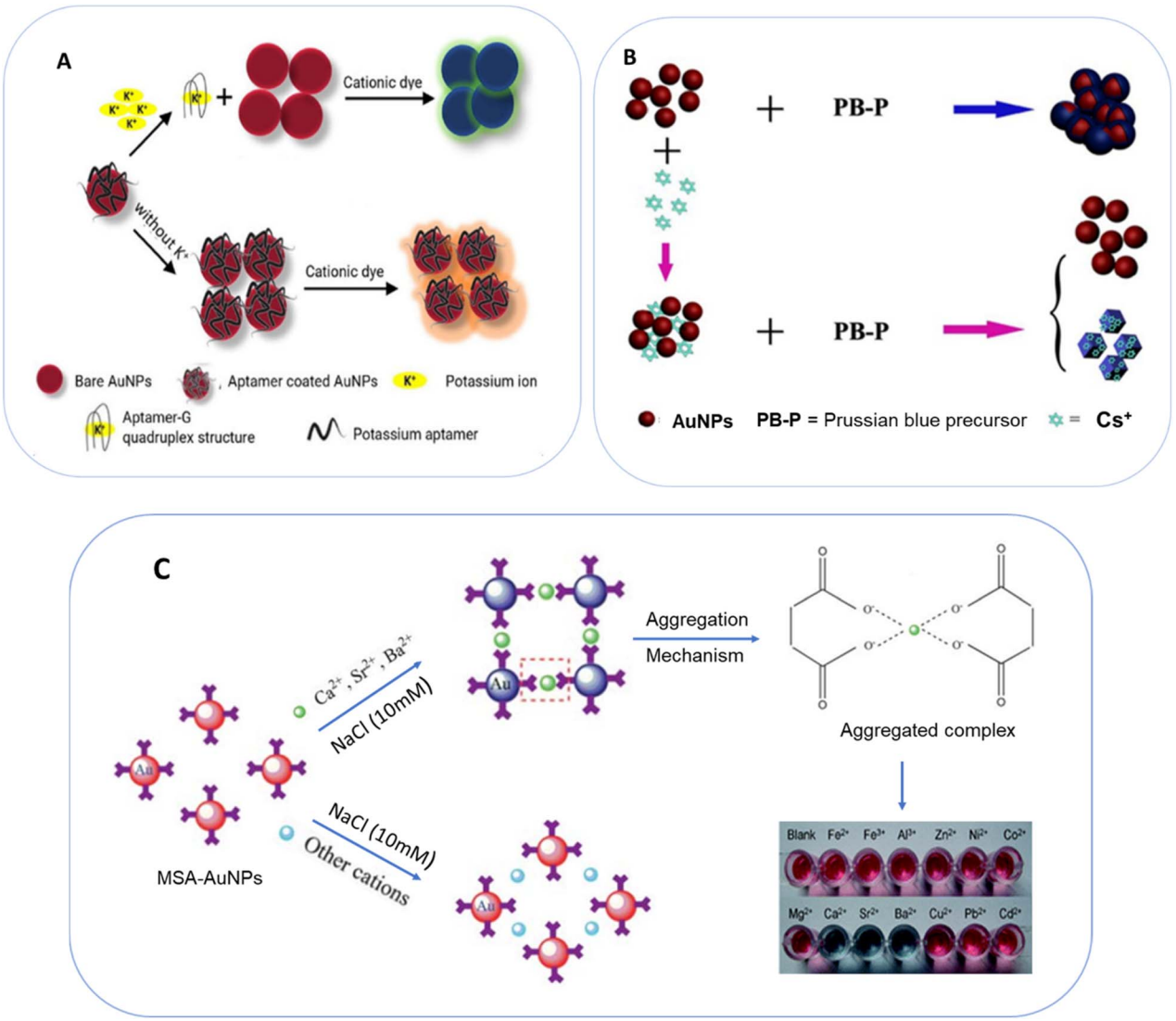

Fig. 12 (A) Selective aptasensor for the detection of potassium ions using aptamer-AuNPs as nanoprobe. This figure has been adapted from ref. 297 with permission from Elsevier, copyright 2018. (B) Detection of cesium ions by nonmorphological transition mechanism. This figure has been adapted from ref. 298 with permission from Royal Society of Chemistry, copyright 2020. (C) The aggregation of MSA-AuNPs in the presence of both alkaline earth cations and NaCl salt induces a color change of solution, a possible mechanism of complex formation between carboxylic group and MSA is illustrated here. This figure has been adapted from ref. 296 with permission from Royal Society of Chemistry, copyright 2011.

found as environmental pollutants. As the metal ions and AuNPs progress faster, so easily it can induce the aggregation phenomenon. In this review, we may summarize that the AuNPs can be decorated with suitable colorimetric chelators and under optimum conditions it can serve as the best target detector (Table 5).

8.1.1.3. Coinage metal and rare earth elements. Copper, silver and gold are considered as coinage metal which exhibits plasmonic properties at the nanoscale level. As a result the nanoparticles of coinage metals can be used to develop analytical devices for the environmental and food sensing system.[215,324] It is also a matter of fact that, these coinage metals can also be detected by using the analytical devices using the coinage nanoparticles. Lu *et al.* has developed an interesting approach to detect Cu^{2+} in the nM level based on the catalytic effect of Cu^{2+} on the $S_2O_3^{2-}$-Ag/Au NPs leaching system. Cu^{2+} can oxidize gold and silver in the presence of $S_2O_3^{2-}$ forming $Cu(S_2O_3)_3^{5-}$ and $Ag(S_2O_3)_2^{3-}$ oxidized by the dissolved oxygen. This complex formation leading to the SPR absorption decreasing of AuNPs results in color change.[325] Another technique has been designed a label-free colorimetric probe for detecting Cu^{2+} ions in aqueous solutions, based on the catalytic etching of gold nanoparticles (AuNPs). The sufficient supply of dissolved oxygen and thus the dissolving rate of AuNPs was remarkably promoted due to the catalytic activity of Cu^{2+} in the etching process. The LOD was detected 5.0 nM with the color change from red to colorless.[326] An anti-aggregation pathway has been developed for the detection of Ag^{+} using unmodified AuNPs. Addition of tris(hydroxymethyl) aminomethane in the AuNPs solution promotes the aggregation of AuNPs showing dark blue

Table 5 Detection of heavy metal contaminants using AuNPs based colorimetric method

Type of contaminants	Analytes	Strategy of colorimetric detection based on AuNPs	Limit of detection	Ref.
Heavy metal	Pb^{2+}	Cross-linking/aggregation	0.5 μg L^{-1}	142
		Anti-aggregation	0.5 μM	309
		Cross-linking	10.0 ppm	310
		Cross-linking	25 μM	311
		Cross-linking	30–300 μM	312
		Cross-linking	100 nM–200 μM	15
	Cd^{2+}	Cross-linking	3.5 nM	313
		Cross-linking	10 nM	314
		Cross-linking	1.0×10^{-7} M	315
		Cross-linking	10 μM	316
	Hg^{2+}	Cross-linking	2.8 nM	313
		Anti-aggregation	6.0 nM	317
		Cross-linking	0.49 μM	318
		Cross-linking	50 nM	319
	Cr^{6+}/Cr^{3+}	Cross-linking	0.1 mg L^{-1}	320
		Cross-linking	0.34 ppb	321
		Cross-linking	0.76 ± 0.013 nM	322
	As^{3+}	Cross-linking	0.7 nM	323
		De-protection	10 nM	18

color change. The color of tris-AuNPs solution changed gradually from dark blue to red due to the complexation formation of Ag^{+} ion trapping the tris molecule and thus inhibiting the aggregation of AuNPs. The detected amount of Ag^{+} by this method was 0.41 μM.[327] Aggregation-based detection offers significant advantages, including greater simplicity, faster response, and high sensitivity at the nM level, in contrast to anti-aggregation approaches, which involve multiple steps and typically achieve detection limits in the μM range.

Rare earth metals refer to the f-block elements of the periodic table including the lanthanides and actinides series. As these elements are used in the technological fields such as sustainable energy construction, electric automobiles, and microchip technology,[328] there is a high chance to circulate its existence throughout the environment and biological tissues of human as well as animals. For instance, Ln^{3+} deposits on the bone tissue of human body[329] while Ce^{3+} accumulate in human tissue[330] and liver causing cancer.[331] For the toxic effects and carcinogenic behavior of these rare earth metals, many detection techniques have been identified till now. In this review, some of the detection techniques will be discussed. A sensing method upon a malonamide-AuNPs has been designed for the detection of trivalent lanthanides (Ln^{3+}) such as Eu^{3+} and Sm^{3+} which was incorporated by the dual function precursor ligands bearing both sodium thiosulfate group and TMMA that is the binding site for Ln^{3+} selection. Lisowski *et al.* estimated the LOD 50 nM for both Eu^{3+} and Sm^{3+} ion by using this method.[332] In the recent years, La^{3+}, Gd^{3+} and Tb^{3+} can also be detected using octadentate hydroxypyridinone chelator functionalized AuNPs based on reduction of their optical signals (LSPR) called quenching of AuNPs. This principle inhibits the particle growth due to interact with Ln^{3+} ions and offered LOD of 3 μM in industrial waste.[333] In another report, biosynthesized AuNPs was used to detect Ce^{3+} on the basis of coordinative bond between –COOH/–NH and AuNPs leading to the aggregation of AuNPs with a color change.[328]

In summary, though the analytical instrument could detect these metal ions, it is not applicable for on-site detection, but it is necessary for Ln^{3+} ions because these are found in rare places. In this case, the colorimetric sensing system paved the easy way for sensing approach.

8.1.2. Detection of anion. Anions are the ionic species which hold negative charge including halides (Cl^{-}, Br^{-}, I^{-}, F^{-}), cyanides (CN^{-}), sulfides (SO_4^{2-}, SO_3^{2-}), Oxo anions (NO_3^{-}, HSO_4^{-}, $H_2PO_4^{-}$, CH_3COO^{-}) *etc.* Anions have a tendency to bind with the biological constituents like DNA, RNA and protein causing serious damage to health.[334] Hence, need on time real detection method to quantify them. A wide range of studies has aimed at developing sensing platforms for anionic species.[335,336] However, their colorimetric detection is very challenging compared to cations because of their lower charge to radius ratio, pH sensitivity, wide range of geometries, solvent dissolving affinity.[244] Recently a report has been documented about the role of nano plasmonic materials for the detection of nitrates and nitric ions through aggregation, anti-aggregation and etching based mechanisms.[337] 4-ATP-AuNPs based colorimetric detection of e ADN-derived nitrite which formed colored product in presence of an azo dye using Griess reaction. Here, the LOD was 0.012 mg L^{-1} for nitrite ion.[338] Br^{-} was detected in rice samples by Plaisen *et al.* using citrate capped AuNPs based on the anti-aggregation method in which Cr^{3+} (cross-linking aggregating agent) induces the aggregation of AuNPs showing red to blue shift. In presence of Br^{-} ion, the solution was changed from blue to red, thus the Br^{-} ion was detected with LOD 0.04 μM.[339] A detection process has been designed for phosphate (Pi) using mercaptoacetic acid (MA)-AuNPs based on anti-aggregation method. Initially Eu^{3+} (aggregating agent) interact with the COO^{-} of MA, the aggregation occurred resulting color change red to blue. The blue color back to the red color, due to the anti-aggregation effect in presence of Pi. The estimated LOD for the Pi was 76 nM.[340] Another colorimetric sensing mechanism was established using adenosine

triphosphate (ATP)-AuNPs with Cu^{2+}-phenanthroline complexes for CN^- detection. In presence of CN^- ion, the phenanthroline group become free and thus the AuNPs goes aggregation and thus the color changed monitored by naked eye. This sensing system allowed the quantitative detection of CN^- down to f 10^{-5} M.[341]

Conclusively, anion is more difficult to detect than cations due to their chemical properties. The nitrite ion detection was carried out by aggregation, anti-aggregation in which an acidic environment was used that needs more exploration than alkaline medium. Further the Griess reaction which is also acid catalyzed. But its good news that colorimetric method made it easier to detect anion so far.

8.1.3. Pesticide monitoring. Pesticides encompass insecticides, fungicides, herbicides, disinfectants, and any agents designed to prevent, eliminate, or manage pest which are rich in active functionalities such as amino, thio, cyano, hydroxyl, carbonyl, and sulfide groups.[342] Nowadays, cultivators use pesticides for maintaining their products quality and quantity. The pesticides residue come in contact with rainwater, river water, and the flooded area through which humans and animals are affected with various diseases also causes the huge impact on environment. The functional group attached with pesticides has great attraction toward negative charged AuNPs, thus helping in visual detection of those chemicals. Organophosphorus pesticides (OP) are widely used pesticides, and these can be detected by the enzyme-mediated colorimetric method due to possess the related activity with acetylcholinesterase (AChE). Bala *et al.* designed a method for parathion detection using cysteine capped gold nanoparticles (Cys-AuNPs) based on anti-aggregation method. Hydrolysis of ATCh form thiocholine (TCh) in presence of AChE which is responsible for aggregation imparting blue color. On the other hand, due to presence of parathion, AChE become inactive so that leading to the formation of thiocholine (TCh), thus, color remains unchanged. The limit of detection was found to be 0.081 ng mL^{-1} for ethyl parathion.[343] OP can also be detected without the enzyme-mediated method. For example, a detection method for malathion has been reported by using citrate-AuNPs based on anti-aggregation method. Firstly, NaOH occurs the aggregation of AuNPs by the electrostatic interaction which overcomes the capping action of citrate ion resulting color change from red to grey. The addition of malathion went hydrolyzed (pH > 7) forming many negative ions which involved interaction with Na^+ making AuNPs free to be well-dispersed

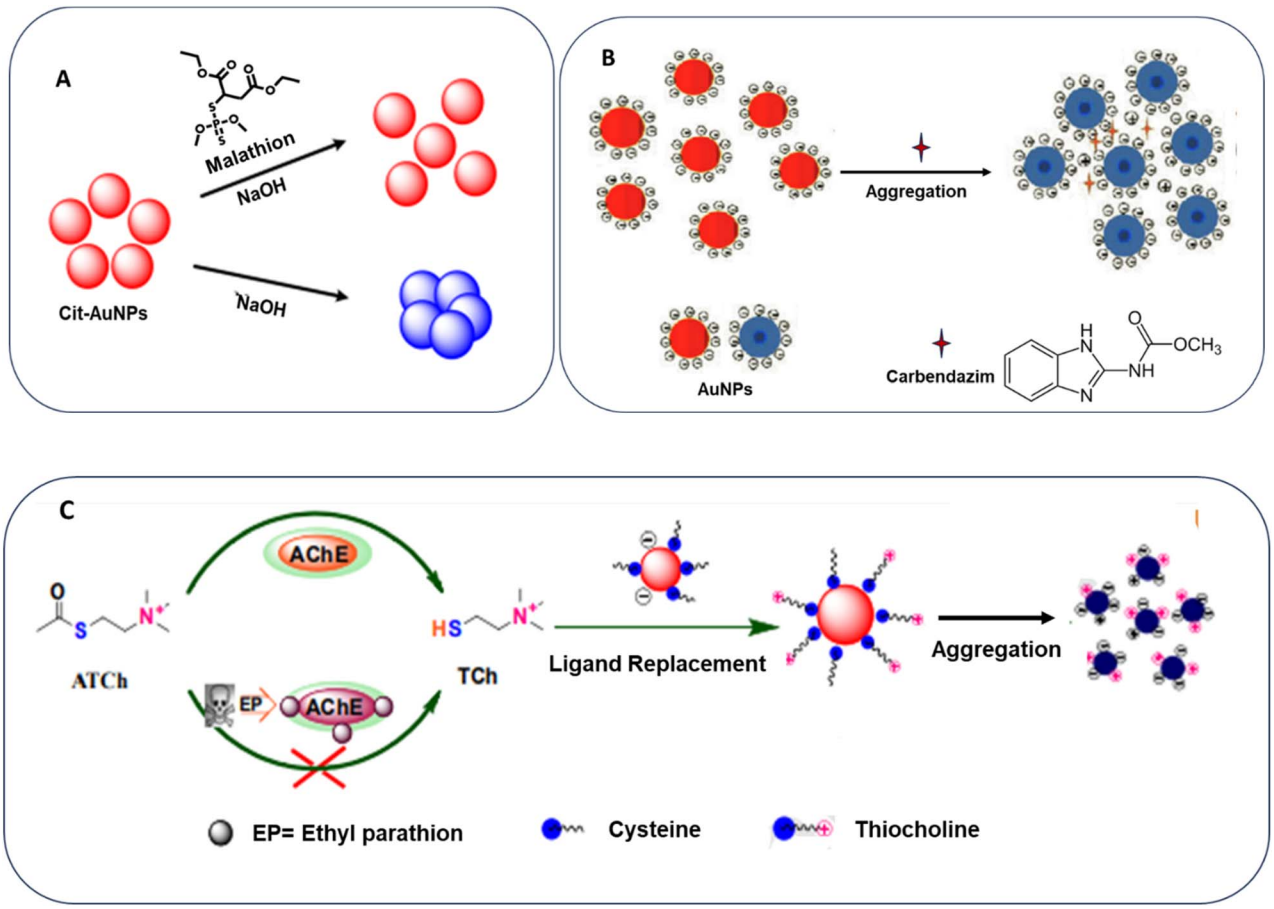

Fig. 13 (A) Detection of malathion based on anti-aggregation mechanism of AuNPs. This figure has been adapted from ref. 344 with permission from Elsevier, copyright 2015.[344] (B) Detection of carbendazim residue using citrate-AuNPs. This figure has been adapted from ref. 345 with permission from Springer Nature, copyright 2017. (C) Ethyl-parathion detection based on ligand replacement reaction of AuNPs. This figure has been adapted from ref. 344 with permission from Elsevier, copyright 2015.

Table 6 Various types of pesticides can be detected by using modified AuNPs. The information of this table has been re-printed with the permission from ref. 66

Pesticides	Sensing method	Modified AuNPs	LOD	Ref.
Atrazine	Aggregation	Melamine-AuNPs	16.5 nM	346
Dithiocarbamate	Aggregation	Citrate-AuNPs	50 μg L^{-1}	347
Triadimenol	Aggregation	Bare-AuNPs	0.182 μM	348
Imidacloprid	De-protection	I-IL-Au NPs	1.0×10^{-5} M	349
Cyromazine	De-protection	Label free AuNPs	252 ng g^{-1}	350
Chlorsulfuron	Anti-aggregation	Acetamiprid-AuNP	0.025 mg L^{-1}	351
Metsulfuron-methyl	Anti-aggregation	Bare-AuNPs	0.05 mg L^{-1}	352

showing color change from grey to red. This technique was able to estimate malathion down to 11.8 nM.[344] Carbendazim is a popular benzimidazole bactericides that is used to boost food production but its residue is very harmful for human lives. In this review, we will discuss a detection method for carbendazim residue using AuNPs. Electron rich nitrogen of carbendazim bind on the surface of AuNPs through Au–N bond. Then the average size of AuNPs decreased and aggregation occurred accompanied by the color of the solution change from red to blue. The LOD of this method was 3.4 ppb (Fig. 13 and Table 6).[345]

In summary, a wide range of pesticides can be detected by using bare and modified AuNPs based on aggregation, anti-aggregation or etching process. The aggregation process is more suitable because of simple operational technique but the LOD detected by this method is little bit high compared to other methods.

8.2. Food-based detection

8.2.1. Illicit additives found in edible items. Food additives are natural or synthetic non-edible substances that are widely used in modern food industry during processing, packaging, and transport which can improve the quality, durability, and stability of food products and adjust their color, smell, and flavor those are prohibited because of the threat they pose to human health.[353,354] However, the addition of illegal additives should be taken under control. Some substances have been reported as illegal food additives including formaldehyde, nitrite, melamine, sodium formaldehyde sulfoxylate, alum, beef extract, clenbuterol, sulfur dioxide, diethylhexyl phthalate (DEHP), fluorescent bleacher, talcum powder *etc.*[355] Besides, there are also some additives are available which are literally forbidden for applying in food items such as SCN^-,[356] SO_3^{2-} (ref. 357) Rhodamine B,[358] Congo red,[359] Sudan dyes.[360] Therefore, it is critically important to develop effective methods for detecting toxic and unauthorized additives in food products to reduce risks to public health. Thiocyanate (SCN^-) plays a crucial role in lactoperoxidase system in milk samples[361] and the inherent content of sodium thiocyanate (NaSCN) is about 40–67 μM.[362] As NaSCN enhances antibacterial activity that extends milk shelf-life, it is often added in milk illegally. Song *et al.* discovered a method to detect this illegal addition of SCN^- using anti-aggregation mechanism of AuNPs. Here, CTAB is used as aggregation agents responsible for aggregation of AuNPs by the electrostatic interaction between them resulting in color change red, blue. but in presence of SCN^- on the surface of AuNPs as a new stabilizing agents made AuNPs free to be dispersed again leading to gain red color back. The calculated LOD by this method was 6.5 nM.[363] Formalin is gradually used illegally as a preserving agent in many edible items such as Fisheries, fruits. It is reported that formalin treatment reduces the quality of protein in fish tissue, and it is harmful for humans as well as the environment. Sultana *et al.* has developed an easy and portable approach for the detection of formaldehyde in which colorimetric method was applied on the cotton-based sensor using Na_2EDTA-AuNPs. In this method, formaldehyde was detected in fruits based on aggregation showing color change from red to blue. The LOD of this technique was 0.11 μM.[172] The AuNPs based colorimetric detection has been widely used for the detection of food additives which has been illustrated in a Table 7.

8.2.2. Hormone-interfering compounds. Hormone-interfering compounds can mimic or interfere with the body's natural hormones, especially estrogen. These types of HICs-

Table 7 Illegal food adulterants are detected qualitatively and quantitively using AuNPs. The table data has been modified with the permission from ref. 364

Source	Adulterants	Sensing method	Modification of AuNPs	LOD	Ref.
Milk	Melamine	Colorimetric	Chitosan-AuNPs	6×10^{-6} g L^{-1}	365
Infant formula	Melamine	Colorimetric	Bare-AuNPs	2.0×10^{-7} g L^{-1}	366
Milk	Melamine	Colorimetric	1,4-Dithiothreitol-GNPs	2.4×10^{-8} M	367
Liquid milk	Melamine	Colorimetric	Methanobactin-GNPs	2.38×10^{-7} M	368
Beef	Ractopamine	Colorimetric	Apt-AuNPs	10 ng g^{-1}	369
Sausages	Nitrite		JanusPEGylated GNP	10.8 μmol L^{-1}	370
Milk	Urea	Colorimetric	GNPs-aptamer	20 mmol L^{-1}	371
Milk	Anionic detergents	Colorimetric	Bare-AuNPs	92 μg mL^{-1}	372

contaminated food are very harmful for humans and threaten the environment. Thus, it becomes quite necessary to detect the HICs as early as possible. Bisphenol A (BPA) is a chemical that is widely used as plasticizers in polycarbonate and epoxy in plastic industry which easily can meet the food items by the packaging materials. BPA leaches to food chain and then environment which is a great threat to nature. The estimated daily intakes (EDIs) of BPA can be 0.007×10^{-4} μg per kg body weight per day *via* migration from PC plastics to food simulants.[373] There are several analytical methods for BPA detection has been emerged recently.[374] BPA was detected in a rice sample using AuNP-aptamer in which the color shifted from red to purple due to aggregation phenomenon due to the presence of NaCl upon addition of BPA. That method was able to quantify and detect with a visual detection limit of 0.004 nM. Although there were so many interferences present such as bisphenol B, bisphenol C, diphenolic acid *etc.* this method could successfully detect the BPA present in one grain of rice.[375] 17β-estradiol (E2) is an estrogen plays important role in human growth and environment such as regulating reproductive system and development of sexual characteristics,[376] but consumption of it even at a very low concentration may harm to livestock farms' effluent and sewage treatment plants.[377] In a current study, E2 has been detected by using AuNPs, E2 specific aptamer and a cationic polymer, (poly(diallyl dimethylammonium chloride)) PDDA. The negatively charged aptamer interacted with the positively charged PDDA, which destroy the possibility of being aggregated. But in presence of E2, aptamer react with it forming E2–aptamer complex and free PDDA induce the aggregation of AuNPs. In this method, the LOD was estimated 1.57 nM.[378]

8.2.3. Detection of microorganisms/pathogens. Foodborne pathogens including pathogenic bacteria, viruses, fungi and parasites can be migrated to food chain and a little amount of digestion of this contaminated food can bring illness to human beings. More than 200 different food-borne diseases have been identified.[379] The symptoms of most of the diseases are nausea, vomiting, retching, diarrhea, abdominal pain, prostration, abdominal cramp and fever. Nowadays, it has become crucial to detect pathogens with great sensitivity and selectiveness. Several methods have been established to detect and quantify the microorganisms present in food items. *Listeria monocytogenes* is a foodborne pathogens whose fatality rate now 30% that is far exceeds other foodborne pathogens.[380] An oligonucleotide probe-conjugated AuNPs has been developed for the detection of *Listeria monocytogenes* based on hybridization which suppress the aggregation of oligonucleotide-AuNPs probe and the detection limit was found 75 copies of *L. monocytogenes*.[380] Depending on pH variation of the experiment, aggregation can also occur. It is known to all that bacteria surface are considered as negative as par physiological conditions.[381] There lies an electrostatic repulsion between the negatively charged bacteria and negatively charged AuNPs surface that hinder the aggregation. On the other hand, at acidic pH, the bacteria surface becomes positively charged which attracts the negatively charged AuNPs causes aggregation showing color change for example, *Escherichia coli* O157:H7 based on the aggregation of HS-Apt@AuNPs. The aggregation/dispersion of HS-Apt@AuNPs was comprehensively caused by the pH-dependent electrostatic interaction in which pH is an important factor to determine the spectral shift of HS-Apt@AuNPs colloids.[382] The etching mechanism is a widely adopted approach in AuNP-based aptasensor designs, enabling selective analyte detection and improved sensitivity. A novel colorimetric immunoassay for the detection of *Staphylococcus aureus* using Fe_3O_4/AuNPs. Further IgY-Fe_3O_4/AuNPs (having peroxidase like catalytic activity) was synthesized which was used for selective enrichment and rapid separation of target *Staphylococcus aureus.* The apt-AuNPs showed peroxidase-like activity revealed by TMB-H_2O_2. Thus, the deep yellow color turned to pale yellow upon increasing the concentration of *Staphylococcus aureus.* The LOD was 10 CFU mL^{-1}.[383] In this review we will try to mention some of the detection method using AuNPs in a table given here (Table 8).

Conclusively, there are various approach available for the detection of pathogens but among all target mediated approaches are simple but very sensitive to pH changes which require a careful handling. Moreover, detection through enhancement of peroxidase like activity due to the catalytic activity of AuNPs is highly sensitive and efficient. Besides, AuNPs-based antibiotic assisted detection process is complex due to the presence of multiple amines, amide or carboxylic acids.

8.2.4. Detection of mycotoxins. Mycotoxins are toxic secondary metabolites predominantly produced by fungi that commonly contaminate food and feed products. Mycotoxins are toxic even at a very low-molecular weight (300–700 Da) which may inter into food chain causing irrecoverable harm to human

Table 8 Various types of food pathogens can also be detected with very accurate detection limits. The information has been modification with permission from ref. 384

Source	Pathogens	Modified-AuNPs	LOD	Ref.
Spiked milk	*S. aureus*	Protein-AuNPs	1.5×10^7 CFU mL^{-1}	385
River and tap water	*E. coli* O157:H7	Protein-AuNPs	10^3 CFU mL^{-1}	386
Natural and tap water	*Francisella tularensis*	Protein-AuNPs	10^3 CFU mL^{-1}	387
Culture	*C. jejuni*	Protein-AuNPs	10^6 CFU mL^{-1}	388
Serum	Hepatitis C virus	Bare-AuNPs	2.5 copies per μL RNA	389
Spiked shrimp	*Vibrio parahaemolyticus*	Bare-AuNPs	10^3 CFU mL^{-1}	390
Spiked pork	*S. aureus*	Bare-AuNPs	10^2 CFU mL^{-1}	391
Culture	*G. lambliacysts*	Protein-AuNPs	1×10^3 cell mL^{-1}	392
Spiked chicken	*Salmonella Typhimurium*	AuNRs	35 CFU mL^{-1}	393
Fresh cut vegetable	*Salmonella*	Bare-AuNPs	6.0×10^1 CFU mL^{-1}	394

Table 9 Summary of some mycotoxins which are detected by colorimetric process. Information has been modified with the permission from ref. 404

Mycotoxin	Sensing method	Modified AuNPs	LOD	Ref.
Aflatoxin B1	Colorimetric	Fe_3O_4-GO	5–250 ng mL^{-1}	405
Aflatoxin B1	Colorimetric	Antibody-AuNPs	12 ng mL^{-1}	406
Aflatoxin B1	Colorimetric	Aptamer-AuNPs	0.36 and 0.18 ng mL^{-1}	407
Aflatoxin B1	Colorimetric	AuNPS@SiNPS-Ab	0.16 ng mL^{-1}	408
Zearalenone	Colorimetric	AuNPs	10 ng mL^{-1}	409
Zearalenone	Colorimetric	Antibody-AuNPs	2.5 ng mL^{-1}	410
Zearalenone	Colorimetric	Aptamer-AuNPs	5 ng mL^{-1}	411

and environment.[395] There are more than 300 types of mycotoxins have been recognized. Among them, some commonly known mycotoxins including aflatoxins,[396] ochratoxin A,[397] T-2 toxin,[398] zearalenone,[399] bongkrekic acid[400] *etc.* Aflatoxin B1 (group 1 carcinogen) a secondary fungal metabolite of *Aspergillus flavus* and *Aspergillus parasiticus*, is one of the most frequently found mycotoxins in contaminated foods. This aflatoxin B1 has been detected using streptavidin functionalized gold nanoparticles as the signal indicators. In presence of AFB1, the aggregation of streptavidin-AuNPs occurs and the color shifts from red to blue the estimated LOD for this method is 2 pM.[401] Aflatoxin M1 is the result of metabolism of aflatoxin B1 and it can be entered into the milk within 12 h following the ingestion of infected foods.[402,403] Jalalian *et al.* developed an optical aptasensor detector for the detection of aflatoxin M1 based on the anti-aggregation method of AuNPs in presence of NaCl. Here, streptavidin coated silica nano particles were modified with aflatoxin M1 aptamer and its complementary strand. In the presence of Aflatoxin M1, AfM1 interacts with aptamer and releases complementary strand which is responsible for the suppression of aggregation of AuNPs in presence of salt. This aptasensor method could detect the aflatoxin M1 down to 30 ng L^{-1}.[396] This review will document the possible colorimetric method to detect mycotoxins in a Table 9.

8.3. Biological detection

8.3.1. Detection of oligonucleotides. The identification of genetic mutations has become a vital focus in diagnostics, prompting increasing interest in nucleic acid-based detection methods for the early diagnosis of various diseases, including cancer.[412,413] Although some conventional methods are available for the detection of oligonucleotides such as fluorescence and radioactive (PCR, RT-PCR, Southern blot, northern blot *etc.*),[414–416] gold nanoparticle (AuNP)-based colorimetric assays have proven to be a highly effective and competitive approach for detecting oligonucleotide targets.[417,418] In this review, we will try to highlight some oligonucleotide detection method using AuNPs based on colorimetric sensing strategy. Owing to the critical role of nucleotide sequences in biological analyses and the notable benefits of using gold nanoparticles—such as ease of preparation, simplicity, cost-effectiveness, and time efficiency—the colorimetric detection method is extensively applied for DNA detection.[419] The colorimetric detection of nucleic acids using metallic nanoparticles, particularly DNA-functionalized gold nanoparticles (GNPs), was initially introduced by Mirkin *et al.* and his colleagues as a method for DNA analysis (DNA sandwich hybridization assay also known cross-linking GNP aggregation assay).[420] Based on their study, the development of gold nanoparticles (AuNPs) functionalized with thiolated DNA strands enabled researchers to customize the properties of the nanoparticle probes to suit specific assay techniques. The majority of DNA detection systems are based on the molecular recognition capability of single-stranded oligonucleotide probes, which hybridize with complementary single-stranded target sequences.[421] When a complementary target oligonucleotide is present, the dispersed oligonucleotide-AuNPs probes undergo hybridization, resulting in their cross-linking into aggregated polymeric structures which results a concomitant color change from red to blue of AuNPs.[418,422] A highly selective colorimetric polynucleotide detection method has been reported based on mercaptoalkyloligonucleotide-AuNPs in which a single-stranded target oligonucleotide was introduced in an appropriate probe resulted in formation of polymeric network of AuNPs due to the hybridization process. This polymeric network changed the color from red to blue.[423] Besides the cross linking manner of DNA-AuNPs, non-cross-linking aggregation configuration is possible even with greater speed and sensitivity.[418,424] Non-cross-linking aggregation occurs when a target containing a single base mismatch at its 5′ terminus mixed with the DNA-AuNPs probe. In this case, no hybridization occurs thus, it is called non-cross-linking aggregation. This process cannot even change color. No color change happens, meaning the system detects the mismatch perfectly thus, the system becomes very sensitive. Non-cross-linking aggregation of DNA-functionalized poly(*N* isopropylacrylamide) (PNIPAAm) nanoparticles was first monitored (Fig. 14).[424]

8.3.2. Detection of protein and enzyme. Proteins are the building blocks and messengers of the body and detection of protein is essential for understanding cellular functions, identifying biomarkers, and diagnosing various diseases, including cancer, infectious disorders, and neurodegenerative conditions due to presence of irregular protein concentration. Nowadays various carbohydrate functionalized AuNPs has been used to detect carbohydrate binding proteins.[425,426] Kim *et al.* developed a convenient and efficient colorimetric method for lysozyme as a protein target using aptamer-AuNPs conjugates. This conjugation system achieved a great sensitivity based on both the

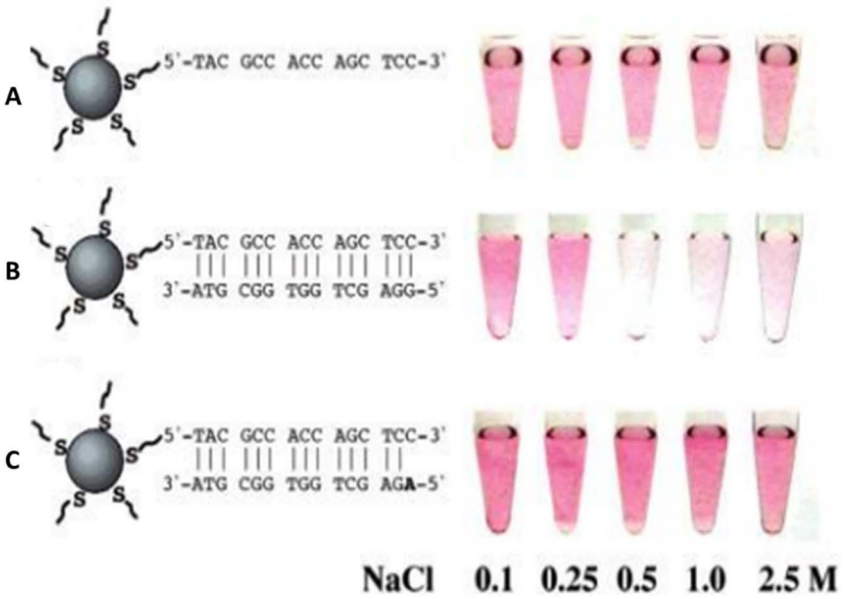

Fig. 14 Aggregation phenomenon of the DNA-gold nanoparticles at different NaCl concentrations (2.3, 500, and 500 nM, respectively) at room temperature: (A) only DNA-AuNPs probe without a target DNA, (B) with the complementary target, and (C) with a target containing a single base mismatch at its 5′ terminus. This figure has been adapted from ref. 425 with permission from American Chemical Society, copyright 2003.

catalytic signal amplification and the aptamer-based target recognition as an artificial enzyme. The catalytic activity of AuNPs was taken under control by masking the surface by target protein. The LOD was 16 nM for lysozyme.[427] Chen *et al.* developed another method to detect lysozyme using HAS-AuNPs. It has been claimed that the Lys-induced aggregation of HSA-AuNPs was suggested based on the London–van der Waals attractive force. In this approach, the lowest detection limit of lysozyme of chicken egg was 50 nM.[428] A facile colorimetric detection method has been designed by Huang *et al.* in which human serum albumin (HSA) was detected using citrate-AuNPs based on the anti-aggregation of AuNPs.[429] A cross-linker named melamine was used to induce the aggregation of AuNPs. After the addition of HAS, the melamine interacts with HSA, made the AuNPs free to be dispersed again. The anti-aggregation process shifts the color change from red-blue-red. The LOD of this process was calculated down to 1.4 nM (Fig. 15).[430]

Dithiols can cause crosslinks with AuNPs. Dithiols functionalized peptides have been used to assembles AuNPs for the colorimetric detection of protease enzyme. C- and N-terminal cysteinyl of peptides help to stick to AuNPs and pull the particles together causing aggregation resulting in color change. Here, nanoparticle aggregation occurs when the intact peptides are present and no target proteases are involved, while peptides that have been cleaved by the protease are unable to connect the gold nanoparticles, preventing aggregation. The color change informs us about the absence of proteas because the peptide was not cleaved. On the other hand, the remaining red solution

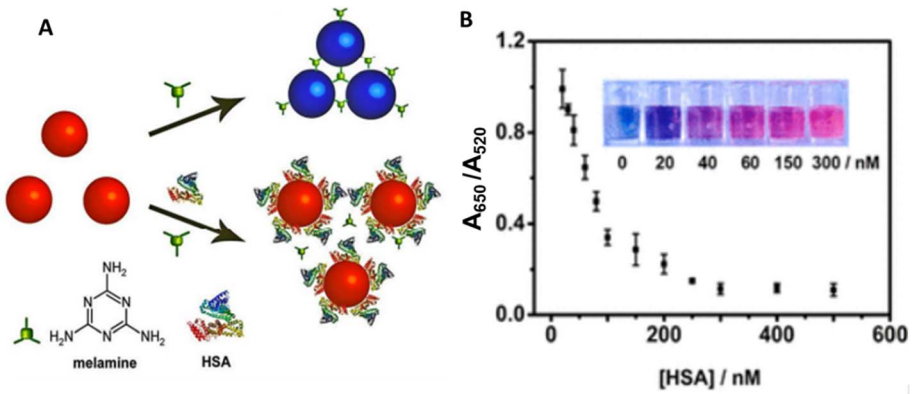

Fig. 15 (A) Schematic illustration of the anti-aggregation effect induced by HSA. (B) Optical photographs of the AuNPs with different conc. of HSA and graph A_{650}/A_{520} *vs.* [HSA]/nM. This figure has been adapted from ref. 429 with permission from American Chemical Society, copyright 2015.

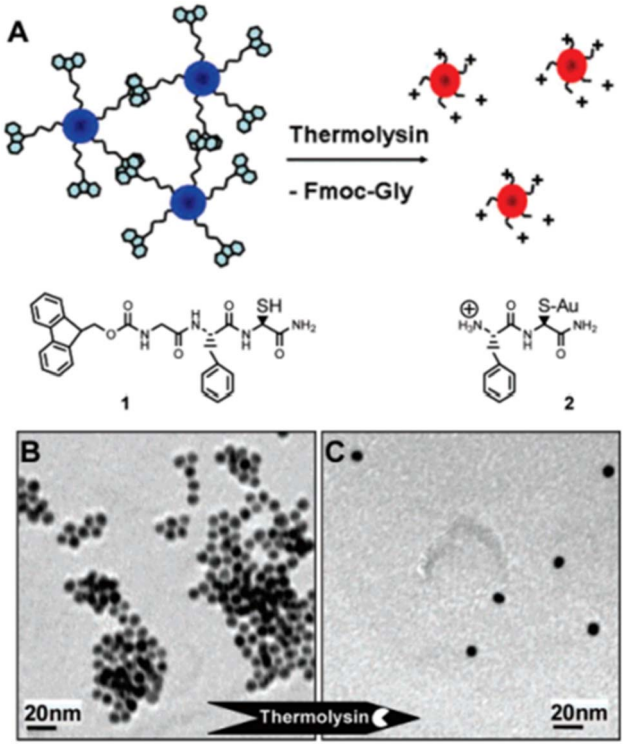

Fig. 16 (A) Schematic representation of the thermolysin-triggered AuNP dispersion approach. (B) TEM image of peptide-AuNPs 1 (8.5 nm at pH 8) (C) TEM image after the addition of thermolysin and formed 2. This figure has been adapted from ref. 431 with permission from PNAS, copyright 2006.

depicts that the protease is present and was able to cut of peptides (Fig. 16).[431]

Another sensitive detection method using peptide-AuNPs has been introduced for proteas detection. Here, dual effect—removing sticky parts and exposing repelling charges—causes the nanoparticles to spread out (disperse) instead of clumping together. Upon enzymatic hydrolysis of peptide-NP conjugate, disassembly occurs through a combination of electrostatic repulsion between particle bound NH_3^+ groups and removal of hydrophobic interactions between Fmoc groups. Thermolysin catalyzes the cleaving process and thus the AuNPs remain dispersed showing red color.[432]

8.3.3. Glucose detection. Glucose serves as the main energy source for cells and functions as a metabolic intermediate, circulating through the bloodstream to supply energy throughout the body.[433,434] Normal glucose levels in human blood typically range from about 3.8 to 6.9 mM (68–124 mg dL^{-1}). However, these levels can fluctuate throughout the day—dropping during fasting and rising after meals (postprandial states).[435] The presence of glucose level over the normal range can cause diabetes mellites which is a chronic disease. For the ease of glucose detection, colorimetric method using AuNPs has been developed by the scientists. A non-enzymatic detection method for glucose detection from real urine samples has been developed using citrate capped AuNPs with good accuracy and precision. This method was able to detect glucose down to 0.043 μM showing color change from violet to red violet.[436] There is various colorimetric method available using functionalized-AuNPs for glucose detection. In this review, we will mention some of them through a Table 10.

Jiang *et al.* developed a colorimetric method for glucose detection from rat's brain using AuNPs. This detection system was carried out by enzyme (GOD) mediated cascade reaction. In this assay, H_2O_2 was produced by the glucose oxidation process in presence of GOD enzyme following to the production of $^{\bullet}OH$ by the Fenton reaction. The $^{\bullet}OH$ radical is responsible for the cleavage of ssDNA thus, the aggregation of AuNPs occurs and red color turns to blue. On the other hand, in absence of glucose, the solution of AuNPs remain dispersed showing red color (Fig. 17 and 18).[443]

8.4. Detection of drugs

Recently, gold nanoparticles (AuNPs) have been widely used to detect a variety of drugs, including neurotransmitters, anti-cancer agents, and polyionic drug molecules, in both pharmaceutical formulations and biological fluids due to its physico-chemical and size dependent properties.[444] Neurotransmitters which are considered as endogenous chemical messengers, play an important role in transmitting, enhancing and converting specific signals in both the central and the peripheral nervous systems.[445] For example, 4-amino-3-hydrazino-5-mercapto 1,2,4-triazol (AHMP)-AuNPs has been used as a colorimetric sensor for dopamine detection in which process dopamine induced the aggregation process by hydrogen bonding interaction causing color change of colloidal solution from red to blue.[446] Moreover, different types of neurotransmitter such as dopamine-, L-DOPA-, adrenaline-, and noradrenaline-induced growth of Au nanoparticles has been introduced for the detection process.[447] Building on this phenomenon, the authors evaluated tyrosinase activity, which can be valuable for the detection of melanoma cells and the diagnosis of Parkinson's disease. Yarbakht and Nikkhah *et al.* developed sensitive

Table 10 Applications of colorimetric strategy based on AuNPs for glucose detection. Revised with the permission from ref. 436

Method	Colorimetric sensor	Linear range (μM)	LOD	Ref.
Colorimetric	AuNPs-nanoceria	0–2000	300 μM	437
Colorimetric	GOx/AgNPs–AuNPs	5–70	3 μM	438
Colorimetric	AuNPs–AgTNPs	0.5–20	0.3 μM	439
Colorimetric	Au@Ag core–shell	0.5 to 400	0.24 μM	440
Colorimetric	HRP-AuNPs	0.05–90	0.02 μM	441
Colorimetric	Green-AuNPs	0.050 to 5.250 mmol L^{-1}	7.615 μM	442

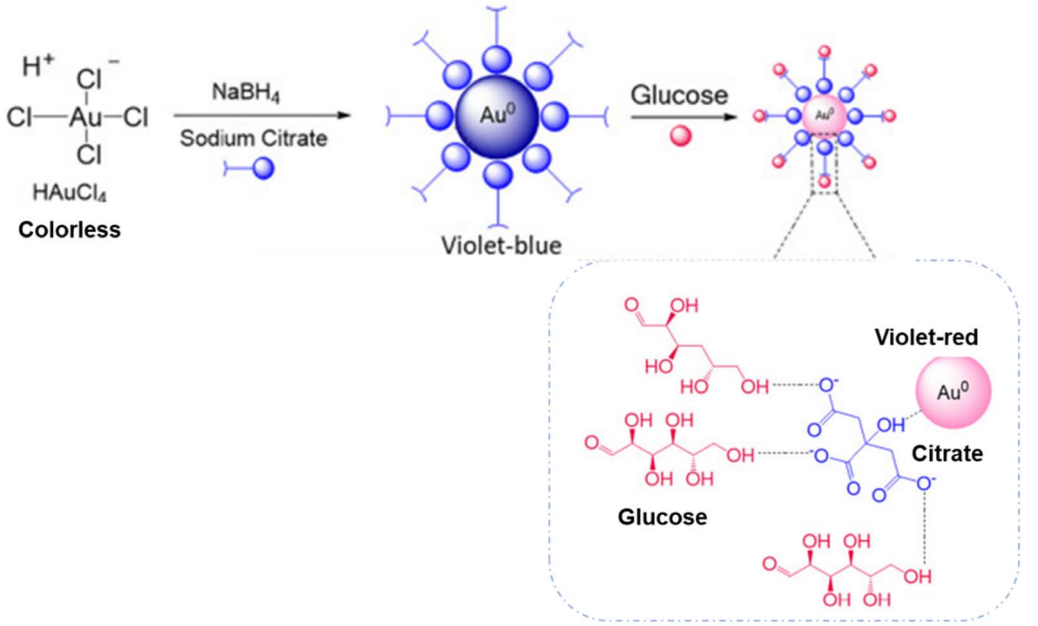

Fig. 17 Schematic mechanism of synthetic route for AuNPs and its application as colorimetric sensor for glucose detection. This figure has been adapted from ref. 431 with permission from PNAS, copyright 2006.

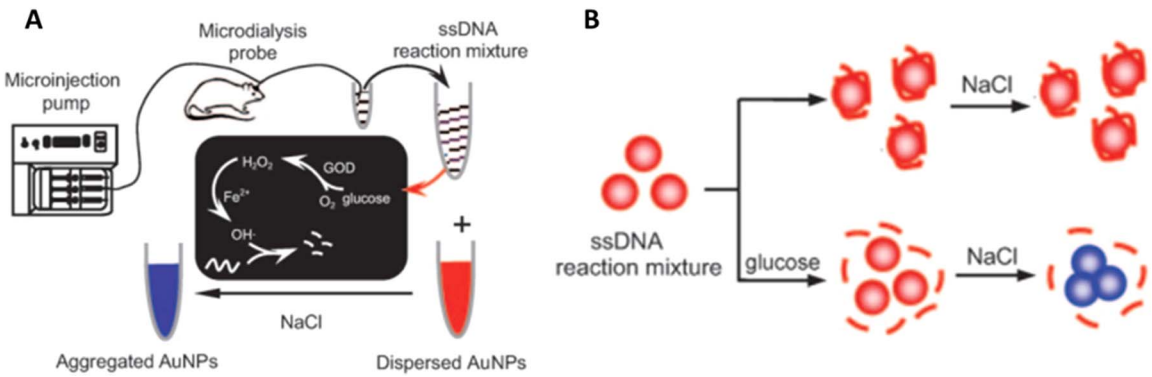

Fig. 18 (A) Schematic representation of glucose detection in rat brain using gold nanoparticles. (B) Glucose-induced color change mechanism. This figure has been adapted from ref. 443 with permission from *Angewandte Chemie*, copyright 2010.

analytical strategy for the detection of methamphetamine (MAMP) in pharmaceutical formulations using Au NPs as a probe. Methamphetamine (MAMP) is known as a highly addictive stimulant drug that affects the central nervous system. In this assay, AptaMeth binds to methamphetamine (MA) forming aptamer–drug complex, losing the ability to protect AuNP from aggregation. Hence, the more the concentration of MA present on the surface of AuNPs, the more aptamer binds with MA leaving fewer aptamer to protect AuNPs leading to the color change from red to blue.[448] Nowadays, AuNPs have been used for anti-cancer drug detection based on optical sensing strategy. For example, 5-fluorouracil (5-FU) is commonly utilized as an anticancer agent due to its significant potential in chemotherapy-based cancer treatment and diagnosis. The nature of binding between 5-FU and gold was investigated by using UV-visible spectroscopy, TEM, cyclic voltammetry.[449] A simple method was developed for the determination of gemcitabine HCl () in bulk drug and pharmaceutical formulation using AuNPs. the complex formation between AuNPs and GMCT changed color of AuNP and forms a dark blue and the detection limit of this method was found 0.44 μg mL^{-1} (Fig. 19).[450]

Glutathione (GSH) is a widely present tripeptide composed of glutamic acid, cysteine, and glycine, and plays a key role in the cellular antioxidant defense system which has been detected in eye drops and medical supplements using AuNPs based colorimetric method. In this method, water-soluble copolymers [poly(*N*-isopropylacrylamide-*co*-acryloyldiethyletriamine)] attached to the surfaces of gold cores which consist of diethylenetriamine group that helps the AuNPs to aggregate forming purplish-blue color. In the presence of GSH, it binds on the AuNPs surface kicking off the diethylenetriamine group,

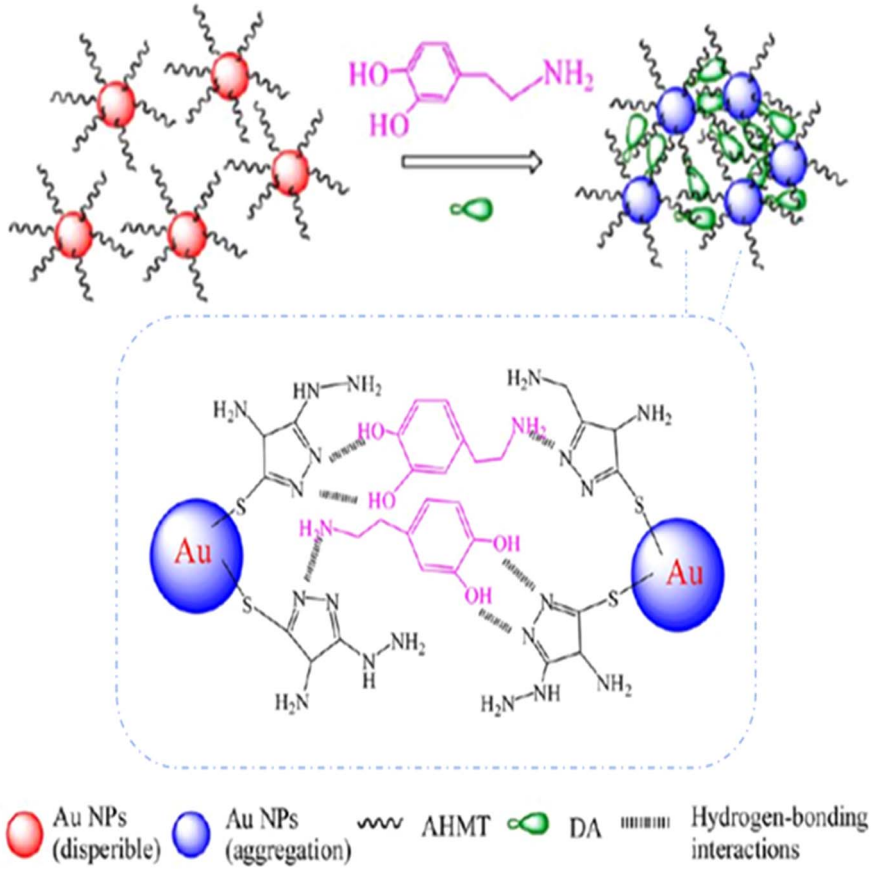

Fig. 19 Colorimetric detection of dopamine using AHMP-AuNPs probe. This figure has been adapted from ref. 446 with permission from American Chemical Society, copyright 2013.

Table 11 Employments of colorimetric strategy using AuNPs for drug detection. The table data is taken from ref. 444

Name of drugs	Modified AuNPs	Linear range (M)	LOD (M)	Ref.
Dopamine	DSP-AuNPs	100–600 nM	2 nM	452
Dopamine	Citrate-AuNPs	5×10^{-7}–1×10^{-5} M	2×10^{-7} M	453
6-Mercaptopurine (6-MP)	BSA-Au NPs	1.0×10^{-7}–1.2×10^{-4} M	1.98×10^{-8} M	454
6-Mercaptopurine (6-MP)	CTAB-AuNPs	0.0681–1.702 μg mL^{-1}	3.32 ng mL^{-1}	455
Protamine and heparin	Citrate-AuNPs	0.1–0.7 and 0.7–1.6 μg mL^{-1}	0.1 μg mL^{-1} and 0.6 μg mL^{-1}	456
Salmeterol xinafoate	CTAB-AuNPs	0.054–6.038 μg mL^{-1}	9.48 ng mL^{-1}	457
APAP, AA and FA	PSMA-Au NPs hydrogel	6–38 $\times 10^{-6}$, 1–7 $\times 10^{-6}$, 5–38 $\times 10^{-6}$ M respectively	1.8×10^{-6} M, 2.7×10^{-7} M, 2×10^{-6} M respectively	458
Berberine	Citrate-AuNPs	0.5–2.5 $\times 10^{-6}$ M	0.06 μg mL^{-1}	459

making free AuNPs to be separate, showing color red. The detection limit of GSH was 2.9×10^{-8} mol L^{-1} (Table 11).[451]

8.4.1. Antibiotic detection. Antibiotics are commonly utilized to treat or prevent diseases in animals by eliminating or suppressing the growth of microorganisms.[460] Wastewater from pharmaceutical factories, farms, or hospitals and the industrial wastage can carry antibiotic residue and also people can be affected by direct exposure of overdose of prescribed antibiotic. In this review, we will discuss the colorimetric method through which different types of antibiotic residue can be detected. Various antibiotics, including oxytetracycline, tetracycline, kanamycin, ofloxacin, chloramphenicol, and ceftriaxone, have been successfully detected using the gold nanoparticle (AuNP)-based colorimetric method.[461–465] A novel colorimetric aptasensor for multiplex antibiotics such as chloramphenicol (CAP) and tetracycline (TET) based on the ssDNA fragment that coordinately control the AuNPs aggregation phenomenon. After the addition of one kind of antibiotics, it specifically recognized fragment could bind with apt, made the AuNPs dispersed with red color and the non-specific one coordinately control the aggregation with support of salt showing blue color. Thus, the antibiotics show different color of AuNPs and the calculated detection limit for CAP and tetracycline TET are 7.0 nM and 32.9 nM.[466] Tobramycin (TOB) is an antibiotic which was

primarily used for the treatment of bacterial infections of the human and its uncontrollable intake causes nephrotoxicity, neuromuscular blocking and hypersensitivity.[467] Colorimetric aptasensors were used to detect TOB in milk and chicken using unmodified AuNPs and ssDNA aptamer. In absence of TOB, ssDNA binds on the AuNPs surface and protect it from aggregation even at present of salt. On the contrary, in the presence of TOB, due to higher affinities between ssDNA and TOB, they bind together and become detach from AuNPs surface, then less protection of DNA may result in the aggregation of AuNPs which is responsible for purple color solution of AuNPs. Thus, the limit of detection of this method was 23.3 nM.[468] Huang *et al.* developed a method for detection of the antibiotic ciprofloxacin (CIP) based on unmodified CIP-aptamer and AuNPs in aqueous solution. Here, in absence of CIP, the aptamer hybridizes PDDA (poly dimethyl diallyl ammonium chloride), forming a duplex structure through electrostatic interactions and made the dispersion of AuNPs. On the other hand, in the presence of target CIP, the aptamer binds with it and then the PDDA reacts with AuNPs causes aggregation. Thus, the CIP was detected down to 0.215 nM (Fig. 20).[469]

Oxytetracycline is among the most widely used antibiotics in the tetracycline class, commonly applied to prevent bacterial infections and promote growth due to its broad-spectrum effectiveness and affordability. To protect humans from the exposure to these drug residues, a colorimetric method for the determination of oxytetracycline has been proposed based on the anti-aggregation of cysteamine-stabilized AuNPs induced by the specific recognition of OBA with oxytetracycline.[470] This method exhibits the detection limit of 0.227 μg mL^{-1}. Another widely used antibiotic named Gentamicin has been detected using cysteamine-modified gold nanoparticles (cys-AuNPs) by colorimetric approach. Here, cysteamine was used to induce the aggregation of AuNPs by the hydrogen bonding interactions between the hydroxyl groups and aliphatic amine groups of gentamicin and the amine groups of cysteamine-modified AuNPs and this method was capable of detecting gentamicin concentrations as low as 12.45 nM in water.[471] However, antibiotic residues in food products can enter the human body through the food chain, veterinary drugs potentially leading to side effects like allergic reactions and the development of antimicrobial resistance in humans.[472] Some drugs are available for the widely used purpose in case of veterinary sectors. AuNPs has been widely used for the detection of many types of drugs which are enlisted in this review in a table format (Table 12).

8.4.2. Detection of allergens. An allergen is a type of antigen, typically a protein or gene product, that provokes an intense immune reaction as the immune system responds to

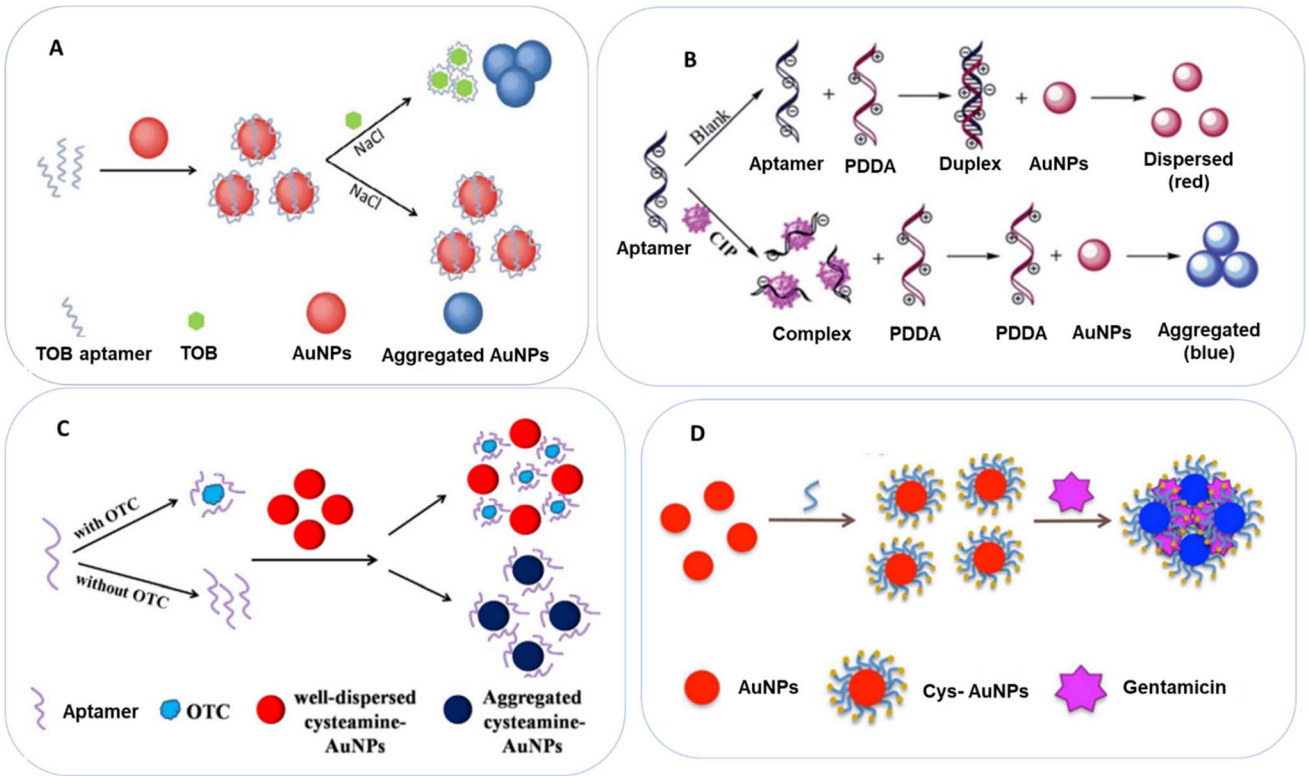

Fig. 20 (A) Schematic description of TOB detection based on colorimetric aptasensors. This figure has been adapted from ref. 468 with permission from Elsevier, copyright 2018. (B) Schematic representation of the colorimetric detection of ciprofloxacin. This figure has been adapted from ref. 469 with permission from Royal Society of Chemistry, copyright 2021. (C) Diagrammatic representation of the colorimetric aptasensor for oxytetracycline detection using cysteamine-modified gold nanoparticles (AuNPs) as the signaling element. This figure has been adapted from ref. 470 with permission from *ScienceDirect*, copyright 2016. (D) Schematic of the gentamicin detection technique on AuNPs modified with cysteamine. This figure has been adapted from ref. 471 with permission from Wiley, copyright 2018.

Table 12 Implementation of AuNP-based colorimetric strategy for veterinary drugs detection

Veterinary drugs	Modification of AuNPs	Linear range	LOD	Ref.
Clenbuterol (CLB), ractopamine (RCT)	(PE-Glu-AuNPs)	0–900 nM	0.23 nM, 0.43 nM respectively	473
Ractopamine (RCT)	Melamine-AuNPs	1×10^{-10}–5×10^{-7} M	1×10^{-11} M	474
Salbutamol		1×10^{-10}–1×10^{-5} M		
Sulfadimethoxine	Unmodified-AuNPs	50 ng mL^{-1}–1 μg mL^{-1}	50 ng mL^{-1}	475
Ampicillin	Unmodified-AuNPs	0.5 to 50 ng mL^{-1}	10 ng mL^{-1}	476
Oxytetracycline	Unmodified-AuNPs	25 nM–1 μM	25 nM	477
Streptomycin	Unmodified-AuNPs	0.2–1.2 μM	N/A	478
Kanamycin	GCNPs	—	2.3 fM	479
Cyromazine	Label-free AuNPs	1–500 ng mL^{-1}	5 ng mL^{-1}	480

what it mistakenly identifies as a threat to the body.[481] Allergen adverse reactions have affected quality of life and have persisted to be one of the most frightening situations among children and infants.[482] Therefore, the easy and rapid detection method for allergen is very necessary. Hence, AuNPs possess great role in colorimetric detection process for allergen present in food samples.[399] Some examples of food allergens are shrimp, fish, eggs, peanuts, soybeans, barley, sesame seeds, walnuts, almonds, pistachios as well as allergenic fungal spore. AuNPs mediated biosensors has proposed a detection procedure for peanut Ara h 1 enabling the visual detection of the target without using any analytical instruments. The detection process was based on the aggregation between switchable linkers (SL) and gold nanoparticles (AuNP) and it was able to detect f 0.19 mg peanut protein per 30 g of cookie.[483] A hybridization chain reaction (HCR) coupled with gold nanoparticles (AuNPs) was designed to detect the allergens presence in peanut, soybean and sesame. In this assay, two specially designed DNA strands called hairpin probes (H1 and H2) were used to occur HCR with the target DNA derived from food allergens. In presence of target DNA, HCR reaction took place and form long dsDNA that was not able to adsorb on AuNPs surface. In this case, the AuNPs underwent aggregation in the presence of salt thus color appears as purple from red. On the other hand, in absence of allergen, no HCR occurred, that's why the AuNPs remained dispersed showing no color change. The detection limit of three allergens detected by this method was as low as 0.5 nM.[484] Colorimetric sensing based on AuNPs is not only used for food allergens but also it can be used for detection of allergenic fungal spores. Lee *et al.* invented a simple and prompt method for *Aspergillus niger* spores using specially peptide-AuNPs. Modified AuNPs bind quickly to *A. niger* spores by phase display screening process. The aggregation of AuNPs cause color change of supernatant and thus, displayed a high sensitivity of ~50 spores.[485]

8.4.3. AuNPs based immunochromatography. Through antigen–antibody interactions, gold nanoparticle-based immunochromatographic assays (GICA) offer a quick, accurate, and field-deployable analytical platform for identifying target analytes.[486] Colloidal gold's deep red hue, which results from localized surface plasmon resonance, allows for simple visual readout without the use of complicated equipment. AuNP-based GICA systems have gained widespread application for on-site detection of pollutants, pathogens, and chemical residues in food, environmental, and clinical samples by incorporating competitive or sandwich immunoassay formats. For instance, scientists created a monoclonal antibody (mAb) based on GICA and used it to examine Imazalil (IMZ) residues in tomato and grape samples to detect IMZ in food samples.[487] Here they designed haptens (small molecules that imitate IMZ) to elicit an immunological response in mice that create AuNPs-linked monoclonal antibodies (AuNPs-mAb). A standard GICA strip was created, consisting of a nitrocellulose membrane (containing both test and control lines), a conjugate pad (containing AuNPs-mAb conjugates), and a sample pad (holding sample liquid). In competitive immunoassay, the immobilized IMZ on the test line and the IMZ in the sample primarily compete for binding to the AuNP-antibody conjugates. When IMZ is present, AuNPs-mAb reacts with it on the test line, producing a faint red or colorless tint. However, when IMZ is not there, the red color stays the same. Therefore, by measuring the color intensity of the test line using a smartphone or portable reader and comparing it to a reference chart, one may quickly identify various kinds of fungicides. In this investigation, the determined LOD for tomatoes and grapes were 4.70 ng g^{-1} and 4.12 ng g^{-1}, respectively.[488] Another study developed an immunochromatographic assay based on gold nanoparticles for the quick identification of the SARS-CoV-2 Omicron variant. Omicron's nucleocapsid protein (NP) was isolated and produced as an antigen. When NP was administered to BALB/c mice, the mice developed anti-NP monoclonal antibodies. In this assay, AuNPs are used for visual detection in a double antibody sandwich format. Based on this study, the researchers used the GICA test strip to detect the recombinant protein and inactivated virus with LODs of 8 pg mL^{-1} and 625 TCID50 per mL, respectively.[489]

8.4.4. Principal component analysis (PCA) and other machine learning methods in AuNPs based sensing. In AuNPs-based sensors, Principal Component Analysis (PCA) is a statistical method that reduces data and extracts characteristics to simplify complex datasets and enhance sensor performance by identifying the most significant variances in sensing strategy.[490] In the realm of AuNPs-based sensors, PCAs have numerous uses. AuNP-based sensors often generate complex, multidimensional datasets (*e.g.*, UV-vis spectra, surface-enhanced Raman spectra, colorimetric image data). PCA simplifies and expedites the detection process by breaking down these massive datasets into a small number of primary components. In order to help differentiate between targets and non-targets, PCA

converts the sensor data into a new coordinate system that emphasizes differences between analytes. For instance, in the context of biomarker identification, PCA has been utilized to distinguish between various polyamines by analyzing the spectral changes in the AuNPs' aggregation process following their addition. In order to increase detection reliability, PCA occasionally eliminates low-variance or redundant features. In order to clearly evaluate sensor performance and analyte separation, this also makes it possible to plot multidimensional sensing data in two or three dimensions. Additionally, the sensing applications use additional machine learning techniques. Machine learning (ML) has been previously applied in conjunction with spectroscopic techniques for the characterisation of nanomaterials, a capacity of particular value for plasmonic nanoparticles.[491,492] To characterize and develop nanoparticles and other nanomaterials, for example, spectroscopic data has been interpreted using machine learning techniques. Convolutional neural networks (CNNs) are a machine learning technique that is particularly relevant for array-structured data, such as spectral profiles and photographs. Because CNNs can analyze complicated data formats like pictures or spectral datasets directly, they frequently eliminate or reduce the need for lengthy preprocessing or dimensionality reduction stages.[493] Machine learning (ML) and deep learning (DL) were used to extract high dimensional data from the responses between various sensing devices and analytes. This technique improved the visual assessment of food safety.[494] Moreover, Linear Discriminant Analysis (LDA), which assists in grouping unknown data into predetermined groups, is used to categorize and quantify pesticide residue in fruits. In the medical diagnostics, Artificial Neural Networks (ANN) which can simulate non-linear interactions in AuNP sensor in case of discriminating between illness biomarkers.

9. Conclusion and future prospects

AuNPs-based colorimetric sensors have become an eminent probe for visual detection process of chemical and biological molecules with high performance, due to having both optoelectronic properties of core AuNPs and its tunable surface properties. There exists a variety of factors including the nature of analyte, the recognition partner, modification of AuNPs and the transduction process which influences the accuracy of limit of detection of AuNPs-based sensors. In this review, detailed information about the synthesis, modification, mechanisms involving visual detection of sensors and the application of AuNPs in various fields have been discussed. The synthetic pathway of AuNPs can be different such as chemical and green synthesis. This review goes over each synthesis process available for AuNPs. The mechanisms including aggregation, anti-aggregation, etching-mediated aggregation, nano enzyme-mediated aggregation *etc.* have been reviewed briefly. Our review has analyzed the sensing approach towards ion detection (cation, anion), metal detection (heavy metals, alkali and alkaline earth metals, coinage metals, rare-earth metals), food analysis (formalin, melamine, rhodamine dye, *etc.*), pathogens detection, mycotoxins detection, oligonucleotides (DNA, nucleic acids, protein *etc.*), glucose detection, drug analysis (antibiotics, allergens *etc.*). Colorimetric methods are acceptable to all the researchers because of their easy-to-use approach, cost effectiveness and visual sensing strategy. But this review reveals that this sensor is not only renowned for easy-to-use approach but also it can quickly respond to target with high accuracy. There is no doubt about the purview of AuNPs in the field of research and nanotechnology. The core benefits of AuNPs have led to a rapid surge in their application in sensing technologies, a trend that is expected to continue transforming the diagnostics field for the foreseeable future. Nevertheless, this detection method has many drawbacks in addition to its benefits. The environment, pH, and temperature can all have an impact on the nanoenzyme's catalytic activity, which lowers AuNPs' catalytic efficiency. Additional care may be required to manage the size and form of AuNPs. Interfering agents occasionally compromise analyte selectivity. Preparing the target analyte from the sample beforehand can help reduce matrix interferences, however this process is time-consuming and complicates the process. Reproducible synthetic methods for AuNPs are advocated since colorimetric detection relies on the colloidal stability of the particles.

It is anticipated that the next generation of AuNP-based probes would advance multifunctional, adaptive, and intelligent nano systems beyond traditional optical and electrochemical sensing. The creation of AuNPs that alter their optical or catalytic characteristics in response to temperature, redox potential, pH, or enzyme activity is one exciting avenue. Real-time, dynamic sensing for *in vivo* monitoring and biological diagnostics will be made possible by this system. The development of plasmonic nanorulers and thermometers that use AuNP's distance-dependent LSPR shifts to detect local temperature changes in biological settings represents another frontier. Stability, multiplex detection, and the integration of optical, electrochemical, and magnetic sensing are improved by further integrating AuNPs with 2D materials (graphene, MXenes), MOFs, and COFs. It may be possible to connect plasmonic AuNPs with quantum sensors like nitrogen-vacancy diamonds to surpass classical detection constraints using entangled photon plasmonic. AuNPs can be precisely arranged in space to produce plasmonic "hotspots" for ultra-sensitive SERS, which can identify single molecules in complicated samples with great selectivity. Translationally speaking, wearable and point-of-care AuNP-based devices will be essential for practical uses, which is why AuNPs must be incorporated into flexible biosensors and portable microfluidic chips. To improve detection accuracy and robustness in heterogeneous samples, these devices can be coupled with artificial intelligence (AI) and machine learning algorithms to enable automatic interpretation of complicated plasmonic signatures. The field will probably move toward biodegradable or renally clearable AuNP analogs to lower the dangers of long-term biological and environmental buildup. Lastly, to ensure reproducibility, speed up commercialization, and promote cross-disciplinary integration of AuNP-based probes into global sensing networks, standardization of fabrication, calibration, and validation protocols as well as open-access databases for nanoparticle-analyte interactions will be crucial.

Author contributions

Evana Sultana: conceptualization, writing original draft; Muhammad Shamim Al Mamun: conceptualization, supervision, writing and reviewing original draft.

Conflicts of interest

There is no conflict of interest regarding this review.

Abbreviation

AuNPs	Gold nanoparticles
OP	Organophosphorus pesticides
Pi	Inorganic phosphate
PNIPAAm	Poly(*N* isopropylacrylamide)
ADN	Ammonium dinitramide
AHMP	4-Amino-6-hydroxy-2-mercaptopyrimidine monohydrate
MA	Mercaptoacetic acid
AChE	Acetylcholinesterase
DEHP	Diethylhexyl phthalate
CTAB	Cetyltrimethylammonium bromide
HIC	Hormone-interfering compounds
EDI	Estimated daily intake
BPA	Bisphenol A
PDDA	Poly(diallyl dimethylammonium chloride)
E2	17β-estradiol
AfM1	Aflatoxin M1
PCR	Polymeric chain reaction
HSA	Human serum albumin
GOD	Glucose oxidase
ssDNA	Single strand DNA
MAMP	Methamphetamine
AptaMeth	Methamphetamine-aptamer
5-FU	5-Fluorouracil
GSH	Glutathione
CAP	Chloramphenicol
TET	Tetracycline
TOB	Tobramycin
CIP	Ciprofloxacin
OBA	Oxytetracycline-binding aptamers
HCR	Hybridization chain reaction
SL	Switchable linkers

Data availability

This study does not generate or analyze any new data. This article does not allow data sharing.

Acknowledgements

Authors love to acknowledge Chemistry Discipline, Khulna University and Chemical and Materials Engineering Department, University of Nevada, Reno for the facilities and lab support to access journals.

References

1 R. P. Schwarzenbach, T. Egli, T. B. Hofstetter, U. Von Gunten and B. Wehrli, *Annu. Rev. Environ. Resour.*, 2010, **35**, 109–136.
2 S. D. Richardson and T. A. Ternes, *Anal. Chem.*, 2018, **90**, 398–428.
3 S. R. Hughes, P. Kay and L. E. Brown, *Environ. Sci. Technol.*, 2013, **47**, 661–677.
4 Y. Luo, W. Guo, H. H. Ngo, L. D. Nghiem, F. I. Hai, J. Zhang, S. Liang and X. C. Wang, *Sci. Total Environ.*, 2014, **473–474**, 619–641.
5 A. Pal, K. Y.-H. Gin, A. Y.-C. Lin and M. Reinhard, *Sci. Total Environ.*, 2010, **408**, 6062–6069.
6 B. Petrie, R. Barden and B. Kasprzyk-Hordern, *Water Res.*, 2015, **72**, 3–27.
7 P. Baptista, E. Pereira, P. Eaton, G. Doria, A. Miranda, I. Gomes, P. Quaresma and R. Franco, *Anal. Bioanal. Chem.*, 2008, **391**, 943–950.
8 M. S. Draz and H. Shafiee, *Theranostics*, 2018, **8**, 1985–2017.
9 P. K. Jain, X. Huang, I. H. El-Sayed and M. A. El-Sayed, *Acc. Chem. Res.*, 2008, **41**, 1578–1586.
10 V. Amendola and M. Meneghetti, *Phys. Chem. Chem. Phys.*, 2009, **11**, 3805.
11 E. Priyadarshini and N. Pradhan, *Sens. Actuators, B*, 2017, **238**, 888–902.
12 J. Turkevich, P. C. Stevenson and J. Hillier, *Discuss. Faraday Soc.*, 1951, **11**, 55.
13 G. Frens, *Nat. Phys. Sci.*, 1973, **241**, 20–22.
14 S. Iravani, *Green Chem.*, 2011, **13**, 2638.
15 J. Liu and Y. Lu, *J. Am. Chem. Soc.*, 2003, **125**, 6642–6643.
16 Z. Wang, J. H. Lee and Y. Lu, *Adv. Mater.*, 2008, **20**, 3263–3267.
17 N. Lavanya, E. Fazio, F. Neri, A. Bonavita, S. G. Leonardi, G. Neri and C. Sekar, *Sens. Actuators, B*, 2015, **221**, 1412–1422.
18 R. Liang, Z. Wang, L. Zhang and J. Qiu, *Chem.–Eur. J.*, 2013, **19**, 5029–5033.
19 M. Arabnejad, I. E. Tothill and I. Chianella, *Biosensors*, 2024, **14**, 624.
20 G. Zheng, F. Patolsky, Y. Cui, W. U. Wang and C. M. Lieber, *Nat. Biotechnol.*, 2005, **23**, 1294–1301.
21 W. Zhao, W. Chiuman, M. A. Brook and Y. Li, *ChemBioChem*, 2007, **8**, 727–731.
22 S. S. Dandu, D. J. Joshi, T. J. Park and S. K. Kailasa, *Appl. Spectrosc.*, 2023, **77**, 360–370.
23 A. K. Yetisen, M. S. Akram and C. R. Lowe, *Lab Chip*, 2013, **13**, 2210.
24 X. Li, X. Shen, W. Jiang, Y. Xi and S. Li, *Ecotoxicol. Environ. Saf.*, 2024, **278**, 116420.
25 R. Levin, C. M. Villanueva, D. Beene, A. L. Cradock, C. Donat-Vargas, J. Lewis, I. Martinez-Morata, D. Minovi, A. E. Nigra, E. D. Olson, L. A. Schaider, M. H. Ward and N. C. Deziel, *J. Expo. Sci. Environ. Epidemiol.*, 2024, **34**, 3–22.
26 H. K. Bayabil, F. T. Teshome and Y. C. Li, *Front. Environ. Sci.*, 2022, **10**, 873499.

27 P. S. Nishmitha, K. A. Akhilghosh, V. P. Aiswriya, A. Ramesh, M. Muthuchamy and A. Muthukumar, *J. Hazard. Mater. Adv.*, 2025, **18**, 100755.
28 S. A. F. Kusuma, J. A. Harmonis, R. Pratiwi and A. N. Hasanah, *Sensors*, 2023, **23**, 8172.
29 S. H. Lee and B.-H. Jun, *Int. J. Mol. Sci.*, 2019, **20**, 865.
30 C. Daruich De Souza, B. Ribeiro Nogueira and M. E. C. M. Rostelato, *J. Alloys Compd.*, 2019, **798**, 714–740.
31 X.-F. Zhang, Z.-G. Liu, W. Shen and S. Gurunathan, *Int. J. Mol. Sci.*, 2016, **17**, 1534.
32 N. Chanda, P. Kan, L. D. Watkinson, R. Shukla, A. Zambre, T. L. Carmack, H. Engelbrecht, J. R. Lever, K. Katti, G. M. Fent, S. W. Casteel, C. J. Smith, W. H. Miller, S. Jurisson, E. Boote, J. D. Robertson, C. Cutler, M. Dobrovolskaia, R. Kannan and K. V. Katti, *Nanomed.: Nanotechnol. Biol. Med.*, 2010, **6**, 201–209.
33 M. L. Yahaya, N. D. Zakaria, R. Noordin and K. Abdul Razak, *Mater. Today Proc.*, 2022, **66**, 2943–2947.
34 B. V. Enustun and J. Turkevich, *J. Am. Chem. Soc.*, 1963, **85**, 3317–3328.
35 S. K. Sivaraman, S. Kumar and V. Santhanam, *J. Colloid Interface Sci.*, 2011, **361**, 543–547.
36 Y. Niidome, K. Nishioka, H. Kawasaki and S. Yamada, *Chem. Commun.*, 2003, 2376–2377.
37 Y. Shao, Y. Jin and S. Dong, *Chem. Commun.*, 2004, 1104–1105.
38 J. Turkevich, P. C. Stevenson and J. Hillier, *Discuss. Faraday Soc.*, 1951, **11**, 55.
39 A. E. F. Oliveira, A. C. Pereira, M. A. C. Resende and L. F. Ferreira, *Analytica*, 2023, **4**, 250–263.
40 J. Turkevich, P. C. Stevenson and J. Hillier, *Discuss. Faraday Soc.*, 1951, **11**, 55.
41 Y. Gao and L. Torrente-Murciano, *Nanoscale*, 2020, **12**, 2740–2751.
42 W. Leng, P. Pati and P. J. Vikesland, *Environ. Sci. Nano*, 2015, **2**, 440–453.
43 S. Kumar, K. S. Gandhi and R. Kumar, *Ind. Eng. Chem. Res.*, 2007, **46**, 3128–3136.
44 T. Yonezawa and T. Kunitake, *Colloids Surf., A*, 1999, **149**, 193–199.
45 K. J. Watson, J. Zhu, S. T. Nguyen and C. A. Mirkin, *J. Am. Chem. Soc.*, 1999, **121**, 462–463.
46 J. Polte, T. T. Ahner, F. Delissen, S. Sokolov, F. Emmerling, A. F. Thünemann and R. Kraehnert, *J. Am. Chem. Soc.*, 2010, **132**, 1296–1301.
47 M. Faraday, *Philos. Trans. R. Soc. London*, 1857, **147**, 145–181.
48 S. R. K. Perala and S. Kumar, *Langmuir*, 2013, **29**, 9863–9873.
49 M. Giersig and P. Mulvaney, *Langmuir*, 1993, **9**, 3408–3413.
50 M. Brust, M. Walker, D. Bethell, D. J. Schiffrin and R. Whyman, *J. Chem. Soc. Chem. Commun.*, 1994, 801–802.
51 D. V. Leff, P. C. Ohara, J. R. Heath and W. M. Gelbart, *J. Phys. Chem.*, 1995, **99**, 7036–7041.
52 M. J. Hostetler, J. E. Wingate, C.-J. Zhong, J. E. Harris, R. W. Vachet, M. R. Clark, J. D. Londono, S. J. Green, J. J. Stokes, G. D. Wignall, G. L. Glish, M. D. Porter, N. D. Evans and R. W. Murray, *Langmuir*, 1998, **14**, 17–30.
53 Y. Negishi, Y. Takasugi, S. Sato, H. Yao, K. Kimura and T. Tsukuda, *J. Phys. Chem. B*, 2006, **110**, 12218–12221.
54 A. C. Templeton, W. P. Wuelfing and R. W. Murray, *Acc. Chem. Res.*, 2000, **33**, 27–36.
55 J. C. Love, L. A. Estroff, J. K. Kriebel, R. G. Nuzzo and G. M. Whitesides, *Chem. Rev.*, 2005, **105**, 1103–1170.
56 S. J. Amina and B. Guo, *Int. J. Nanomed.*, 2020, **15**, 9823–9857.
57 A. Gole and C. J. Murphy, *Chem. Mater.*, 2004, **16**, 3633–3640.
58 T. K. Sau and C. J. Murphy, *J. Am. Chem. Soc.*, 2004, **126**, 8648–8649.
59 Y. Chen, X. Gu, C.-G. Nie, Z.-Y. Jiang, Z.-X. Xie and C.-J. Lin, *Chem. Commun.*, 2005, 4181.
60 C. R. Bridges, P. M. DiCarmine, A. Fokina, D. Huesmann and D. S. Seferos, *J. Mater. Chem. A*, 2013, **1**, 1127–1133.
61 J. A. Jenkins, T. J. Wax and J. Zhao, *J. Chem. Educ.*, 2017, **94**, 1090–1093.
62 Z. Sadiq, S. H. Safiabadi Tali, H. Hajimiri, M. Al-Kassawneh and S. Jahanshahi-Anbuhi, *Crit. Rev. Anal. Chem.*, 2023, 1–36.
63 L. Qin, G. Zeng, C. Lai, D. Huang, P. Xu, C. Zhang, M. Cheng, X. Liu, S. Liu, B. Li and H. Yi, *Coord. Chem. Rev.*, 2018, **359**, 1–31.
64 N. R. Jana and X. Peng, *J. Am. Chem. Soc.*, 2003, **125**, 14280–14281.
65 D. Gentili, G. Ori and M. Comes Franchini, *Chem. Commun.*, 2009, 5874.
66 G. Liu, M. Lu, X. Huang, T. Li and D. Xu, *Sensors*, 2018, **18**, 4166.
67 R. Sharma, U. S. Akshath, P. Bhatt, M. S. Thakur and K. S. M. S. Raghavarao, *Procedia Technol.*, 2017, **27**, 282–286.
68 Y.-C. Yang, C.-H. Wang, Y.-K. Hwu and J.-H. Je, *Mater. Chem. Phys.*, 2006, **100**, 72–76.
69 B. Akar, K. Pushpavanam, E. Narayanan, K. Rege and J. J. Heys, *Biomed. Phys. Eng. Express*, 2018, **4**, 065011.
70 A. M. Abdelghany, E. M. Abdelrazek, S. I. Badr, M. S. Abdel-Aziz and M. A. Morsi, *J. Saudi Chem. Soc.*, 2017, **21**, 528–537.
71 C. Fan, W. Li, S. Zhao, J. Chen and X. Li, *Mater. Lett.*, 2008, **62**, 3518–3520.
72 V. K. T. Ngo, D. G. Nguyen, T. P. Huynh and Q. V. Lam, *Adv. Nat. Sci. Nanosci. Nanotechnol.*, 2016, **7**, 035016.
73 M. D. P. Rodríguez-Torres, L. A. Diaz -Torres, M. Olmos-López, P. Salas and C. Gutiérrez, *Conference Plasmonics: Metallic Nanostructures and Their Optical Properties XI*, ed. M. I. Stockman, 2013, p. 88092R.
74 F. Correard, K. Maximova, C. Villard, M. Roy, A. Al-Kattan, M. Sentis, M. Gingras, A. Kabashin, M.-A. Esteve and D. Braguer, *Int. J. Nanomed.*, 2014, 5415–5430.
75 H. R. Tiyyagura, P. Majerič, I. Anžel and R. Rudolf, *Mater. Res. Express*, 2020, **7**, 055017.
76 L. Gao, S. Mei, H. Ma and X. Chen, *Ultrason. Sonochem.*, 2022, **83**, 105940.
77 K. D. N. Vo, C. Kowandy, L. Dupont, X. Coqueret and N. Q. Hien, *Radiat. Phys. Chem.*, 2014, **94**, 84–87.

78 A. Kumar, M. Bhatt, G. Vyas, S. Bhatt and P. Paul, *ACS Appl. Mater. Interfaces*, 2017, **9**, 17359–17368.
79 C. Fan, W. Li, S. Zhao, J. Chen and X. Li, *Mater. Lett.*, 2008, **62**, 3518–3520.
80 M. E. El-Naggar, T. I. Shaheen, M. M. G. Fouda and A. A. Hebeish, *Carbohydr. Polym.*, 2016, **136**, 1128–1136.
81 X. Hong, J. Bai, Y. Peng, X. Zhang, Z. Gao, B. Ning, M. Li, Y. Pu, Y. Ying, F. Su and X. Zhang, *Sens. Actuators, B*, 2020, **321**, 128493.
82 J. Qiao and L. Qi, *Talanta*, 2021, **223**, 121396.
83 T. H. A. Nguyen, V.-C. Nguyen, T. N. H. Phan, V. T. Le, Y. Vasseghian, M. A. Trubitsyn, A.-T. Nguyen, T. P. Chau and V.-D. Doan, *Chemosphere*, 2022, **287**, 132271.
84 P. Kuppusamy, M. M. Yusoff, G. P. Maniam and N. Govindan, *Saudi Pharm. J.*, 2016, **24**, 473–484.
85 P. B. Santhosh, J. Genova and H. Chamati, *Chemistry*, 2022, **4**, 345–369.
86 A. I. Usman, A. Abdul Aziz and O. Abu Noqta, *J. Teknol.*, 2019, **81**, 171–182.
87 M. Nadeem, B. H. Abbasi, M. Younas, W. Ahmad and T. Khan, *Green Chem. Lett. Rev.*, 2017, **10**, 216–227.
88 S. Ying, Z. Guan, P. C. Ofoegbu, P. Clubb, C. Rico, F. He and J. Hong, *Environ. Technol. Innov.*, 2022, **26**, 102336.
89 M. Noruzi, D. Zare, K. Khoshnevisan and D. Davoodi, *Spectrochim. Acta, Part A*, 2011, **79**, 1461–1465.
90 K. Xin Lee, K. Shameli, M. Miyake, N. Kuwano, N. B. Bt Ahmad Khairudin, S. E. Bt Mohamad and Y. P. Yew, *J. Nanomater.*, 2016, **2016**, 1–7.
91 J. Y. Song, H.-K. Jang and B. S. Kim, *Process Biochem.*, 2009, **44**, 1133–1138.
92 V. Ganesh Kumar, S. Dinesh Gokavarapu, A. Rajeswari, T. Stalin Dhas, V. Karthick, Z. Kapadia, T. Shrestha, I. A. Barathy, A. Roy and S. Sinha, *Colloids Surf., B*, 2011, **87**, 159–163.
93 P. Dauthal and M. Mukhopadhyay, *Ind. Eng. Chem. Res.*, 2012, **51**, 13014–13020.
94 K. P. Kumar, W. Paul and C. P. Sharma, *Process Biochem.*, 2011, **46**, 2007–2013.
95 M. H. Oueslati, L. Ben Tahar and A. H. Harrath, *Green Chem. Lett. Rev.*, 2020, **13**, 18–26.
96 K. Ghule, A. V. Ghule, J.-Y. Liu and Y.-C. Ling, *J. Nanosci. Nanotechnol.*, 2006, **6**, 3746–3751.
97 R. K. Das, N. Gogoi and U. Bora, *Bioprocess Biosyst. Eng.*, 2011, **34**, 615–619.
98 S. Ghosh, S. Patil, M. Ahire, R. Kitture, D. D. Gurav, A. M. Jabgunde, S. Kale, K. Pardesi, V. Shinde, J. Bellare, D. D. Dhavale and B. A. Chopade, *J. Nanobiotechnol.*, 2012, **10**, 17.
99 K. B. Narayanan and N. Sakthivel, *Adv. Colloid Interface Sci.*, 2010, **156**, 1–13.
100 N. Chakraborty, A. Banerjee, S. Lahiri, A. Panda, A. N. Ghosh and R. Pal, *J. Appl. Phycol.*, 2009, **21**, 145–152.
101 G. Li, D. He, Y. Qian, B. Guan, S. Gao, Y. Cui, K. Yokoyama and L. Wang, *Int. J. Mol. Sci.*, 2011, **13**, 466–476.
102 J. Verma, C. Kumar, M. Sharma and S. Saxena, *3 Biotech*, 2024, **14**, 263.
103 N. Soni and S. Prakash, *Rep. Parasitol.*, 2012, **1**, 1–7.
104 Y. Konishi, T. Tsukiyama, T. Tachimi, N. Saitoh, T. Nomura and S. Nagamine, *Electrochim. Acta*, 2007, **53**, 186–192.
105 S. R. Rajasree and T. Suman, *Asian Pac. J. Trop. Dis.*, 2012, **2**, S796–S799.
106 N. Sharma, A. K. Pinnaka, M. Raje, A. Fnu, M. S. Bhattacharyya and A. R. Choudhury, *Microb. Cell Factories*, 2012, **11**, 86.
107 Y. Nangia, N. Wangoo, N. Goyal, G. Shekhawat and C. R. Suri, *Microb. Cell Factories*, 2009, **8**, 39.
108 S. He, Z. Guo, Y. Zhang, S. Zhang, J. Wang and N. Gu, *Mater. Lett.*, 2007, **61**, 3984–3987.
109 D. Inbakandan, R. Venkatesan and S. Ajmal Khan, *Colloids Surf., B*, 2010, **81**, 634–639.
110 G. Singaravelu, J. S. Arockiamary, V. G. Kumar and K. Govindaraju, *Colloids Surf., B*, 2007, **57**, 97–101.
111 A. Chauhan, S. Zubair, S. Tufail, A. Sherwani, M. Sajid, S. C. Raman, A. Azam and M. Owais, *Int. J. Nanomed.*, 2011, **6**, 2305–2319.
112 M. Gholami-Shabani, M. Shams-Ghahfarokhi, Z. Gholami-Shabani, A. Akbarzadeh, G. Riazi, S. Ajdari, A. Amani and M. Razzaghi-Abyaneh, *Process Biochem.*, 2015, **50**, 1076–1085.
113 T. Maruyama, Y. Fujimoto and T. Maekawa, *J. Colloid Interface Sci.*, 2015, **447**, 254–257.
114 V. D. Badwaik, J. J. Bartonojo, J. W. Evans, S. V. Sahi, C. B. Willis and R. Dakshinamurthy, *Langmuir*, 2011, **27**, 5549–5554.
115 P. De La Presa, M. Multigner, J. De La Venta, M. A. García and M. L. Ruiz-González, *J. Appl. Phys.*, 2006, **100**, 123915.
116 C. C. Berry and A. S. G. Curtis, *J. Phys. Appl. Phys.*, 2003, **36**, R198–R206.
117 D. V. Leff, L. Brandt and J. R. Heath, *Langmuir*, 1996, **12**, 4723–4730.
118 M. Aslam, L. Fu, M. Su, K. Vijayamohanan and V. P. Dravid, *J. Mater. Chem.*, 2004, **14**, 1795.
119 J. D. S. Newman and G. J. Blanchard, *Langmuir*, 2006, **22**, 5882–5887.
120 S. K. Bhargava, J. M. Booth, S. Agrawal, P. Coloe and G. Kar, *Langmuir*, 2005, **21**, 5949–5956.
121 S. Mandal, P. R. Selvakannan, S. Phadtare, R. Pasricha and M. Sastry, *J. Chem. Sci.*, 2002, **114**, 513–520.
122 Pr. Selvakannan, P. S. Kumar, A. S. More, R. D. Shingte, P. P. Wadgaonkar and M. Sastry, *Langmuir*, 2004, **20**, 295–298.
123 F. Dumur, E. Dumas and C. R. Mayer, *Nanomaterials*, 2020, **10**, 548.
124 A. P. Alivisatos, K. P. Johnsson, X. Peng, T. E. Wilson, C. J. Loweth, M. P. Bruchez and P. G. Schultz, *Nature*, 1996, **382**, 609–611.
125 C. A. Mirkin, R. L. Letsinger, R. C. Mucic and J. J. Storhoff, *Nature*, 1996, **382**, 607–609.
126 M. Rahmati, E. A. Silva, J. E. Reseland, C. A. Heyward and H. J. Haugen, *Chem. Soc. Rev.*, 2020, **49**, 5178–5224.
127 J. Song, S. Park, S. Kim, K. Im and N. Park, *New J. Chem.*, 2017, **41**, 9590–9593.
128 C. Liu, J. Zhang, X. Zhang, L. Zhao and S. Li, *Microchim. Acta*, 2018, **185**, 227.

129 W. C. Song, B. Kim, S. Y. Park, G. Park and J.-W. Oh, *Arab. J. Chem.*, 2022, **15**, 104056.
130 J. H. Heo, H. H. Cho and J. H. Lee, *Analyst*, 2014, **139**, 5936–5944.
131 J. R. Nicol, D. Dixon and J. A. Coulter, *Nanomed*, 2015, **10**, 1315–1326.
132 H. Li and L. Rothberg, *Proc. Natl. Acad. Sci. U. S. A.*, 2004, **101**, 14036–14039.
133 L. Xu, S. Dong, J. Hao, J. Cui and H. Hoffmann, *Langmuir*, 2017, **33**, 3047–3055.
134 H. Li and L. J. Rothberg, *J. Am. Chem. Soc.*, 2004, **126**, 10958–10961.
135 T. Fellows, L. Ho, S. Flanagan, R. Fogel, D. Ojo and J. Limson, *Analyst*, 2020, **145**, 5180–5193.
136 K. Abnous, N. M. Danesh, M. Ramezani, A. S. Emrani and S. M. Taghdisi, *Biosens. Bioelectron.*, 2016, **78**, 80–86.
137 S. Alex and A. Tiwari, *J. Nanosci. Nanotechnol.*, 2015, **15**, 1869–1894.
138 K. G. Thomas and P. V. Kamat, *Acc. Chem. Res.*, 2003, **36**, 888–898.
139 Y. Song, T. Huang and R. W. Murray, *J. Am. Chem. Soc.*, 2003, **125**, 11694–11701.
140 V. Poornima, V. Alexandar, S. Iswariya, P. T. Perumal and T. S. Uma, *RSC Adv.*, 2016, **6**, 46711–46722.
141 S. Kim, N. H. Lee, S. H. Seo, M. S. Eom, S. Ahn and M. S. Han, *Chem.–Asian J.*, 2010, **5**, 2463–2466.
142 N. Ratnarathorn, O. Chailapakul and W. Dungchai, *Talanta*, 2015, **132**, 613–618.
143 J. M. Abad, S. F. L. Mertens, M. Pita, V. M. Fernández and D. J. Schiffrin, *J. Am. Chem. Soc.*, 2005, **127**, 5689–5694.
144 K. Hamaguchi, H. Kawasaki and R. Arakawa, *Colloids Surf., A*, 2010, **367**, 167–173.
145 Y.-R. Kim, R. K. Mahajan, J. S. Kim and H. Kim, *ACS Appl. Mater. Interfaces*, 2010, **2**, 292–295.
146 G. Wang, C. Yan, S. Gao and Y. Liu, *Mater. Sci. Eng., C*, 2019, **103**, 109856.
147 Y. Guo, Z. Wang, W. Qu, H. Shao and X. Jiang, *Biosens. Bioelectron.*, 2011, **26**, 4064–4069.
148 D. Li, A. Wieckowska and I. Willner, *Angew. Chem.*, 2008, **120**, 3991–3995.
149 W. Yang, J. J. Gooding, Z. He, Q. Li and G. Chen, *J. Nanosci. Nanotechnol.*, 2007, **7**, 712–716.
150 T. Lou, Z. Chen, Y. Wang and L. Chen, *ACS Appl. Mater. Interfaces*, 2011, **3**, 1568–1573.
151 L. Chen, X. Fu, W. Lu and L. Chen, *ACS Appl. Mater. Interfaces*, 2013, **5**, 284–290.
152 C.-J. Yu, T.-L. Cheng and W.-L. Tseng, *Biosens. Bioelectron.*, 2009, **25**, 204–210.
153 C.-J. Yu and W.-L. Tseng, *Langmuir*, 2008, **24**, 12717–12722.
154 G. K. Darbha, A. K. Singh, U. S. Rai, E. Yu, H. Yu and P. Chandra Ray, *J. Am. Chem. Soc.*, 2008, **130**, 8038–8043.
155 Z. Jiang, G. Wen, Y. Fan, C. Jiang, Q. Liu, Z. Huang and A. Liang, *Talanta*, 2010, **80**, 1287–1291.
156 R. Manjumeena, D. Duraibabu, T. Rajamuthuramalingam, R. Venkatesan and P. T. Kalaichelvan, *RSC Adv.*, 2015, **5**, 69124–69133.
157 F. Boussoufi, S. Navarro Gallón, R. Chang and T. Webster, *Int. J. Nanomed.*, 2018, **13**, 6199–6205.
158 F. Chai, C. Wang, T. Wang, Z. Ma and Z. Su, *Nanotechnology*, 2010, **21**, 025501.
159 S. H. Lee, K. H. Bae, S. H. Kim, K. R. Lee and T. G. Park, *Int. J. Pharm.*, 2008, **364**, 94–101.
160 S. M. Louie, J. M. Gorham, J. Tan and V. A. Hackley, *Environ. Sci. Nano*, 2017, **4**, 1866–1875.
161 S. Sangwan and R. Seth, *Int. J. Dairy Technol.*, 2023, **76**, 351–363.
162 D. A. Giljohann, D. S. Seferos, A. E. Prigodich, P. C. Patel and C. A. Mirkin, *J. Am. Chem. Soc.*, 2009, **131**, 2072–2073.
163 X. Chen, Y. Zu, H. Xie, A. M. Kemas and Z. Gao, *Analyst*, 2011, **136**, 1690.
164 S. K. Kailasa, T. P. Nguyen, S. H. Baek, L. M. Tu Phan, R. Rafique and T. J. Park, *Talanta*, 2019, **205**, 120087.
165 A. R. Esfahani, Z. Sadiq, O. D. Oyewunmi, S. H. Safiabadi Tali, N. Usen, D. C. Boffito and S. Jahanshahi-Anbuhi, *Analyst*, 2021, **146**, 3697–3708.
166 E. Buhr, N. Senftleben, T. Klein, D. Bergmann, D. Gnieser, C. G. Frase and H. Bosse, *Meas. Sci. Technol.*, 2009, **20**, 084025.
167 E. Sultana, M. Z. Rana, M. S. Al Mamun, M. A. Saad Aly, G. E. Khedr, J. Ahmed and W. Alahmad, *Chemosphere*, 2025, **372**, 144095.
168 T. Zheng, S. Bott and Q. Huo, *ACS Appl. Mater. Interfaces*, 2016, **8**, 21585–21594.
169 A. L. Suherman, G. Zampardi, S. Kuss, E. E. L. Tanner, H. M. A. Amin, N. P. Young and R. G. Compton, *Phys. Chem. Chem. Phys.*, 2018, **20**, 28300–28307.
170 C. L. Nehl and J. H. Hafner, *J. Mater. Chem.*, 2008, **18**, 2415.
171 A. R. Esfahani, Z. Sadiq, O. D. Oyewunmi, S. H. Safiabadi Tali, N. Usen, D. C. Boffito and S. Jahanshahi-Anbuhi, *Analyst*, 2021, **146**, 3697–3708.
172 E. Sultana, Md. Z. Rana, M. S. A. Mamun, M. Aly Saad Aly, G. E. Khedr, M. Nasiruddin and Md Z. H. Khan, *RSC Adv.*, 2025, **15**, 10442–10452.
173 N. D. Israelsen, C. Hanson and E. Vargis, *Sci. World J.*, 2015, **2015**, 124582.
174 S. S. An, M. Ramasamy, S. J. Ahn, K.-S. Yun, S. Govindaraju and R. Baskaran, *Int. J. Nanomed.*, 2015, **67**.
175 J. Liu, R. Papadakis and H. Li, *Appl. Phys. Lett.*, 2018, **113**, 083108.
176 E. Meyer, *Prog. Surf. Sci.*, 1992, **41**, 3–49.
177 A. Ramanaviciene, J. Voronovic, A. Popov, R. Drevinskas, A. Kausaite-Minkstimiene and A. Ramanavicius, *Colloids Surf., A*, 2016, **510**, 183–189.
178 D. N. Correa-Llantén, S. A. Muñoz-Ibacache, M. E. Castro, P. A. Muñoz and J. M. Blamey, *Microb. Cell Factories*, 2013, **12**, 75.
179 T. Pellegrino, R. A. Sperling, A. P. Alivisatos and W. J. Parak, *J. Biomed. Biotechnol.*, 2007, **2007**, 1–9.
180 P. K. Harimech, S. R. Gerrard, A. H. El-Sagheer, T. Brown and A. G. Kanaras, *J. Am. Chem. Soc.*, 2015, **137**, 9242–9245.
181 B. A. N. Asbaghi, A. Alsadig, L. Casalis, P. Parisse, J. Niemela, S. Bellucci and H. Cabrera, *Microchem. J.*, 2022, **173**, 106961.

182 D. Titus, E. James Jebaseelan Samuel and S. M. Roopan, in *Green Synthesis, Characterization and Applications of Nanoparticles*, Elsevier, 2019, pp. 303–319.
183 R. Xu, *Particuology*, 2008, **6**, 112–115.
184 A. V. Delgado, F. González-Caballero, R. J. Hunter, L. K. Koopal and J. Lyklema, *J. Colloid Interface Sci.*, 2007, **309**, 194–224.
185 F. Arockiya Aarthi Rajathi, C. Parthiban, V. Ganesh Kumar and P. Anantharaman, *Spectrochim. Acta, Part A*, 2012, **99**, 166–173.
186 A. W. Khan, N. S. Lali, F. Y. Sabei, M. I. Irfan, M. Naeem-ul-Hassan, M. Sher, A. Y. Safhi, A. Alsalhi, A. H. Albariqi, F. Kamli, H. M. A. Amin and A. Abbas, *J. Environ. Chem. Eng.*, 2024, **12**, 112576.
187 A. Shah, S. Akhtar, F. Mahmood, S. Urooj, A. B. Siddique, M. I. Irfan, M. Naeem-ul-Hassan, M. Sher, A. Alhoshani, A. Rauf, H. M. A. Amin and A. Abbas, *Surf. Interfaces*, 2024, **51**, 104556.
188 N. Elahi, M. Kamali and M. H. Baghersad, *Talanta*, 2018, **184**, 537–556.
189 C. L. Nehl, H. Liao and J. H. Hafner, *Nano Lett.*, 2006, **6**, 683–688.
190 C. A. Foss, G. L. Hornyak, J. A. Stockert and C. R. Martin, *J. Phys. Chem.*, 1994, **98**, 2963–2971.
191 S. Zeng, K.-T. Yong, I. Roy, X.-Q. Dinh, X. Yu and F. Luan, *Plasmonics*, 2011, **6**, 491–506.
192 F. Yuan, H. Chen, J. Xu, Y. Zhang, Y. Wu and L. Wang, *Chem.–Eur. J.*, 2014, **20**, 2888–2894.
193 P. K. Jain, K. S. Lee, I. H. El-Sayed and M. A. El-Sayed, *J. Phys. Chem. B*, 2006, **110**, 7238–7248.
194 S. Eustis and M. A. El-Sayed, *Chem. Soc. Rev.*, 2006, **35**, 209–217.
195 Y. Zhang, I. D. McKelvie, R. W. Cattrall and S. D. Kolev, *Talanta*, 2016, **152**, 410–422.
196 S. C. B. Gopinath, T. Lakshmipriya and K. Awazu, *Biosens. Bioelectron.*, 2014, **51**, 115–123.
197 N. Xia, B. Zhou, N. Huang, M. Jiang, J. Zhang and L. Liu, *Biosens. Bioelectron.*, 2016, **85**, 625–632.
198 Y. Cho, S. S. Lee and J. H. Jung, *Analyst*, 2010, **135**, 1551.
199 K. Saha, S. S. Agasti, C. Kim, X. Li and V. M. Rotello, *Chem. Rev.*, 2012, **112**, 2739–2779.
200 M. I. Mishchenko and L. D. Travis, *Bull. Am. Meteorol. Soc.*, 2008, **89**, 1853–1862.
201 C. Fang, R. Dharmarajan, M. Megharaj and R. Naidu, *Trac. Trends Anal. Chem.*, 2017, **86**, 143–154.
202 G.-H. Chen, W.-Y. Chen, Y.-C. Yen, C.-W. Wang, H.-T. Chang and C.-F. Chen, *Anal. Chem.*, 2014, **86**, 6843–6849.
203 S. Link and M. A. El-Sayed, *J. Phys. Chem. B*, 1999, **103**, 4212–4217.
204 A. C. Templeton, J. J. Pietron, R. W. Murray and P. Mulvaney, *J. Phys. Chem. B*, 2000, **104**, 564–570.
205 K.-H. Su, Q.-H. Wei, X. Zhang, J. J. Mock, D. R. Smith and S. Schultz, *Nano Lett.*, 2003, **3**, 1087–1090.
206 S. Srivastava, B. L. Frankamp and V. M. Rotello, *Chem. Mater.*, 2005, **17**, 487–490.
207 P. N. Njoki, I.-I. S. Lim, D. Mott, H.-Y. Park, B. Khan, S. Mishra, R. Sujakumar, J. Luo and C.-J. Zhong, *J. Phys. Chem. C*, 2007, **111**, 14664–14669.
208 L. Polavarapu, J. Pérez-Juste, Q.-H. Xu and L. M. Liz-Marzán, *J. Mater. Chem. C*, 2014, **2**, 7460.
209 J. R. Reimers, M. J. Ford, S. M. Marcuccio, J. Ulstrup and N. S. Hush, *Nat. Rev. Chem.*, 2017, **1**, 0017.
210 Y. Chen, Y. Xianyu and X. Jiang, *Acc. Chem. Res.*, 2017, **50**, 310–319.
211 C. Couto, R. Vitorino and A. L. Daniel-da-Silva, *Crit. Rev. Biotechnol.*, 2017, **37**, 238–250.
212 R. Cao-Milán and L. M. Liz-Marzán, *Expet Opin. Drug Deliv.*, 2014, **11**, 741–752.
213 Y. Li, H. J. Schluesener and S. Xu, *Gold Bull.*, 2010, **43**, 29–41.
214 R. Sharma, K. V. Ragavan, M. S. Thakur and K. S. M. S. Raghavarao, *Biosens. Bioelectron.*, 2015, **74**, 612–627.
215 E. Morales-Narváez, H. Golmohammadi, T. Naghdi, H. Yousefi, U. Kostiv, D. Horák, N. Pourreza and A. Merkoçi, *ACS Nano*, 2015, **9**, 7296–7305.
216 Z. Luo, J. Zhang, Y. Wang, J. Chen, Y. Li and Y. Duan, *Sens. Actuators, B*, 2016, **236**, 474–479.
217 S.-H. Lo, M.-C. Wu, P. Venkatesan and S.-P. Wu, *Sens. Actuators, B*, 2015, **220**, 772–778.
218 G. Yue, S. Su, N. Li, M. Shuai, X. Lai, D. Astruc and P. Zhao, *Coord. Chem. Rev.*, 2016, **311**, 75–84.
219 Md. Nazmul Islam, S. Yadav, Md. Hakimul Haque, A. Munaz, F. Islam, M. S. Al Hossain, V. Gopalan, A. K. Lam, N.-T. Nguyen and M. J. A. Shiddiky, *Biosens. Bioelectron.*, 2017, **92**, 668–678.
220 H. Wang, H. Rao, M. Luo, X. Xue, Z. Xue and X. Lu, *Coord. Chem. Rev.*, 2019, **398**, 113003.
221 S.-I. Yeh, W.-F. Fang, C.-J. Huang, T.-M. Wang and J.-T. Yang, *J. Vis. Exp.*, 2016, **115**, e54424.
222 N. Sattarahmady, G. H. Tondro, M. Gholchin and H. Heli, *Biochem. Eng. J.*, 2015, **97**, 1–7.
223 I. A. Trantakis and S. J. Sturla, *Chem. Commun.*, 2014, **50**, 15517–15520.
224 C.-C. Chang, S.-C. Wei, T.-H. Wu, C.-H. Lee and C.-W. Lin, *Biosens. Bioelectron.*, 2013, **42**, 119–123.
225 C.-C. Chang, C.-Y. Chen, C.-P. Chen and C.-W. Lin, *Anal. Methods*, 2015, **7**, 29–33.
226 W. Bai, C. Zhu, J. Liu, M. Yan, S. Yang and A. Chen, *Environ. Toxicol. Chem.*, 2015, **34**, 2244–2249.
227 J. Du, B. Zhu, W. R. Leow, S. Chen, T. C. Sum, X. Peng and X. Chen, *Small*, 2015, **11**, 4104–4110.
228 S. Megarajan and A. Veerappan, *Opt. Mater.*, 2020, **108**, 110177.
229 R. De La Rica and M. M. Stevens, *Nat. Nanotechnol.*, 2012, **7**, 821–824.
230 M. Zayats, R. Baron, I. Popov and I. Willner, *Nano Lett.*, 2005, **5**, 21–25.
231 Y. Zhou and Z. Ma, *Sens. Actuators, B*, 2017, **241**, 1063–1068.
232 C. Lai, L. Qin, L. Chen, G.-M. Zeng, D.-L. Huang, C. Zhang, P. Xu and M. Cheng, *Int. J. Environ. Anal. Chem.*, 2017, **97**, 71–84.

233 D. Liu, J. Yang, H.-F. Wang, Z. Wang, X. Huang, Z. Wang, G. Niu, A. R. Hight Walker and X. Chen, *Anal. Chem.*, 2014, **86**, 5800–5806.
234 J. H. Soh, Y. Lin, S. Rana, J. Y. Ying and M. M. Stevens, *Anal. Chem.*, 2015, **87**, 7644–7652.
235 Y. Zhao, L. Gui and Z. Chen, *Sens. Actuators, B*, 2017, **241**, 262–267.
236 L. Shen, J. Chen, N. Li, P. He and Z. Li, *Anal. Chim. Acta*, 2014, **839**, 83–90.
237 Y. Wang, N. S. Reddy Satyavolu and Y. Lu, *Curr. Opin. Colloid Interface Sci.*, 2018, **38**, 158–169.
238 L. H. Tan, Y. Yue, N. S. R. Satyavolu, A. S. Ali, Z. Wang, Y. Wu and Y. Lu, *J. Am. Chem. Soc.*, 2015, **137**, 14456–14464.
239 Z. Gao, K. Deng, X.-D. Wang, M. Miró and D. Tang, *ACS Appl. Mater. Interfaces*, 2014, **6**, 18243–18250.
240 C.-C. Chang, C.-P. Chen, T.-H. Wu, C.-H. Yang, C.-W. Lin and C.-Y. Chen, *Nanomaterials*, 2019, **9**, 861.
241 X. Ma, Z. Guo, Z. Mao, Y. Tang and P. Miao, *Microchim. Acta*, 2018, **185**, 33.
242 G. Z. Tsogas, F. A. Kappi, A. G. Vlessidis and D. L. Giokas, *Anal. Lett.*, 2018, **51**, 443–468.
243 H. Häkkinen, *Nat. Chem.*, 2012, **4**, 443–455.
244 D. Liu, Z. Wang and X. Jiang, *Nanoscale*, 2011, **3**, 1421.
245 P. Liu, L. Han, F. Wang, V. A. Petrenko and A. Liu, *Biosens. Bioelectron.*, 2016, **82**, 195–203.
246 B. Sajjanar, B. Kakodia, D. Bisht, S. Saxena, A. K. Singh, V. Joshi, A. K. Tiwari and S. Kumar, *J. Nanoparticle Res.*, 2015, **17**, 234.
247 A. Parnsubsakul, S. Oaew and W. Surareungchai, *Nanoscale*, 2018, **10**, 5466–5473.
248 R. Chandrawati and M. M. Stevens, *Chem. Commun.*, 2014, **50**, 5431.
249 G. Liu, X. Yang, T. Li, H. Yu, X. Du, Y. She, J. Wang, S. Wang, F. Jin, M. Jin, H. Shao, L. Zheng, Y. Zhang and P. Zhou, *Microchim. Acta*, 2015, **182**, 1983–1989.
250 N. Gao, P. Huang and F. Wu, *Spectrochim. Acta, Part A*, 2018, **192**, 174–180.
251 G. Wang, Y. Akiyama, S. Shiraishi, N. Kanayama, T. Takarada and M. Maeda, *Bioconjug. Chem.*, 2017, **28**, 270–277.
252 C. McVey, F. Huang, C. Elliott and C. Cao, *Biosens. Bioelectron.*, 2017, **92**, 502–508.
253 H. S. Aldewachi, N. Woodroofe, S. Turega and P. H. E. Gardiner, *Talanta*, 2017, **169**, 13–19.
254 H. Aldewachi, N. Woodroofe and P. Gardiner, *Appl. Sci.*, 2018, **8**, 2589.
255 S. Liu, Z. Du, P. Li and F. Li, *Biosens. Bioelectron.*, 2012, **35**, 443–446.
256 F. Sang, X. Zhang, J. Liu, S. Yin and Z. Zhang, *Spectrochim. Acta, Part A*, 2019, **217**, 122–127.
257 H.-H. Deng, C.-L. Wu, A.-L. Liu, G.-W. Li, W. Chen and X.-H. Lin, *Sens. Actuators, B*, 2014, **191**, 479–484.
258 X. Ma, X. Kou, Y. Xu, D. Yang and P. Miao, *Nanoscale Adv.*, 2019, **1**, 486–489.
259 S. Wang, Z. Chen, L. Chen, R. Liu and L. Chen, *Analyst*, 2013, **138**, 2080.
260 G. Weng, X. Dong, J. Zhao, J. Li, J. Zhu and J. Zhao, *J. Nanoparticle Res.*, 2018, **20**, 256.
261 J. Wang, H. Z. Zhang, J. J. Liu, D. Yuan, R. S. Li and C. Z. Huang, *Analyst*, 2018, **143**, 824–828.
262 C. J. Murphy, L. B. Thompson, A. M. Alkilany, P. N. Sisco, S. P. Boulos, S. T. Sivapalan, J. A. Yang, D. J. Chernak and J. Huang, *J. Phys. Chem. Lett.*, 2010, **1**, 2867–2875.
263 Z. Zhang, Z. Chen, D. Pan and L. Chen, *Langmuir*, 2015, **31**, 643–650.
264 Z. Zhang, Z. Chen, F. Cheng, Y. Zhang and L. Chen, *Analyst*, 2016, **141**, 2955–2961.
265 Y.-Y. Chen, H.-T. Chang, Y.-C. Shiang, Y.-L. Hung, C.-K. Chiang and C.-C. Huang, *Anal. Chem.*, 2009, **81**, 9433–9439.
266 G. Weng, J. Li, J. Zhu and J. Zhao, *J. Nanoparticle Res.*, 2014, **16**, 2728.
267 L. Saa, M. Coronado-Puchau, V. Pavlov and L. M. Liz-Marzán, *Nanoscale*, 2014, **6**, 7405–7409.
268 J. Guo, D. Huo, M. Yang, C. Hou, J. Li, H. Fa, H. Luo and P. Yang, *Talanta*, 2016, **161**, 819–825.
269 S. Wu, D. Li, J. Wang, Y. Zhao, S. Dong and X. Wang, *Sens. Actuators, B*, 2017, **238**, 427–433.
270 F.-M. Li, J.-M. Liu, X.-X. Wang, L.-P. Lin, W.-L. Cai, X. Lin, Y.-N. Zeng, Z.-M. Li and S.-Q. Lin, *Sens. Actuators, B*, 2011, **155**, 817–822.
271 Q. Zhu, J. Wu, J. Zhao and W. Ni, *Langmuir*, 2015, **31**, 4072–4077.
272 J. S. DuChene, W. Niu, J. M. Abendroth, Q. Sun, W. Zhao, F. Huo and W. D. Wei, *Chem. Mater.*, 2013, **25**, 1392–1399.
273 G. Weng, X. Dong, J. Li and J. Zhao, *J. Mater. Sci.*, 2016, **51**, 7678–7690.
274 X. Cheng, Y. Huang, C. Yuan, K. Dai, H. Jiang and J. Ma, *Sens. Actuators, B*, 2019, **282**, 838–843.
275 Q. Zhong, Y. Chen, X. Qin, Y. Wang, C. Yuan and Y. Xu, *Microchim. Acta*, 2019, **186**, 161.
276 S. Sun, M. Gao, G. Lei, H. Zou, J. Ma and C. Huang, *Nano Res.*, 2016, **9**, 1125–1134.
277 S. Wu, D. Li, Z. Gao and J. Wang, *Microchim. Acta*, 2017, **184**, 4383–4391.
278 Z. Zhang, Z. Chen and L. Chen, *Langmuir*, 2015, **31**, 9253–9259.
279 J. Guo, D. Huo, M. Yang, C. Hou, J. Li, H. Fa, H. Luo and P. Yang, *Talanta*, 2016, **161**, 819–825.
280 W. Liu, L. Tian, J. Du, J. Wu, Y. Liu, G. Wu and X. Lu, *Analyst*, 2020, **145**, 5500–5507.
281 R. Das, A. Dhiman, A. Kapil, V. Bansal and T. K. Sharma, *Anal. Bioanal. Chem.*, 2019, **411**, 1229–1238.
282 Y. Xu, C. Lu, Y. Sun, Y. Shao, Y. Cai, Y. Zhang, J. Miao and P. Miao, *Microchim. Acta*, 2018, **185**, 548.
283 J. Lou-Franco, B. Das, C. Elliott and C. Cao, *Nano-Micro Lett.*, 2021, **13**, 10.
284 D. Zhao, C. Chen, L. Lu, F. Yang and X. Yang, *Sens. Actuators, B*, 2015, **215**, 437–444.
285 Y. Liu, C. Wang, N. Cai, S. Long and F. Yu, *J. Mater. Sci.*, 2014, **49**, 7143–7150.
286 Y. Jv, B. Li and R. Cao, *Chem. Commun.*, 2010, **46**, 8017.

287 H. Cui, Z.-F. Zhang, M.-J. Shi, Y. Xu and Y.-L. Wu, *Anal. Chem.*, 2005, **77**, 6402–6406.
288 Z. Zhang, A. Berg, H. Levanon, R. W. Fessenden and D. Meisel, *J. Am. Chem. Soc.*, 2003, **125**, 7959–7963.
289 A. Henglein, *J. Phys. Chem.*, 1993, **97**, 5457–5471.
290 J. Shah, R. Purohit, R. Singh, A. S. Karakoti and S. Singh, *J. Colloid Interface Sci.*, 2015, **456**, 100–107.
291 Y. Zhao, Y. Huang, H. Zhu, Q. Zhu and Y. Xia, *J. Am. Chem. Soc.*, 2016, **138**, 16645–16654.
292 Z. Chen, L. Tan, L. Hu, Y. Zhang, S. Wang and F. Lv, *ACS Appl. Mater. Interfaces*, 2016, **8**, 102–108.
293 C.-T. Kung, C.-Y. Hou, Y.-N. Wang and L.-M. Fu, *Sens. Actuators, B*, 2019, **301**, 126855.
294 J. Briffa, E. Sinagra and R. Blundell, *Heliyon*, 2020, **6**, e04691.
295 J. Zhang, Y. Wang, X. Xu and X. Yang, *Analyst*, 2011, **136**, 3865.
296 Z. Chen, J. Guo, H. Ma, T. Zhou and X. Li, *Anal. Methods*, 2014, **6**, 8018–8021.
297 M. Naderi, M. Hosseini and M. R. Ganjali, *Spectrochim. Acta, Part A*, 2018, **195**, 75–83.
298 J. Qiu, L. Fu, H. Wang, R. Zou, Y. Zhang, X. Li and A. Wu, *New J. Chem.*, 2020, **44**, 2241–2246.
299 P. Duenchay, O. Chailapakul and W. Siangproh, *Int. J. Mol. Sci.*, 2019, **20**, 2954.
300 L.-Y. Bai, Y.-P. Zhang, N. Chen, J. Chen, X.-M. Zhou and L.-F. Hu, *Nano-Micro Lett.*, 2011, **6**, 337–341.
301 P. B. Tchounwou, C. G. Yedjou, A. K. Patlolla and D. J. Sutton, in *Molecular, Clinical and Environmental Toxicology*, ed. A. Luch, Springer Basel, Basel, 2012, vol. 101, pp. 133–164.
302 M. Jaishankar, T. Tseten, N. Anbalagan, B. B. Mathew and K. N. Beeregowda, *Interdiscip. Toxicol.*, 2014, **7**, 60–72.
303 S. Ali, X. Chen, W. Shi, G. Huang, L. Yuan, L. Meng, S. Chen, X. Zhonghao and X. Chen, *Crit. Rev. Anal. Chem.*, 2023, **53**, 718–750.
304 L. Zhang, D. Huang, G. Yue, J. Zhu, L. Yang, L. Yang, W. Dan and P. Zhao, *Chem. Phys. Lett.*, 2021, **784**, 139101.
305 F. Chai, C. Wang, T. Wang, L. Li and Z. Su, *ACS Appl. Mater. Interfaces*, 2010, **2**, 1466–1470.
306 A. M. S. Mendes, G. P. Duda, C. W. A. D. Nascimento and M. O. Silva, *Agric. Sci.*, 2006, **63**, 328–332.
307 Y. Gan, T. Liang, Q. Hu, L. Zhong, X. Wang, H. Wan and P. Wang, *Talanta*, 2020, **208**, 120231.
308 Y. Qi, J. Ma, F.-R. Xiu and X. Gao, *Microchim. Acta*, 2021, **188**, 273.
309 Z. Zhou, Y. Zhang, J. Kang, C. Dong, N. Chen, X. Li, Z. Guo and A. Wu, *Anal. Methods*, 2017, **9**, 2890–2896.
310 R. Gunupuru, D. Maity, G. R. Bhadu, A. Chakraborty, D. N. Srivastava and P. Paul, *J. Chem. Sci.*, 2014, **126**, 627–635.
311 Y. Kim, R. C. Johnson and J. T. Hupp, *Nano Lett.*, 2001, **1**, 165–167.
312 K. Yoosaf, B. I. Ipe, C. H. Suresh and K. G. Thomas, *J. Phys. Chem. C*, 2007, **111**, 12839–12847.
313 J. Wang, X. Fang, X. Cui, Y. Zhang, H. Zhao, X. Li and Y. He, *Talanta*, 2018, **188**, 266–272.
314 J. R. Bhamore, A. R. Gul, S. K. Kailasa, K.-W. Kim, J. S. Lee, H. Park and T. J. Park, *Sens. Actuators, B*, 2021, **334**, 129685.
315 Y. Xue, H. Zhao, Z. Wu, X. Li, Y. He and Z. Yuan, *Analyst*, 2011, **136**, 3725.
316 Y. Guo, Y. Zhang, H. Shao, Z. Wang, X. Wang and X. Jiang, *Anal. Chem.*, 2014, **86**, 8530–8534.
317 W. Jin, P. Huang, G. Wei, Y. Cao and F. Wu, *Sens. Actuators, B*, 2016, **233**, 223–229.
318 N. Zohora, D. Kumar, M. Yazdani, V. M. Rotello, R. Ramanathan and V. Bansal, *Colloids Surf., A*, 2017, **532**, 451–457.
319 X. Liu, X. Cheng, T. Bing, C. Fang and D. Shangguan, *Anal. Sci.*, 2010, **26**, 1169–1172.
320 A. Mohamed, X. Li, C. Li, X. Li, C. Yuan and H. Barakat, *Appl. Sci.*, 2021, **11**, 10894.
321 S. Y. Ejeta and T. Imae, *Anal. Chim. Acta*, 2021, **1152**, 338272.
322 M. Shellaiah, N. Thirumalaivasan, K. W. Sun and S.-P. Wu, *Microchem. J.*, 2021, **160**, 105754.
323 S.-J. Yoon, Y.-S. Nam, Y. Lee, I. H. Oh and K.-B. Lee, *RSC Adv.*, 2021, **11**, 5456–5465.
324 A. Hyder, J. A. Buledi, M. Nawaz, D. B. Rajpar, Z.-H. Shah, Y. Orooji, M. L. Yola, H. Karimi-Maleh, H. Lin and A. R. Solangi, *Environ. Res.*, 2022, **205**, 112475.
325 T. Lou, L. Chen, Z. Chen, Y. Wang, L. Chen and J. Li, *ACS Appl. Mater. Interfaces*, 2011, **3**, 4215–4220.
326 R. Liu, Z. Chen, S. Wang, C. Qu, L. Chen and Z. Wang, *Talanta*, 2013, **112**, 37–42.
327 A. Safavi, R. Ahmadi and Z. Mohammadpour, *Sens. Actuators, B*, 2017, **242**, 609–615.
328 E. Priyadarshini, N. Pradhan, P. K. Panda and B. K. Mishra, *Biosens. Bioelectron.*, 2015, **68**, 598–603.
329 M. Rogosnitzky and S. Branch, *BioMetals*, 2016, **29**, 365–376.
330 K. Park, J. Park, H. Lee, J. Choi, W.-J. Yu and J. Lee, *Arch Pharm. Res.*, 2018, **41**, 1108–1116.
331 B. He, J. Wang, J. Lin, J. Chen, Z. Zhuang, Y. Hong, L. Yan, L. Lin, B. Shi, Y. Qiu, L. Pan, X. Zheng, F. Liu and F. Chen, *Front. Public Health*, 2021, **9**, 647120.
332 C. E. Lisowski and J. E. Hutchison, *Anal. Chem.*, 2009, **81**, 10246–10253.
333 R. M. Pallares, K. P. Carter, S. E. Zeltmann, T. Tratnjek, A. M. Minor and R. J. Abergel, *Inorg. Chem.*, 2020, **59**, 2030–2036.
334 A. Ducatman, M. Luster and T. Fletcher, *Environ. Toxicol. Pharmacol.*, 2021, **85**, 103650.
335 R. Martínez-Máñez and F. Sancenón, *Chem. Rev.*, 2003, **103**, 4419–4476.
336 F. P. Schmidtchen and M. Berger, *Chem. Rev.*, 1997, **97**, 1609–1646.
337 M. Sepahvand, F. Ghasemi and H. M. Seyed Hosseini, *Food Chem. Toxicol.*, 2021, **149**, 112025.
338 F. Mamatioğlu, A. Üzer, E. Erçağ and R. Apak, *Talanta*, 2021, **226**, 122187.
339 S. Plaisen, W. Cheewasedtham and T. Rujiralai, *RSC Adv.*, 2018, **8**, 21566–21576.

340 W. Liu, Z. Du, Y. Qian and F. Li, *Sens. Actuators, B*, 2013, **176**, 927–931.
341 M. H. Kim, S. Kim, H. H. Jang, S. Yi, S. H. Seo and M. S. Han, *Tetrahedron Lett.*, 2010, **51**, 4712–4716.
342 V. L. Zikankuba, G. Mwanyika, J. E. Ntwenya and A. James, *Cogent Food Agric.*, 2019, **5**, 1601544.
343 R. Bala, R. K. Sharma and N. Wangoo, *Sens. Actuators, B*, 2015, **210**, 425–430.
344 D. Li, S. Wang, L. Wang, H. Zhang and J. Hu, *Anal. Bioanal. Chem.*, 2019, **411**, 2645–2652.
345 Y. Ma, H. Jiang, C. Shen, Ch. Hou, D. Huo, H. Wu and M. Yang, *J. Appl. Spectrosc.*, 2017, **84**, 460–465.
346 G. Liu, X. Yang, T. Li, H. Yu, X. Du, Y. She, J. Wang, S. Wang, F. Jin, M. Jin, H. Shao, L. Zheng, Y. Zhang and P. Zhou, *Microchim. Acta*, 2015, **182**, 1983–1989.
347 K. M. Giannoulis, D. L. Giokas, G. Z. Tsogas and A. G. Vlessidis, *Talanta*, 2014, **119**, 276–283.
348 G. Liu, X. Huang, S. Zheng, L. Li, D. Xu, X. Xu, Y. Zhang and H. Lin, *Dyes Pigments*, 2018, **149**, 229–235.
349 X. Zhang, Z. Sun, Z. Cui and H. Li, *Sens. Actuators, B*, 2014, **191**, 313–319.
350 J. Liu, W. Bai, C. Zhu, M. Yan, S. Yang and A. Chen, *Analyst*, 2015, **140**, 3064–3069.
351 G. Liu, R. Zhang, L. Li, X. Huang, T. Li, M. Lu, D. Xu and J. Wang, *Nanomaterials*, 2018, **8**, 499.
352 G. Liu, R. Zhang, X. Huang, L. Li, N. Liu, J. Wang and D. Xu, *Sensors*, 2018, **18**, 1595.
353 F. C. O. L. Martins, M. A. Sentanin and D. De Souza, *Food Chem.*, 2019, **272**, 732–750.
354 D. Xiao, Y. Jiang and Y. Bi, *Microchim. Acta*, 2018, **185**, 247.
355 W. Zhang and J. Xue, *Food Control*, 2016, **67**, 192–198.
356 X. Cui, T. Wei, M. Hao, Q. Qi, H. Wang and Z. Dai, *J. Hazard. Mater.*, 2020, **391**, 122217.
357 J. Du, Q. Shao, S. Yin, L. Jiang, J. Ma and X. Chen, *Small*, 2012, **8**, 3412–3416.
358 H. Wang, X. Guo, S. Fu, T. Yang, Y. Wen and H. Yang, *Food Chem.*, 2015, **188**, 137–142.
359 Q. Yang, Y. Wang, J. Wang, F. Liu, N. Hu, H. Pei, W. Yang, Z. Li, Y. Suo and J. Wang, *Food Chem.*, 2018, **254**, 241–248.
360 C. Zhang, G. Li and Z. Zhang, *J. Chromatogr., A*, 2015, **1419**, 1–9.
361 P. Kanthale, A. Kumar, N. Upadhyay, D. Lal, G. Rathod and V. Sharma, *J. Food Sci. Technol.*, 2015, **52**, 1698–1704.
362 X. Lin, W. Hasi, X. Lou, S. Lin, F. Yang, B. Jia, Y. Cui, D. Ba, D. Lin and Z. Lu, *J. Raman Spectrosc.*, 2014, **45**, 162–167.
363 J. Song, P.-C. Huang, Y.-Q. Wan and F.-Y. Wu, *Sens. Actuators, B*, 2016, **222**, 790–796.
364 L. Li, M. Zhang and W. Chen, *J. Food Drug Anal.*, 2020, **28**, 642–654.
365 H. Guan, J. Yu and D. Chi, *Food Control*, 2013, **32**, 35–41.
366 W. Chen, H.-H. Deng, L. Hong, Z.-Q. Wu, S. Wang, A.-L. Liu, X.-H. Lin and X.-H. Xia, *Analyst*, 2012, **137**, 5382.
367 C. Xiao, X. Zhang, J. Liu, A. Yang, H. Zhao, X. Li, Y. He and Z. Yuan, *Anal. Methods*, 2015, **7**, 924–929.
368 J. Xin, L. Zhang, D. Chen, K. Lin, H. Fan, Y. Wang and C. Xia, *Food Chem.*, 2015, **174**, 473–479.
369 P. Wang, X. Su, L. Shi and Y. Yuan, *Microchim. Acta*, 2016, **183**, 2899–2905.
370 Y. Xiong, M. Li, H. Liu, Z. Xuan, J. Yang and D. Liu, *Nanoscale*, 2017, **9**, 1811–1815.
371 P. Kumar, P. Ramulu Lambadi and N. Kumar Navani, *Biosens. Bioelectron.*, 2015, **72**, 340–347.
372 P. Kumar, P. Kumar, S. Manhas and N. K. Navani, *Sens. Actuators, B*, 2016, **233**, 157–161.
373 S.-R. Park, S.-J. Park, M.-J. Jeong, J. C. Choi and M. Kim, *Chemosphere*, 2018, **203**, 300–306.
374 F. Sun, L. Kang, X. Xiang, H. Li, X. Luo, R. Luo, C. Lu and X. Peng, *Anal. Bioanal. Chem.*, 2016, **408**, 6913–6927.
375 E.-H. Lee, S. K. Lee, M. J. Kim and S.-W. Lee, *Food Chem.*, 2019, **287**, 205–213.
376 D. deCatanzaro, *Horm. Behav.*, 2015, **68**, 103–116.
377 M. Adeel, X. Song, Y. Wang, D. Francis and Y. Yang, *Environ. Int.*, 2017, **99**, 107–119.
378 D. Zhang, W. Zhang, J. Ye, S. Zhan, B. Xia, J. Lv, H. Xu, G. Du and L. Wang, *Aust. J. Chem.*, 2016, **69**, 12.
379 P. S. Mead, L. Slutsker, V. Dietz, L. F. McCaig, J. S. Bresee, C. Shapiro, P. M. Griffin and R. V. Tauxe, *Emerg. Infect. Dis.*, 1999, **5**, 607–625.
380 Z. Fu, X. Zhou and D. Xing, *Methods*, 2013, **64**, 260–266.
381 J. Du, Z. Yu, Z. Hu, J. Chen, J. Zhao and Y. Bai, *J. Microbiol. Methods*, 2021, **180**, 106110.
382 Y. Xie, Y. Huang, J. Li and J. Wu, *Sens. Actuators, B*, 2021, **339**, 129865.
383 S. Yao, J. Li, B. Pang, X. Wang, Y. Shi, X. Song, K. Xu, J. Wang and C. Zhao, *Microchim. Acta*, 2020, **187**, 504.
384 S.-H. Park and Y. You, *Foods*, 2023, **13**, 95.
385 Y. J. Sung, H.-J. Suk, H. Y. Sung, T. Li, H. Poo and M.-G. Kim, *Biosens. Bioelectron.*, 2013, **43**, 432–439.
386 N. Amin, A. S. Torralba, R. Álvarez-Diduk, A. Afkhami and A. Merkoçi, *Anal. Chem.*, 2020, **92**, 4209–4216.
387 N. A. Byzova, A. V. Zherdev, A. A. Gorbatov, A. G. Shevyakov, S. F. Biketov and B. B. Dzantiev, *Micromachines*, 2022, **13**, 2194.
388 C. Cao, L. C. Gontard, L. L. Thuy Tram, A. Wolff and D. D. Bang, *Small*, 2011, **7**, 1701–1708.
389 S. M. Shawky, D. Bald and H. M. E. Azzazy, *Clin. Biochem.*, 2010, **43**, 1163–1168.
390 P. Wang, G. Yu, J. Wei, X. Liao, Y. Zhang, Y. Ren, C. Zhang, Y. Wang, D. Zhang, J. Wang and Y. Wang, *J. Hazard. Mater.*, 2023, **443**, 130157.
391 Y. Guo, J. Li, X. Song, K. Xu, J. Wang and C. Zhao, *ACS Appl. Bio Mater.*, 2021, **4**, 420–427.
392 X. X. Li, C. Cao, S. J. Han and S. J. Sim, *Water Res.*, 2009, **43**, 1425–1431.
393 R. Guo, F. Huang, G. Cai, L. Zheng, L. Xue, Y. Li, M. Liao, M. Wang and J. Lin, *Microchim. Acta*, 2020, **187**, 197.
394 Y. Man, M. Ban, A. Li, X. Jin, Y. Du and L. Pan, *Food Chem.*, 2021, **354**, 129578.
395 J. Singh and A. Mehta, *Food Sci. Nutr.*, 2020, **8**, 2183–2204.
396 S. H. Jalalian, P. Lavaee, M. Ramezani, N. M. Danesh, M. Alibolandi, K. Abnous and S. M. Taghdisi, *Spectrochim. Acta, Part A*, 2021, **246**, 119062.

397 Y. Luan, J. Chen, C. Li, G. Xie, H. Fu, Z. Ma and A. Lu, *Toxins*, 2015, **7**, 5377–5385.
398 W. Zhang, Y. Wang, M. Nan, Y. Li, J. Yun, Y. Wang and Y. Bi, *Food Chem.*, 2021, **348**, 129128.
399 K. Xing, J. Peng, W. Chen, B. Fang, D. Liu, S. Shan, G. Zhang, Y. Huang and W. Lai, *Food Chem.*, 2022, **370**, 131365.
400 Y. Zhang, S. Hou, H. Song, X. Luo, D. Wu, F. Zheng, W. Liu and S. Ji, *Food Control*, 2022, **136**, 108887.
401 J. Chen, J. Wen, L. Zhuang and S. Zhou, *Nanoscale*, 2016, **8**, 9791–9797.
402 G. Battacone, A. Nudda, A. Cannas, A. C. Borlino, G. Bomboi and G. Pulina, *J. Dairy Sci.*, 2003, **86**, 2667–2675.
403 N. Unusan, *Food Chem. Toxicol.*, 2006, **44**, 1897–1900.
404 V. Sharma, B. Javed, H. J. Byrne and F. Tian, *Biosensors*, 2024, **14**, 491.
405 W. Zhu, L. Li, Z. Zhou, X. Yang, N. Hao, Y. Guo and K. Wang, *Food Chem.*, 2020, **319**, 126544.
406 X. Wang, R. Niessner and D. Knopp, *Sensors*, 2014, **14**, 21535–21548.
407 J. Lerdsri, W. Chananchana, J. Upan, T. Sridara and J. Jakmunee, *Sens. Actuators, B*, 2020, **320**, 128356.
408 I. I. Althagafi, S. A. Ahmed and W. A. El-Said, *Spectrochim. Acta, Part A*, 2021, **246**, 118999.
409 S. Sun, R. Zhao, S. Feng and Y. Xie, *Microchim. Acta*, 2018, **185**, 535.
410 W.-B. Shim, K.-Y. Kim and D.-H. Chung, *J. Agric. Food Chem.*, 2009, **57**, 4035–4041.
411 L. Zhang, J. Chen, L. Lu, R. Yu and D. Zhang, *Food Chem.: X*, 2023, **19**, 100792.
412 J. A. Ludwig and J. N. Weinstein, *Nat. Rev. Cancer*, 2005, **5**, 845–856.
413 P. Cairns, *Nat. Rev. Cancer*, 2007, **7**, 531–543.
414 K.-Y. Lien and G.-B. Lee, *Analyst*, 2010, **135**, 1499.
415 A. A. Martí, S. Jockusch, N. Stevens, J. Ju and N. J. Turro, *Acc. Chem. Res.*, 2007, **40**, 402–409.
416 A. Sassolas, B. D. Leca-Bouvier and L. J. Blum, *Chem. Rev.*, 2008, **108**, 109–139.
417 C. S. Thaxton, D. G. Georganopoulou and C. A. Mirkin, *Clin. Chim. Acta*, 2006, **363**, 120–126.
418 K. Sato, K. Hosokawa and M. Maeda, *Anal. Sci.*, 2007, **23**, 17–20.
419 Y. Liu, Z. Wu, G. Zhou, Z. He, X. Zhou, A. Shen and J. Hu, *Chem. Commun.*, 2012, **48**, 3164.
420 *Spherical Nucleic Acids*, ed. C. A. Mirkin, Jenny Stanford Publishing, Singapore, 2020.
421 R. A. Reynolds, C. A. Mirkin and R. L. Letsinger, *J. Am. Chem. Soc.*, 2000, **122**, 3795–3796.
422 R. A. Reynolds, C. A. Mirkin and R. L. Letsinger, *Pure Appl. Chem.*, 2000, **72**, 229–235.
423 R. Elghanian, J. J. Storhoff, R. C. Mucic, R. L. Letsinger and C. A. Mirkin, *Science*, 1997, **277**, 1078–1081.
424 K. Sato, K. Hosokawa and M. Maeda, *J. Am. Chem. Soc.*, 2003, **125**, 8102–8103.
425 C. L. Schofield, A. H. Haines, R. A. Field and D. A. Russell, *Langmuir*, 2006, **22**, 6707–6711.
426 S. Watanabe, K. Yoshida, K. Shinkawa, D. Kumagawa and H. Seguchi, *Colloids Surf., B*, 2010, **81**, 570–577.
427 B.-H. Kim, I. S. Yoon and J.-S. Lee, *Anal. Chem.*, 2013, **85**, 10542–10548.
428 Y.-M. Chen, C.-J. Yu, T.-L. Cheng and W.-L. Tseng, *Langmuir*, 2008, **24**, 3654–3660.
429 Z. Huang, H. Wang and W. Yang, *ACS Appl. Mater. Interfaces*, 2015, **7**, 8990–8998.
430 Z. Huang, H. Wang and W. Yang, *ACS Appl. Mater. Interfaces*, 2015, **7**, 8990–8998.
431 C. Guarise, L. Pasquato, V. De Filippis and P. Scrimin, *Proc. Natl. Acad. Sci. U. S. A.*, 2006, **103**, 3978–3982.
432 A. Laromaine, L. Koh, M. Murugesan, R. V. Ulijn and M. M. Stevens, *J. Am. Chem. Soc.*, 2007, **129**, 4156–4157.
433 M. N. Costa, B. Veigas, J. M. Jacob, D. S. Santos, J. Gomes, P. V. Baptista, R. Martins, J. Inácio and E. Fortunato, *Nanotechnology*, 2014, **25**, 094006.
434 X. Chen, J. Chen, F. Wang, X. Xiang, M. Luo, X. Ji and Z. He, *Biosens. Bioelectron.*, 2012, **35**, 363–368.
435 S. Liu, W. Su and X. Ding, *Sensors*, 2016, **16**, 2086.
436 M. L. Firdaus, E. Saputra, S. M. Ginting, S. Wyantuti, D. R. Eddy, L. Rahmidar and B. Yuliarto, *Sens. Bio-Sens. Res.*, 2022, **35**, 100472.
437 N. J. Lang, B. Liu and J. Liu, *J. Colloid Interface Sci.*, 2014, **428**, 78–83.
438 Y. Gao, Y. Wu and J. Di, *Spectrochim. Acta, Part A*, 2017, **173**, 207–212.
439 T. Cai, Y. Gao, J. Yan, Y. Wu and J. Di, *RSC Adv.*, 2017, **7**, 29122–29128.
440 X. Zhang, M. Wei, B. Lv, Y. Liu, X. Liu and W. Wei, *RSC Adv.*, 2016, **6**, 35001–35007.
441 S. Xu, L. Jiang, Y. Liu, P. Liu, W. Wang and X. Luo, *Anal. Chim. Acta*, 2019, **1071**, 53–58.
442 Y. Chen and H. Guan, *Spectrochim. Acta, Part A*, 2025, **329**, 125523.
443 Y. Jiang, H. Zhao, Y. Lin, N. Zhu, Y. Ma and L. Mao, *Angew. Chem.*, 2010, **122**, 4910–4914.
444 S. K. Kailasa, J. R. Koduru, M. L. Desai, T. J. Park, R. K. Singhal and H. Basu, *Trac. Trends Anal. Chem.*, 2018, **105**, 106–120.
445 N. Yusoff, A. Pandikumar, R. Ramaraj, H. N. Lim and N. M. Huang, *Microchim. Acta*, 2015, **182**, 2091–2114.
446 J.-J. Feng, H. Guo, Y.-F. Li, Y.-H. Wang, W.-Y. Chen and A.-J. Wang, *ACS Appl. Mater. Interfaces*, 2013, **5**, 1226–1231.
447 R. Baron, M. Zayats and I. Willner, *Anal. Chem.*, 2005, **77**, 1566–1571.
448 M. Yarbakht and M. Nikkhah, *J. Exp. Nanosci.*, 2016, **11**, 593–601.
449 V. Selvaraj and M. Alagar, *Int. J. Pharm.*, 2007, **337**, 275–281.
450 S. K. Menon, B. R. Mistry, K. V. Joshi, P. G. Sutariya and R. V. Patel, *Spectrochim. Acta, Part A*, 2012, **94**, 235–242.
451 N. Uehara, K. Ookubo and T. Shimizu, *Langmuir*, 2010, **26**, 6818–6825.
452 L. Liu, S. Li, L. Liu, D. Deng and N. Xia, *Analyst*, 2012, **137**, 3794.
453 H. Su, B. Sun, L. Chen, Z. Xu and S. Ai, *Anal. Methods*, 2012, **4**, 3981.

454 Z. Chen, G. Zhang, X. Chen, J. Chen, J. Liu and H. Yuan, *Biosens. Bioelectron.*, 2013, **41**, 844–847.
455 Z. Li, S. Bi, T. Wang, Y. Wang, H. Zhou and J. Wu, *Luminescence*, 2017, **32**, 502–508.
456 B. K. Jena and C. R. Raj, *Biosens. Bioelectron.*, 2008, **23**, 1285–1290.
457 S. Bi, T. Wang, Y. Wang, T. Zhao and H. Zhou, *Spectrochim. Acta, Part A*, 2015, **135**, 1074–1079.
458 M. Bahram, F. Hoseinzadeh, K. Farhadi, M. Saadat, P. Najafi-Moghaddam and A. Afkhami, *Colloids Surf., A*, 2014, **441**, 517–524.
459 Z. Hu, M. Xie, D. Yang, D. Chen, J. Jian, H. Li, K. Yuan, Z. Jiang and H. Zhou, *RSC Adv.*, 2017, **7**, 34746–34754.
460 J. D. G. McEvoy, *Anal. Chim. Acta*, 2002, **473**, 3–26.
461 J. Zhou, Y. Li, W. Wang, Z. Lu, H. Han and J. Liu, *Langmuir*, 2020, **36**, 11490–11498.
462 X. Zhou, L. Wang, G. Shen, D. Zhang, J. Xie, A. Mamut, W. Huang and S. Zhou, *Microchim. Acta*, 2018, **185**, 355.
463 Z. Zhang, Y. Tian, P. Huang and F.-Y. Wu, *Talanta*, 2020, **208**, 120342.
464 D. A. Raja, S. G. Musharraf, M. R. Shah, A. Jabbar, M. I. Bhanger and M. I. Malik, *J. Ind. Eng. Chem.*, 2020, **87**, 180–186.
465 S. Khurana, S. Kukreti and M. Kaushik, *Spectrochim. Acta, Part A*, 2021, **246**, 119039.
466 Y.-Y. Wu, P. Huang and F.-Y. Wu, *Food Chem.*, 2020, **304**, 125377.
467 H. S. Santos, G. M. De França, E. C. Romani, D. G. Larrudé, A. L. M. C. Da Cunha, R. Q. Aucélio and A. R. Da Silva, *Microchem. J.*, 2014, **116**, 206–215.
468 Q. Ma, Y. Wang, J. Jia and Y. Xiang, *Food Chem.*, 2018, **249**, 98–103.
469 W. Huang, Y. Wang, L. Wang, C. Pan and G. Shen, *Anal. Methods*, 2021, **13**, 90–98.
470 R. Su, J. Xu, Y. Luo, Y. Li, X. Liu, J. Bie and C. Sun, *Mater. Lett.*, 2016, **180**, 31–34.
471 J. C. Gukowsky, C. Tan, Z. Han and L. He, *J. Food Sci.*, 2018, **83**, 1631–1638.
472 T. Delatour, L. Racault, T. Bessaire and A. Desmarchelier, *Food Addit. Contam.,: Part A*, 2018, **35**, 633–646.
473 T. Simon, M. Shellaiah, P. Steffi, K. W. Sun and F.-H. Ko, *Anal. Chim. Acta*, 2018, **1023**, 96–104.
474 Y. Zhou, P. Wang, X. Su, H. Zhao and Y. He, *Talanta*, 2013, **112**, 20–25.
475 A. Chen, X. Jiang, W. Zhang, G. Chen, Y. Zhao, T. M. Tunio, J. Liu, Z. Lv, C. Li and S. Yang, *Biosens. Bioelectron.*, 2013, **42**, 419–425.
476 K.-M. Song, E. Jeong, W. Jeon, M. Cho and C. Ban, *Anal. Bioanal. Chem.*, 2012, **402**, 2153–2161.
477 Y. S. Kim, J. H. Kim, I. A. Kim, S. J. Lee, J. Jurng and M. B. Gu, *Biosens. Bioelectron.*, 2010, **26**, 1644–1649.
478 N. Zhou, J. Wang, J. Zhang, C. Li, Y. Tian and J. Wang, *Talanta*, 2013, **108**, 109–116.
479 Q. Chen, R. Tian, G. Liu, Y. Wen, X. Bian, D. Luan, H. Wang, K. Lai and J. Yan, *Biosens. Bioelectron.*, 2022, **207**, 114187.
480 J. Liu, W. Bai, C. Zhu, M. Yan, S. Yang and A. Chen, *Analyst*, 2015, **140**, 3064–3069.
481 V. Turcanu, H. A. Brough, G. Du Toit, R.-X. Foong, T. Marrs, A. F. Santos and G. Lack, *Curr. Opin. Immunol.*, 2017, **48**, 92–98.
482 T. R. Pavase, H. Lin, M. A. Soomro, H. Zheng, X. Li, K. Wang and Z. Li, *Mar. Life Sci. & Technol.*, 2021, **3**, 382–394.
483 E. Kim, J. Hahn, C. Ban, Y. Jo, H. Han, S. Lim and Y. J. Choi, *Food Chem.*, 2021, **352**, 129354.
484 D. Yuan, X. Fang, Y. Liu, J. Kong and Q. Chen, *Analyst*, 2019, **144**, 3886–3891.
485 J. I. Lee, S. C. Jang, J. Chung, W.-K. Choi, C. Hong, G. R. Ahn, S. H. Kim, B. Y. Lee and W.-J. Chung, *Sens. Actuators, B*, 2021, **327**, 128894.
486 S. Lou, J. Ye, K. Li and A. Wu, *Analyst*, 2012, **137**, 1174–1181.
487 X. Xu, A. Wu, L. Guo, H. Kuang, L. Xu, C. Xu and L. Liu, *Nanoscale Horiz.*, 2024, **9**, 123–131.
488 X. Xu, A. Wu, L. Guo, H. Kuang, L. Xu, C. Xu and L. Liu, *Nanoscale Horiz.*, 2024, **9**, 123–131.
489 L. Ye, X. Lei, L. Xu, H. Kuang, C. Xu and X. Xu, *Mater. Chem. Front.*, 2023, **7**, 4063–4072.
490 I. T. Jolliffe and J. Cadima, *Philos. Trans. R. Soc. A: Math. Phys. Eng. Sci.*, 2016, **374**, 20150202.
491 E. X. Tan, Y. Chen, Y. H. Lee, Y. X. Leong, S. X. Leong, C. V. Stanley, C. S. Pun and X. Y. Ling, *Nanoscale Horiz.*, 2022, **7**, 626–633.
492 B. Karlik, M. F. Yilmaz, M. Ozdemir, C. T. Yavuz and Y. Danisman, *Plasmonics*, 2021, **16**, 147–155.
493 F. Bilén, P. Ekborg-Tanner, A. Balzano, M. Ughetto, R. R. Da Silva, H. Schomaker, P. Erhart, K. Moth-Poulsen and R. Bordes, *J. Phys. Chem. C*, 2024, **128**, 13909–13916.
494 Y. Lin, J.-H. Cheng, J. Ma, C. Zhou and D.-W. Sun, *Crit. Rev. Food Sci. Nutr.*, 2025, **65**, 3628–3649.